AN ABSTRACT OF THE THESIS OF

Nevenka Obušković for the degree of Doctor of Philosophy

in Chemical Engineering presented on September 28, 1988.

Title: Heat Transfer Between Moving Beds of Solids and a Vertical Tube

Redacted for privacy

Abstract approved: _____
Dr. James G. Knudsen

Heat transfer to moving packed beds of solids has been studied extensively but predictions are usually specific to the experimenter's own equipment. In order to obtain a more general predictive equation, the heat transfer coefficient was measured for a single vertical tube immersed in a moving packed bed of glass beads, sand, or copper in air at atmospheric pressure and compared to measurements performed by independent researchers with various experimental configurations.

High speed photography was used to observe the motion of the particles as they flowed past the heated wall. The particle separation from the wall could not be determined. There was little interchange of the wall particles with the particles in the bulk beyond the wall layer. Likewise, the particles in the layer adjacent to the wall showed very little rotational or cross-flow motion.

A numerical method, based on the unsteady state conduction equation, was developed to predict the heat transfer coefficient between the wall and the flowing bed of solid particles. This method could be used to predict the experimental heat transfer coefficients obtained provided the correct value of the particle separation from the wall was used in the numerical solution. This separation cannot be

predicted a priori so that the numerical method is, therefore, not suitable for predicting the heat transfer coefficient.

The experimental data showed good agreement with the analytic solution obtained by Mickley and Fairbanks (1) at long contact times. At short contact times, the data do not agree with the Mickley and Fairbanks solution but the heat transfer coefficient tends to level off at an asymptotic value.

An empirical correlation was obtained by which the contact time at which the data depart from the Mickley and Fairbanks solution may be predicted. The following equation, was found to be valid for the data of the present work and for data of other researchers who used different geometries in their work.

$$\frac{t_{cr}}{d_p \rho_s} = 0.3622 + 9.691\ L.$$

This equation may be used in conjunction with the Mickley and Fairbanks solution to predict the heat transfer coefficient for a given flowing packed bed over a wide range of contact times.

Heat Transfer Between Moving Beds of Solids and a Vertical Tube

by

Nevenka S. Obušković

A THESIS

submitted to

Oregon State University

in partial fulfilment of
the requirements for the
degree of

Doctor of Philosophy

Completed Sept. 28, 1988

Commencement June 1989

Approved:

Redacted for privacy

Professor of Chemical Engineering in charge of major

Redacted for privacy

Chairman of Chemical Engineering Department

Redacted for privacy

Dean of Graduate School

Date thesis is presented Sept. 28, 1988

Typed by Kevin Greek for Nevenka Obušković

ACKNOWLEDGEMENT

I would like to express my thanks to my major professor Dr. James G. Knudsen for all the understanding and financial support at times when this job seemed to be a neverending story; also for reading and correcting the manuscript and the final draft.

Special thanks are extended to my dear professor Dr. Octave Levenspiel not only for his insistent questions on music, art, geography, history and life in general but also for the lost backgammon games, jokes and free lunches that anyone could get if he shows up in front of his office around 12pm (students only). Acknowledgments are also extended to my professors and chairmen Dr. Charles Wicks and Dr. Robert Mrazek and Dr. Jim Fredericks for enormous understanding and support in the completion of this thesis.

My thanks also go to Nick Wannenmacher for his invaluable help in experimental research whenever necessary and to Jordana Chambers expert in solving all my administrative problems.

I wish to express gratitude to my friend and "computer-wiz" Kevin Greek or as I call him Mr. Blasius who was unselfishly available whenever the word "computer" was mentioned; also for correcting and typing the manuscript.

Special thanks go to my mother Vera and dear friend Dr. Vojislav Bogic for their everlasting support understanding and suggestions.

I also want to thank the rest of faculty members for their help and encouragement during the course of this research.

Thanks also to all my "beanery" friends for being there when necessary.

Finally, my greatest appreciation goes to my very dear friend Hubert called Mici for all the lengthy hours of listening to my complaints about this work and his criticism that I did not always accept.

NOMENCLATURE

Symbol	Description	Units
A_{rod}	- surface area of the heated section available for heat transfer.	m^2
C_{ps}	- heat capacity of the solids.	J/kgK
D	- heated rod diameter.	m
d_p	- particle diameter.	m
d_{pi}	- diameter of particles of size "i".	m
f_D (f_W)	- friction coefficient between a tube and dry (wet) solids.	
h	- heat transfer coefficient.	W/m^2K
h_i	- local heat transfer coefficient.	W/m^2K
k_g	- thermal conductivity of gas.	W/mK
k_e	- effective thermal conductivity of solids-gas emulsion.	W/mK
k_{gs}	- reduced thermal conductivity of gas.	W/mK
L	- heated length parallel to the flow path of solids.	m
L_C	- heated length across the flow path of solids (characteristic length).	m
n	- number of sides of polygon.	
$Nu_d = \frac{hd_p}{k_g}$	- Nusselt number based on particle radius (d_p).	
$Nu_D = \frac{h\ D}{k_g}$	- Nusselt number based on heated rod diameter (D).	
P	- power input to the heater.	W

Symbol	Description	Units
$Pe_d = \frac{C_{ps} d_p \rho_b U_s}{k_g}$	- Peclet number based on particle diameter (d_p).	
$Pe_D = \frac{C_{ps} D \rho_b U_s}{k_g}$	- Peclet number based on heated rod diameter (D).	
r_p	- particle radius.	m
R_c	- contact resistance (due to gas film).	m_2K/W
s,x	- distance from heated wall.	m
T_g	- temperature of the gas.	K
T_s	- bulk temperature of the solids.	K
T_W	- steady-state average surface temperature of the rod.	K
t	- residence time.	s
t_{cr}	- critical or separation time.	s
t_{max}	- time where maximum heat transfer occurs.	s
U_s	- linear solids velocity.	m/s
X_i	- mass fraction of particles of size "i".	

GREEK SYMBOLS

Symbol	Description	Units
α_e	- effective thermal diffusivity (emulsion).	m^2/s
α_s	- effective thermal diffusivity (solids).	m^2/s
δ	- ratio of gap width to particle radius.	

Symbol	Description	Units
ϵ	- porosity of packed bed.	
ϵ_0	- void fraction for wall separation distance greater than $0.7d_p$.	
ϵ_r	- void fraction for wall separation distance less than $0.7d_p$.	
γ	- accomodation coefficient.	
λ	- mean free path of gas particle.	m
ρ_b, ρ_e	- bulk density of solids.	kg/m^3
ρ_s	- density of solids.	kg/m^3
σ	- thickness of the gas layer.	m
τ_D, (τ_W)	- effective shear stress for dry (wet) solids.	N/m^3

TABLE OF CONTENTS

Chapter		Page
I.	INTRODUCTION	1
II.	SELECTED PREVIOUS WORK	3
III.	EXPERIMENTAL EQUIPMENT	8
III.A.	Solids	8
III.B.	Heater rod	11
III.C.	Test section and solids transport system	13
III.D.	Particle motion and porosity measurement equipment	15
III.E.	Experimental procedure	18
III.E.1.	Heat transfer coefficient measurement	18
III.E.2.	Velocity measurements	20
III.E.3.	Particle motion and porosity measurement	21
IV.	HEAT TRANSFER RESULTS	24
IV.A.	Present study	24
IV.B.	Data comparison with other researchers	29
V.	MODEL ASSUMPTIONS	37
V.A.	The role of the gas phase	38
V.B.	Contact resistance	40
V.C.	Particle shape	44
V.D.	Flow and porosity distribution	45
V.D.1.	Flow properties	46
V.D.2.	Static properties	49

Chapter		Page
V.E.	Summary	54
VI.	HEAT TRANSFER COEFFICIENT MODELS	56
VI.A.	Analytic models	56
VI.B.	Numerical model	61
VI.C.	Empirical model	66
VII.	CONCLUSIONS	77
VII.A.	Summary of Findings	77
VII.A.	Furthure Work	79
BIBLIOGRAPHY		80
APPENDICES		
A.	Analytic heat transfer coefficient for rod	84
B.	Heat transfer coefficient for two region semi-infinite slab	91
C.	Heat transfer from wall to particle through interstitial fluid	95
D.	Finite difference calculation of heat transfer coefficient to packed beds	102
E.	Experimental data	161
F.	Statistical analysis	170
G.	Particle size distribution	171

LIST OF FIGURES

Figure		Page
(III.B.1)	Heated stainless steel tube.	12
(III.C.1)	General layout of moving bed apparatus.	14
(III.D.1)	Transparent test section used with high speed camera.	17
(IV.A.1)	Comparison between heat transfer coefficients as a function of the linear solids velocity for 0.18mm and 0.8mm diameter glass beads.	25
(IV.A.2)	Comparison between heat transfer coefficients as a function of contact time with the heated surface for 0.044mm, 0.18mm, and 0.8mm diameter glass beads.	26
(IV.A.3)	Comparison between heat transfer coefficients as a function of the contact time with the heated surface for 0.11mm and 0.8mm diameter sand.	27
(IV.A.4)	Comparison between heat transfer coefficient as a function of contact time with the heated surface for 0.044mm, 0.18mm, 0.8mm glass beads and copper of 0.21mm in diameter.	28
(IV.B.1)	Comparison between heat transfer coefficients as a function of the linear solids velocity for Colakyan's (10) data and the present study for 0.11mm, 0.27mm and 0.8mm diameter sand.	30
(IV.B.2)	Comparison between heat transfer coefficients as a function of the linear solids velocity for horizontal finned (11) and vertical tube for 0.11mm and 0.8mm diameter sand.	31
(IV.B.3)	Comparison between heat transfer coefficients as a function of contact time for Colakyan's (10) data and this study for 0.11m, 0.27mm, and 0.8mm diameter sand.	32

(IV.B.4)	Comparison between heat transfer coefficients as a function of contact time for the author's (11) data and the present study for 0.11mm and 0.8mm diameter sand.	33
(IV.B.5)	Comparison between heat transfer coefficients as a function of contact time with the heated surface for Ernst's (9), Schlunder's (13), and the present data.	35
(IV.B.6)	Comparison between heat transfer coefficients as a function of contact time with the heated surface for Sullivan's (3) data and the present study.	36
(V.A.1)	Comparison between heat transfer coefficients as a function of contact time with the heated surface for glass in air and vacuum conditions (reproduced from Wunschmann (13)).	39
(V.D.2.1)	Particles in orthorhombic array.	51
(V.D.2.2)	Scheme for porosity calculation by penetration s into orthorhombic array of spheres.	53
(VI.A.1)	Heat transfer coefficient comparison by contact time to rod and slab analytic models and experimental data.	59
(VI.B.1)	Heat transfer coefficient comparison as a function of contact time with the heated surface for the M&F (1) model and the numerical solution for 0.8mm diameter glass beads.	62
(VI.B.2)	Heat transfer coefficient comparison as a function of contact time with the heated surface for the M&F (1) model and the numerical solution for 0.18mm diameter glass beads.	63

(VI.B.3)	Heat transfer coefficient as a function of contact time with the heated surface for M&F (1) model and the numerical solution by gap width for 0.18mm diameter glass beads.	65
(VI.C.1)	Comparison between heat transfer coefficients as a function of contact time with the heated surface for the present data and the M&F (1) model.	68
(VI.C.2)	Empirical prediction of t_{cr} by Eq. (VI.C.1) and Ernst's (9) data.	72
(VI.C.3)	Empirical prediction of tcr by Eq. (VI.C.1) and Desai's (21) data for glass.	73
(VI.C.4)	Empirical prediction of t_{cr} by Eq. (VI.C.1) and Desai's (21) data for copper.	74
(VI.C.5)	Empirical prediction of t_{cr} by Eq. (VI.C.1) and t_{max} by Eq. (VI.C.2) for data of the present study.	75
(VI.C.6)	Comparison between heat transfer coefficients by contact time with the heated surface for Ernst's (9), Wunschmann's (12), Harakas (2) and the present data.	76
(B.1)	Representation of composite slab.	92
(C.1)	Representation of separation distance between a spherical particle and wall.	96
(D.1)	Finite difference map to model wall-to-bed heat transfer.	107
(D.2)	Example of cell noding scheme.	108
(D.3)	Finite difference scheme at wall to obtain axial average heat transfer coefficient.	120
(D.4)	Error introduced by modeling a semi-infinite slab as a finite slab.	124

(D.5) Accurary of heat transfer solution to a semi-infinite slab on Fo_d value. 128

LIST OF TABLES

Table		Page
(III.A.1)	Properties of Materials Used and Operating Conditions.	9
(III.A.2)	Properties of Solids.	10
(E.1)	Table of Experimental Conditions and Heat Transfer Coefficients for Glass Beads.	161
(E.2)	Table of Experimental Conditions and Heat Transfer Coefficients for Sand.	163
(E.3)	Table of Experimental Conditions and Heat Transfer Coefficients for Copper.	165
(E.4)	Table of Experimental Conditions and Heat Transfer Coefficients for Falling Solids.	166
(F.1)	Regression Analysis of Model.	170
(F.2)	List of All Data used to Fit the Model.	170
(G.1)	Size Distributions of Particles	171

Heat Transfer Between Moving Beds of Solids and a Vertical Tube

I. INTRODUCTION

The most important aspect of heat transfer information for any kind of heat exchanger is the average heat transfer coefficient to an immersed heated surface. This quantity is usually obtained by measuring the power dissipation from the surface to the surrounding media. Reliable data and correlations for the average heat transfer coefficient have great commercial importance, therefore an increase in heat transfer can nearly proportionally reduce the cost of the exchanger.

Ever since gas-solid systems have been recognized for their excellent heat transfer characteristic, considerable research has been conducted in this field especially for fluidized beds. However, less data is available for moving packed beds of solids than for fluidized beds. Existing predictions have generally been compared against the researcher's own data instead of equally considering data from the literature. Consequently, there has been little study to explain deviations between data by various experimental setups. The knowledge of these heat transfer variations over a wide range of particle sizes and velocities would be of great interest when designing or selecting materials for

solid-gas heat exchangers.

For this purpose, this study presents heat transfer coefficient measurements to granular media flowing by gravity past a vertical heated tube and compares it to the limited number of data available in the literature. The comparison shows that the heat transfer coefficient to vertically oriented heaters may be predicted graphically and a unique empirical solution to predict the heat transfer coefficient is proposed.

II. SELECTED PREVIOUS WORK

A considerable amount of work has been done on the flow patterns as well as heat transfer behavior of granular media in systems such as fluidized beds, packed beds, moving beds, and suspension. In spite of many attempts, the mechanism of convective heat transfer to/from surfaces immersed in flowing solids is not yet well understood. Related past research is briefly reviewed in this chapter.

Mickley and Fairbanks (1) were among the first to obtain data for the instantaneous heat transfer coefficient in fluidized beds and provided an analytical solution for the proposed version of the "packet" theory. The packet (i.e. moving particles with entrained gas) is assumed to be in contact with the heated surface for a short time and then is replaced by a new packet from the bulk of the bed. They considered the packet to be homogeneous with uniform thermal properties and derived an expression for the local instantaneous heat transfer coefficient h_i,

$$h_i = \sqrt{\frac{k_e C_{ps} \rho_b}{\pi t}} \qquad \text{(II.1)}$$

Their results indicated that heat transfer resistance exists in the layers of particles closest to the wall,

but the independent effect of particle size is not included.

Harakas and Beatty (2) considered the heat transfer from a flat plate immersed in a rotating bed of granular material (the flow of particles was parallel to the plate). They varied particle size as well as interstitial gas and observed an increase in average heat transfer coefficient by either increasing interstitial gas conductivity or decreasing particle diameter. Their experimental findings are presented in Chapter IV. Fine grained materials were considered a one-component continuum and effective properties of this continuum were used to predict a mean heat transfer coefficient. However, great discrepancies in the model predictions occurred as the particle size increased. This result is expected since the thermal gradient which forms within the "packet" in a short residence time does not extend beyond one or two particle diameters from the surface.

The convective heat transfer from a vertical flat plate to various granular materials was investigated by Sullivan and Sabersky (3). To explain their observations analytically, they defined an idealized model called the "discrete particle model". In this model it was assumed that the conductance at the wall was the same as that existing between adjacent rows of

particles and that the conductance was inversely proportional to the average thickness of the gas film between particles and the heated plate.

Studying the mechanism of heat transfer between a fluidized bed and immersed surfaces Baskakov (4) introduced an additional contact resistance R_c, in series with the thermal resistance of the packets, R_e, as defined by Mickley and Fairbanks (1). The contact resistance, R_c, is assumed to represent the additional thermal resistance of the layer next to the wall due to increased porosity.

Denloye and Botterill (5) studied the heat transfer in flowing packed beds. They obtained data by varying the particle sizes of different interstitial gases. They concluded that the heat transfer coefficient increases with increasing gas thermal conductivity, decreasing particle size, and particle residence time.

Spelt (6) investigated the heat transfer to a granular material flowing in an inclined chute. He found that the heat transfer coefficient increased to a maximum and that decreased as the velocity of the solids across the plate increased. The phenomena is believed to occur due to changes in the packing density of the flowing media.

Russian researchers Donskov (7) and Kurockin (8) also experimented with flowing packed beds. Donskov (7)

investigated the heat transfer coefficient by varying the tube diameter and pitch of the tubes in a tube bank. The results showed that the heat transfer coefficient increases with a decrease in the ratio between pitch and tube diameter. Kurockin (8) investigated the heat transfer coefficient between dry and wet material, and a single tube. He concluded that heat transfer increased as the velocities of the granular material increased, and he correlated his results with the following equation:

$$Nu_D = 0.22\ Pe_D \left(\frac{D}{d_p}\right) \left(\frac{f_d}{f_w}\right) \left(\frac{\tau_D}{\tau_w}\right)^{0.33}$$

Ernst Rudolf (9) concluded that for moving beds of solids and vertical or horizontal tubes at "short" contact times the heat transfer coefficient is only important within 0.1mm to 1mm away from the heated surface. He also found that the heat transfer coefficient at short contact times exhibits a maximum value which is independent of the physical properties of the particles but depends on particle size.

Colakyan's (10) work on heat transfer from a single tube to various granular materials flowing in a direction perpendicular to the cylinder axis provided an empirical value for the contact resistance R_c first introduced by Baskakov (4). The resistance was

estimated to be

$$R_c = \frac{6.7 \times 10^{-5}\ d_p^2}{k_g}$$

Previous work preformed by the author (11) upon the heat transfer coefficient between a horizontal finned tube and moving beds of solids led to the following empirical correlation:

$$Nu_d = 2.37\ Pe_d^{0.25} \left(\frac{k_e}{k_g}\right)^{0.3} \left(\frac{d_p}{L_c}\right)^{0.33}$$

The equation predicts the heat transfer coefficients for plain and finned tubes within ±20%, but is restricted to tubes with fin heights equal to or smaller than that used for this research.

It was observed that the heat transfer coefficient is greatest for particles with small diameters as compared to the large diameter particles of the same substance. The heat transfer coefficient also depends on the velocity of the particle flow over the heated surface as explained later.

Other research concerning flow of solid material, porosity distribution, gas properties, surface influence, etc. is discussed elsewhere in the related sections.

III. EXPERIMENTAL EQUIPMENT

An experimental test system was developed to determine the heat transfer coefficient for granular materials flowing by gravity past a vertical heated tube. Particles having various solids properties and sizes were selected for measurement as a function of transport velocity. A physical description of each component is reviewed here.

III.A. Solids

In the present work only granular materials are considered; porous materials in which a solid medium has a closed gaseous space were not considered. Four types of solids, sand, glass beads, copper, and iron were used as the granular media. Properties of the materials used in the experiments as well as the range of operating conditions are given in Table (III.A.1). Table (III.A.2) lists all the properties of the four different solids used in the experiments. Effective properties were calculated using Eq. A.2 in Appendix A.

Microscopic photographs of these particles revealed the glass beads had the most smooth and regular shape distribution. In contrast, the iron solids have a

Table (III.A.1). Properties of Materials Used and Operating Conditions.

Material		Range of Operating Conditions
Particle Diameter, d_p	=	0.044 - 0.8 mm
Solids Density, ρ_s	=	2500 - 8900 kg/m^3
Bulk Density, ρ_b	=	1500 - 5360 kg/m^3
Solids Thermal Conductivity, k_s	=	0.8 - 384 W/mK
Solids Heat Capacity, Cps	=	380 - 1080 J/kgK
Linear Solids Velocity, Us	=	0.004 - 0.3 m/s

Table (III.A.2). Properties of Solids.

Material	d_p (mm)	k_s (W/mK)	ρ_s (kg/m^3)	C_{ps} (J/kgK)	ϵ	ρ_b (kg/m^3)	k_e (W/mK)	$\alpha_e x10^8$ (m^2/s)	$\alpha_s x10^8$ (m^2/s)
Sand	0.11	0.80	2700	780	0.488	1280	0.14	14.0	0.38
Sand	0.80	0.80	2700	780	0.436	1410	0.17	15.5	0.38
Sand	1.2	0.80	2700	780	0.424	1440	0.18	16.2	0.38
Glass	0.044	1.04	2500	1080	0.426	1435	0.26	16.6	0.53
Glass	0.18	1.04	2500	1080	0.400	1500	0.28	17.3	0.53
Glass	0.80	1.04	2500	1080	0.400	1500	0.29	17.7	0.53
Copper	0.21	384	8950	383	0.419	5200	0.46	22.4	11000

wide size distribution and a flaky texture. When pressed together, the iron would cling in clumps.

The mean diameter, d_p, of each solid was calculated according to the following formula:

$$d_p = \frac{1}{\sum \frac{x_i}{d_{pi}}} \qquad \text{(III.A.1)}$$

where

x_i = mass fraction of particles of size "i".

d_{pi} = diameter of particles of size "i".

III.B. Heater Rod

The instrument illustrated in Figure (III.B.1) consists of a stainless steel tube 0.0127m O.D., 0.4572m long with a 600W (115V) heating element 0.1524m long imbedded in it. Temperature at the inside surface of the stainless steel rod was measured with a single imbedded T-type thermocouple positioned along the axial center of the heater element. Power to the heater was regulated by a 115V 5amp variac and measured with a Jewell electric wattmeter to 5% tolerance. A calibration procedure was performed to determine the metal resistance (k/x) between the thermocouple and the rod outside surface. Corrected temperatures were then used for calculations of the heat transfer coefficient. A table for heat transfer coefficients using corrected

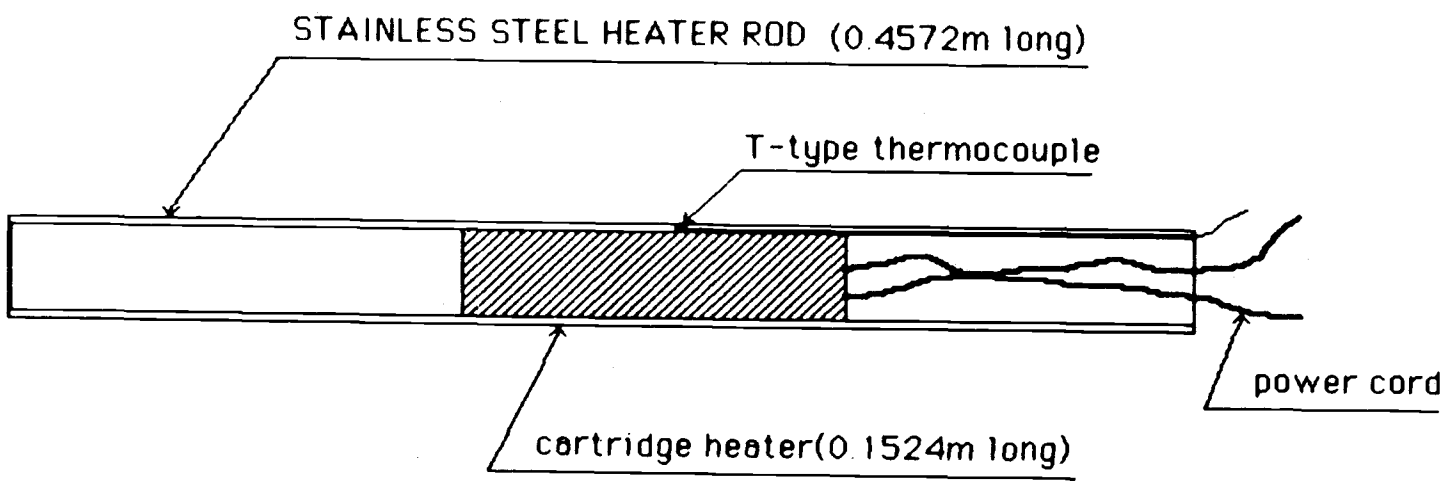

Figure (III.B.1). Heated stainless steel tube.

temperatures is presented in Appendix E.

The surface of the heated rod, in which the heating element is installed, maintains a constant temperature axially over a 0.1524m length. Some experiments were conducted to verify this condition and temperatures along this length were observed within 0.5F deviation.

III.C. Test Section and Solids Transport System

The heater rod was centered within a 0.0381m I.D. tube and its position was maintained by three retaining screws at either end of this 0.4572m long tube. The tube was made of clear plexiglass to permit visual examination of granular flow about the heater rod. A small hole in this vertical test section near the center of the heated section of the rod allowed a thermocouple to penetrate and measure solid temperature near the tube wall during the experiment. A cone centered at the base of the heater rod and inside the bottom opening of the test section maintained an equal radial distribution of solids flow about the rod length and its height could be adjusted to vary the flow rate of solids leaving the bottom of the test section.

A ten gallon supply hopper acted as a solids reservoir and emptied its contents through a 2in I.D. pipe which was kept capped until the experiment was

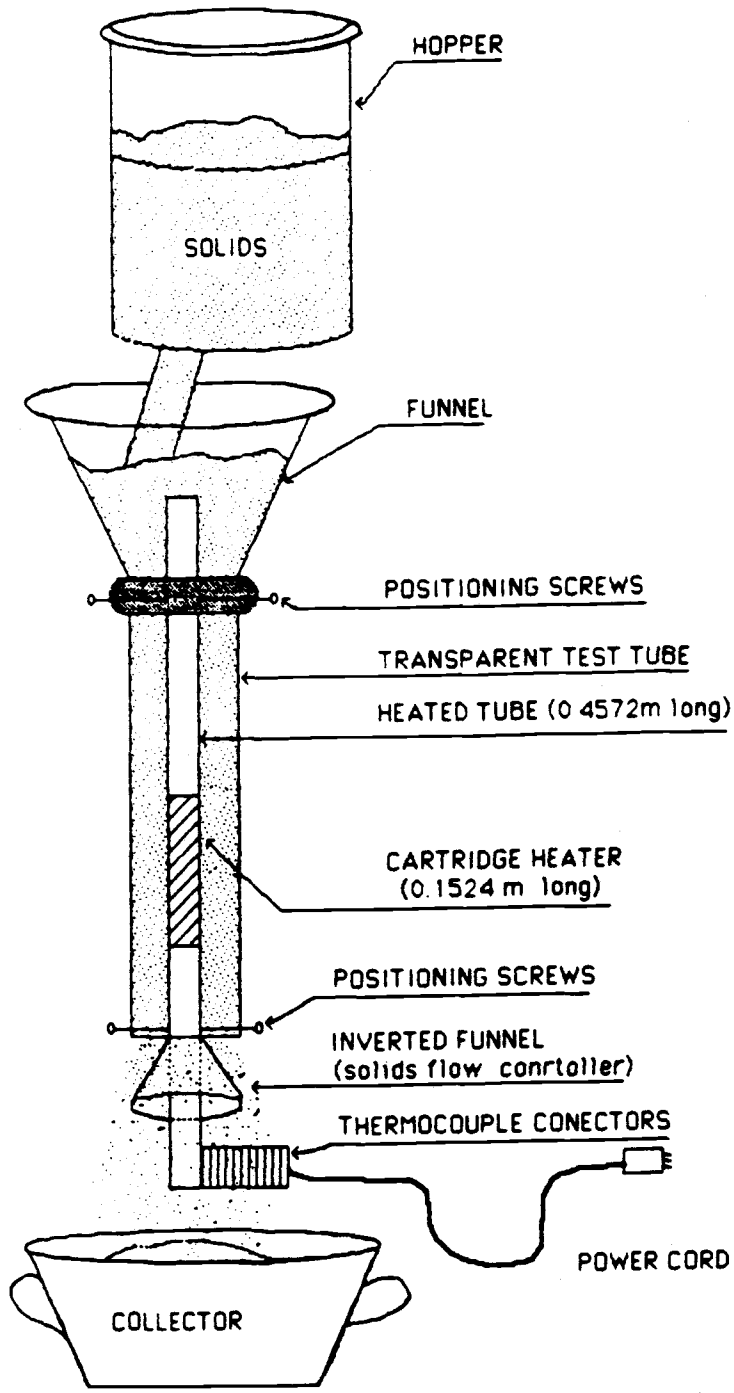

Figure (III.C.1). General layout of moving bed apparatus.

ready to begin. Solids were fed through a funnel into the test section and collected into a bucket below. To recirculate the flow, solids were manually transferred into the supply hopper. The depth of the supply hopper outlet pipe into the funnel was kept constant throughout experiments with all materials and the height of solids in the hopper was maintained at the same level as much as possible. Maintaining these positions constant was essential to assure constant flow rate. The funnel outlet size limited the rate of mass flow into the test section and was largely responsible for the maximum transport velocities achieved (Figure III.C.1).

Two thermocouples, one to measure ambient air, the other to measure solids leaving the funnel, were employed to determine static two phase (gas-air) temperatures. These two thermocouples, including the heater rod thermocouple, were wired through a selector switch to a ±0.1F digital thermocouple reader.

III.D. Particle Motion and Porosity Measurement Equipment

In order to record motion of particles which slide against the surface of the heating rod, an apparatus was devised whereby a high speed motion picture camera could be focused upon a small portion of the rod. A plexiglass tube with an outer radius identical to the

heater rod was constructed within a test section to enable photography of particles through the tube wall under conditions closely resembling particle contact with the heater (Figure III.D.1). A small vertical section of both this tube and the test section wall was removed and a tunnel between the two openings was installed. A Hycam model 41-0004 rotating prism camera was focused through the tunnel upon the outside edge of the tube and the subject was illuminated from 3 feet by a 1000W tungsten-halogen spotlight. To assure focus and alignment, the test section was firmly clamped to the equipment support column and the camera was positioned on a level surface over a rubber mat. Framing speeds may be measured directly from the film margin since timing marks are exposed on the film during camera operation by an internal time dot generator. The motion was recorded at speeds to 2000 frames per second on a high speed 16mm film, Kodak RAR 2484, developed for 8min in D19 developer at 20C to a sensitivity of 1250 ASA. Film spools of approximately 40ft were used for each run. When imaged with a Sopelem macro zoom lens set for highest magnification (250mm f/5), a view field of 3mm x 5mm was obtained, the latter dimension closely approximating the arc length of rod surface in view. Due to this high magnification, an extremely short depth of field ensured only those particles within 1mm of the

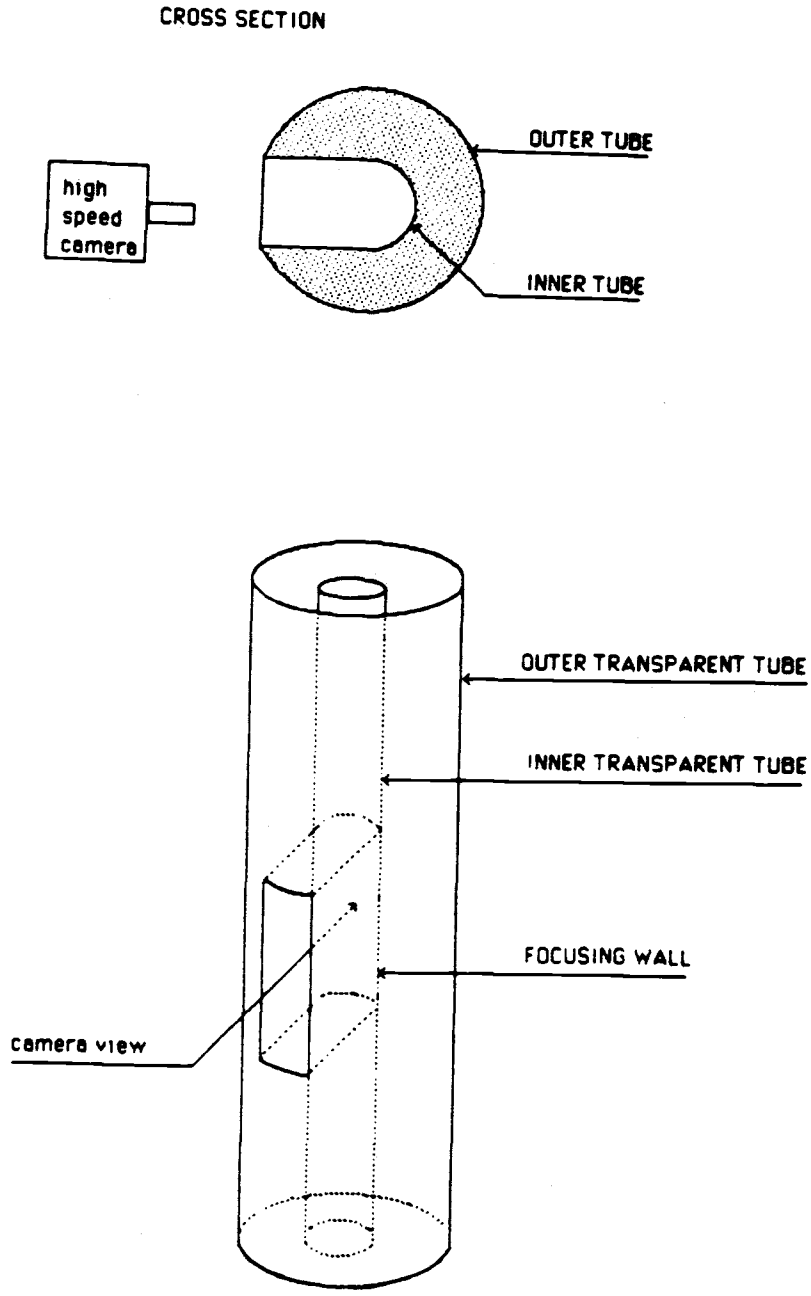

Figure (III.D.1). Transparent test section used with high speed camera.

tube wall could be imaged.

Spherical particles of glass (0.8mm) and copper (mixed sizes of 0.8 to 0.2mm) were filmed for porosity measurements for moving packed beds. The glass beads, in an attempt to obtain a better photographic image, were colored with blue paint.

III.E. Experimental Procedure

III.E.1 Heat Transfer Coefficient Measurement

This section provides details of the steps performed in the experiment, experimental equipment operation constraints or criteria chosen to select a particular range of operation, and calculations required to obtain a measured value of the heat transfer coefficient as a function of solids velocity. The experimental procedure required the heat transfer coefficient to be measured under steady state temperature conditions. Once the cap of the supply hopper was removed and the flow rate through the test section was adjusted, power to the heating rod was applied. Steady state was reached when the temperature variation at the surface of the rod was negligible with time (a deviation of not more than 0.1 to 0.2F over a few minutes). When the rod temperature stabilized, the time required for solids leaving the test section to

collect in a beaker for mass survey was measured and the thermocouple readings and power were recorded. Measurements were repeated several times for a single solids type, flow setting, and power level.

Precautions regarding power levels, and therefore operating temperatures of the rod, were taken. First, the rod surface temperature could not exceed 300C to avoid errors introduced by T-type thermocouples which are not designed to operate at these higher temperatures. Second, by providing the maximum possible temperature difference Tw-Ts the highest precision was ensured. In all experiments this difference is at least 50C. It was also observed that at power levels below 75W significant deviation existed in heat transfer coefficient calculations from rod temperatures compared to those calculations at all higher power levels. Therefore, experimental power levels were maintained within a range of 75 to 200W.

Solids depth in the supply hopper influenced flow velocity and therefore rod temperature changed a small percentage as the hopper was replenished. Maintaining an equal level within the hopper as well as performing multiple measurements reduced what affect this variation might have.

In a large number of test runs under different conditions of solids velocity, the test section was

rotated with respect to the rod to confirm that the rod thermocouple gave identical readings when placed in different radial positions.

The heat transfer coefficient h is calculated for each run using the following relationship.

$$h = \frac{P}{A_{rod}(T_w - T_s)}$$

where

P = power input to the heater (W)

Arod = surface area of the heated section available for heat transfer ($0.00608048 m^2$).

Ts = bulk temperature of the solids (K).

Tw = steady state average surface temperature of the rod (K).

Flow velocity was calculated from the time required for solids discharged from the test section to fill a survey beaker and the mass which accumulated.

III.E.2. Velocity Measurements

The velocity was measured in two different ways:

1. The amount of solids discharged from the test section in a given time was collected and weighed. Knowing the properties of the material and the limiting cross sectional area available for flow, the velocity was estimated

using the following relationship

$$U_s = \frac{\text{(mass flow rate)}}{\text{(bulk density) (flow area)}}.$$

2. The velocities were estimated by visual observation of the particles near the transparent wall by measuring the time taken for the particles to travel a given distance. This method assumes that solids are flowing in plug flow.

For data analysis, velocities measured by the first method were used. Flow velocities at the wall were also recorded for comparison by high speed photography.

III.E.3. Particle Motion and Porosity Measurement

At the high magnification required to photograph particle movement, alignment and stability of the camera and test section was critical. Film changes were therefore performed without moving the camera position and both alignment and focus were verified prior loading each film. Also, the solids were allowed to flow through the section before switching on the spotlight and camera and precautions were taken to isolate movement by the operator from the equipment while the exposure was taking place. Solids velocity was regulated by the height of an inverted funnel centered at the bottom of the test section and a different

velocity was set for each run. A solids velocity measurement by sampling the mass and duration of solids accumulated from the test section occurred simultaneously.

The photographic experiment was exposure limited because of the recording speed required. Therefore, the lens aperture was opened fully throughout the experiment so the inherent camera aperture of f/3 was the only restriction on the intensity of exposure. Due to the narrow opening of the view tunnel into the test section, spotlight placement had an effect on the intensity and clarity of the image of the particles viewed through the lens. Some experimentation with spotlight placement was therefore necessary for initial runs.

Film processing occurred on site to minimize delay for analysis. To analyze the films, a 16mm film editor was used to view particle motion and velocity whereas an enlarger displayed individual frames for porosity and particle separation. A film of a static packed bed for each particle type was used for comparison. Particle speed was computed by tracking a vertically moving particle throughout the height of the frame image, counting the consecutive frames, and calculating the corresponding elapsed time using the timing marks exposed on the film. Individual frames selected for appearance of distinct particles were projected upon a

sheet of paper where the measurements were recorded. At least 10 to 20 distinct frames were sampled from each film to measure particle separation and interpret particle number per frame touching the rod wall.

IV. HEAT TRANSFER RESULTS

The following section provides a graphical presentation of the experimental results for heat transfer from a vertical bare tube and moving beds of solids. A graphical comparison between results of the present study and some available data from the literature for various experimental setups accumulated from either tables or digitized from original figures is also included.

IV.A. Present Study

Figure (IV.A.1) presents the heat transfer coefficient as a function of the linear solids velocity for glass beads of 0.8mm, 0.18mm and 0.044mm in diameter. As expected from the results of the previous workers, the heat transfer coefficient increases with a corresponding increase of the solids velocity. The heat transfer coefficient can be observed to level off with increasing velocity for all three sizes and the maximum value for the heat transfer coefficient decreases as particle size increases. When data are plotted on a log-log scale all three particle diameters follow a straight line with a slope of 0.4 and only the heat transfer coefficient for glass beads of 0.8mm diameter

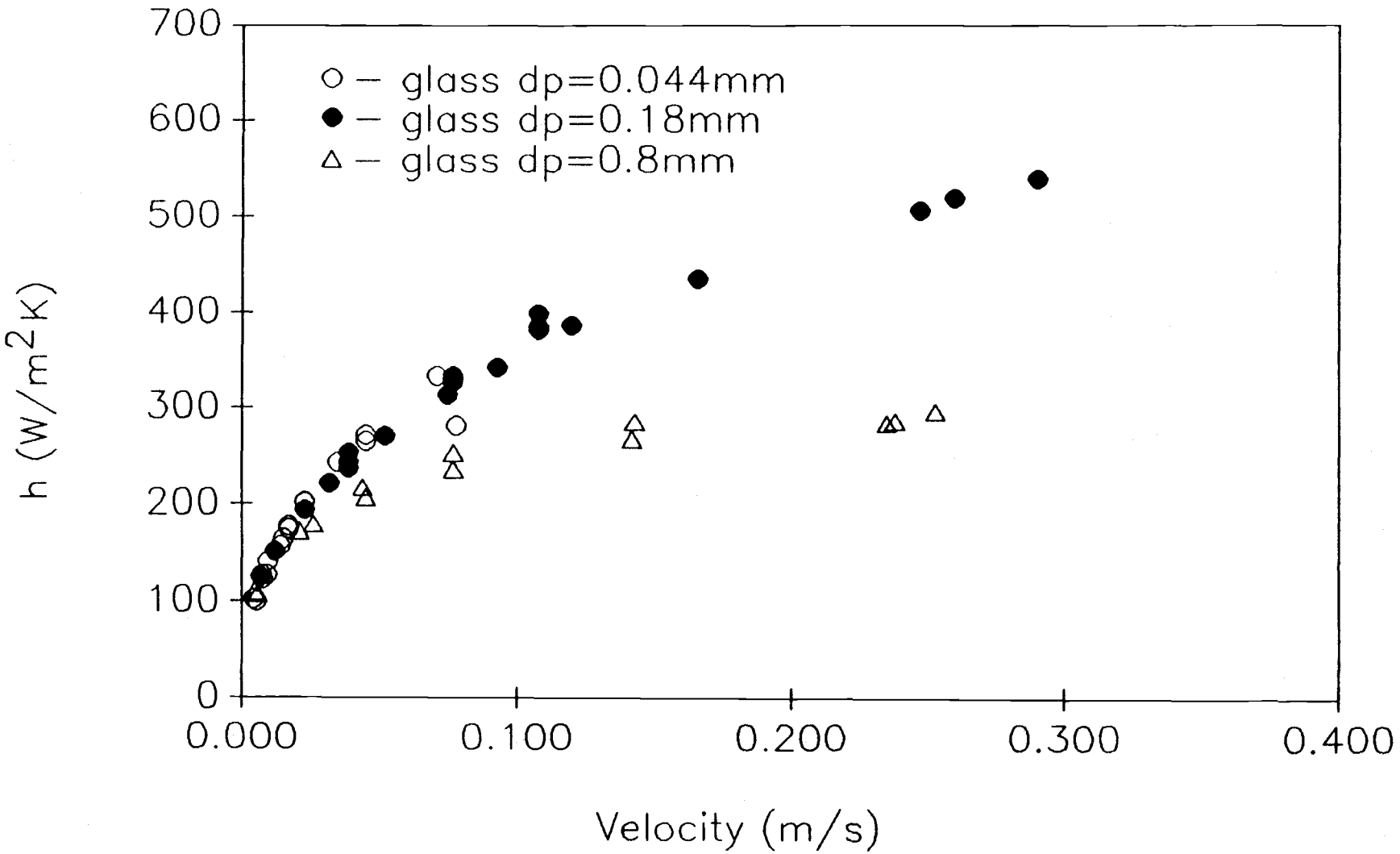

Figure (IV.A.1). Comparison between heat transfer coefficients as a function of the linear solids velocity for 0.18mm and 0.8mm diameter glass beads.

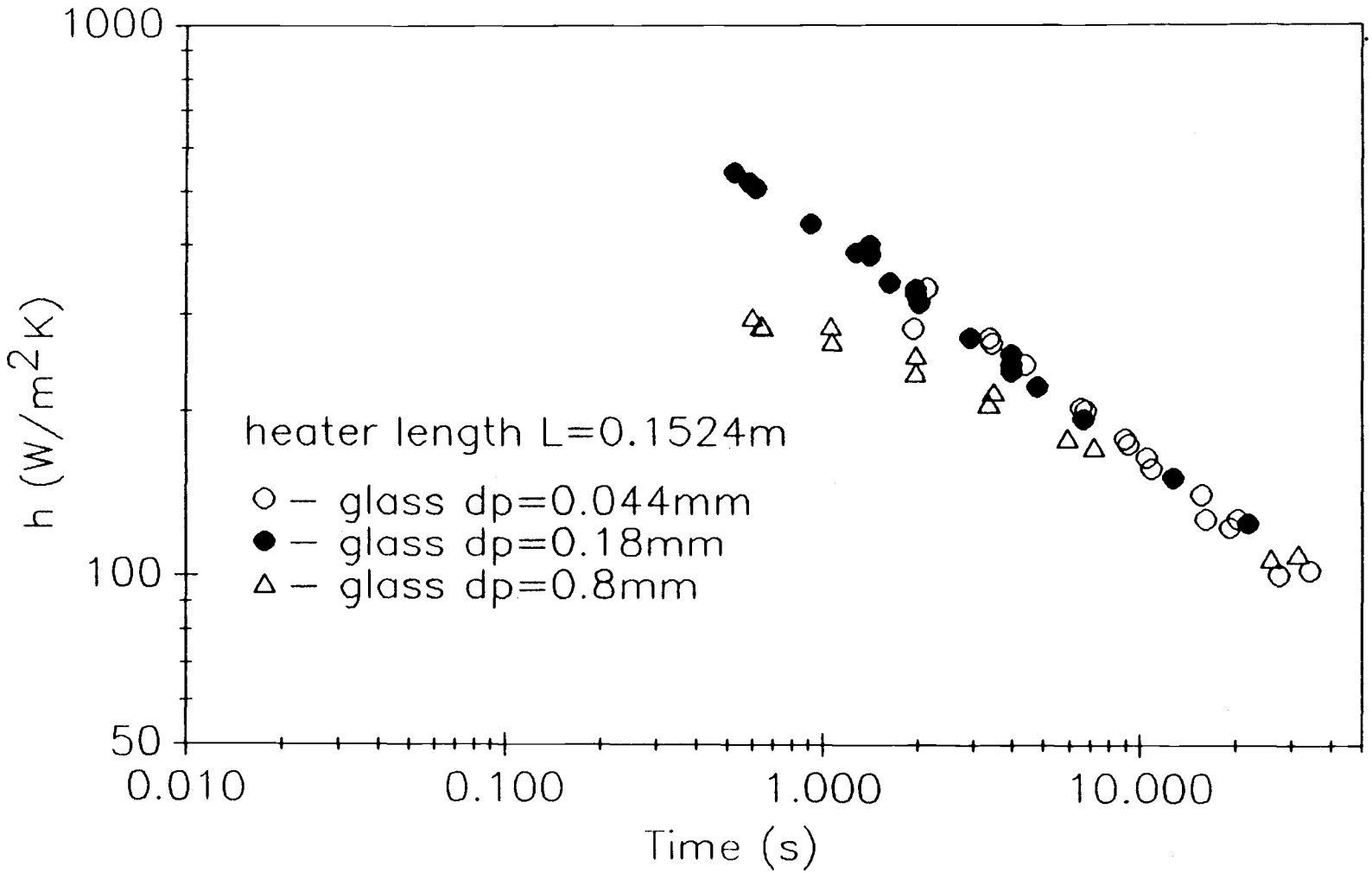

Figure (IV.A.2). Comparison between heat transfer coefficients as a function of contact time with the heated surface for 0.044mm, 0.18mm, and 0.8mm diameter glass beads.

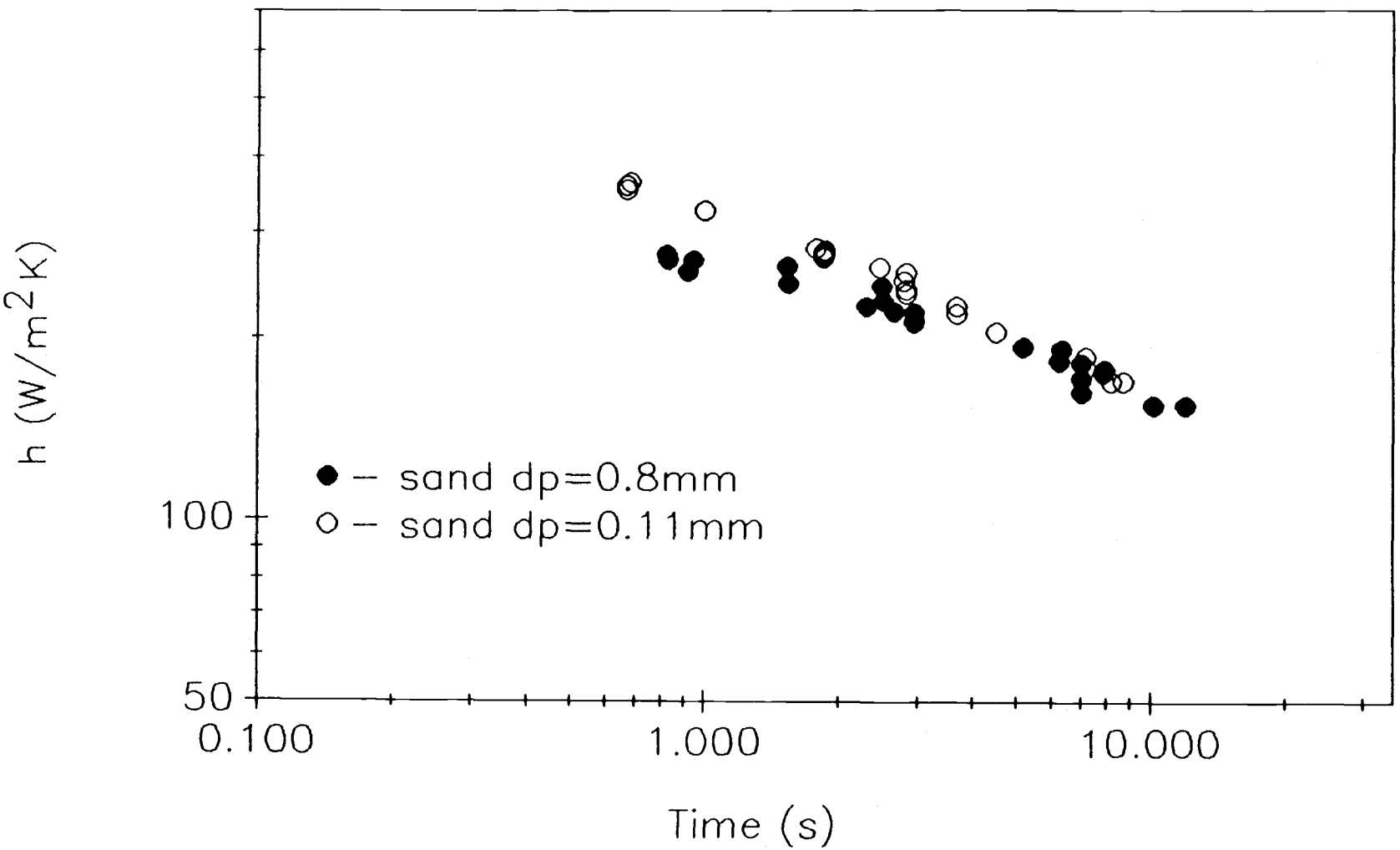

Figure (IV.A.3). Comparison between heat transfer coefficients as a function of the contact time with the heated surface for 0.11mm and 0.8mm diameter sand.

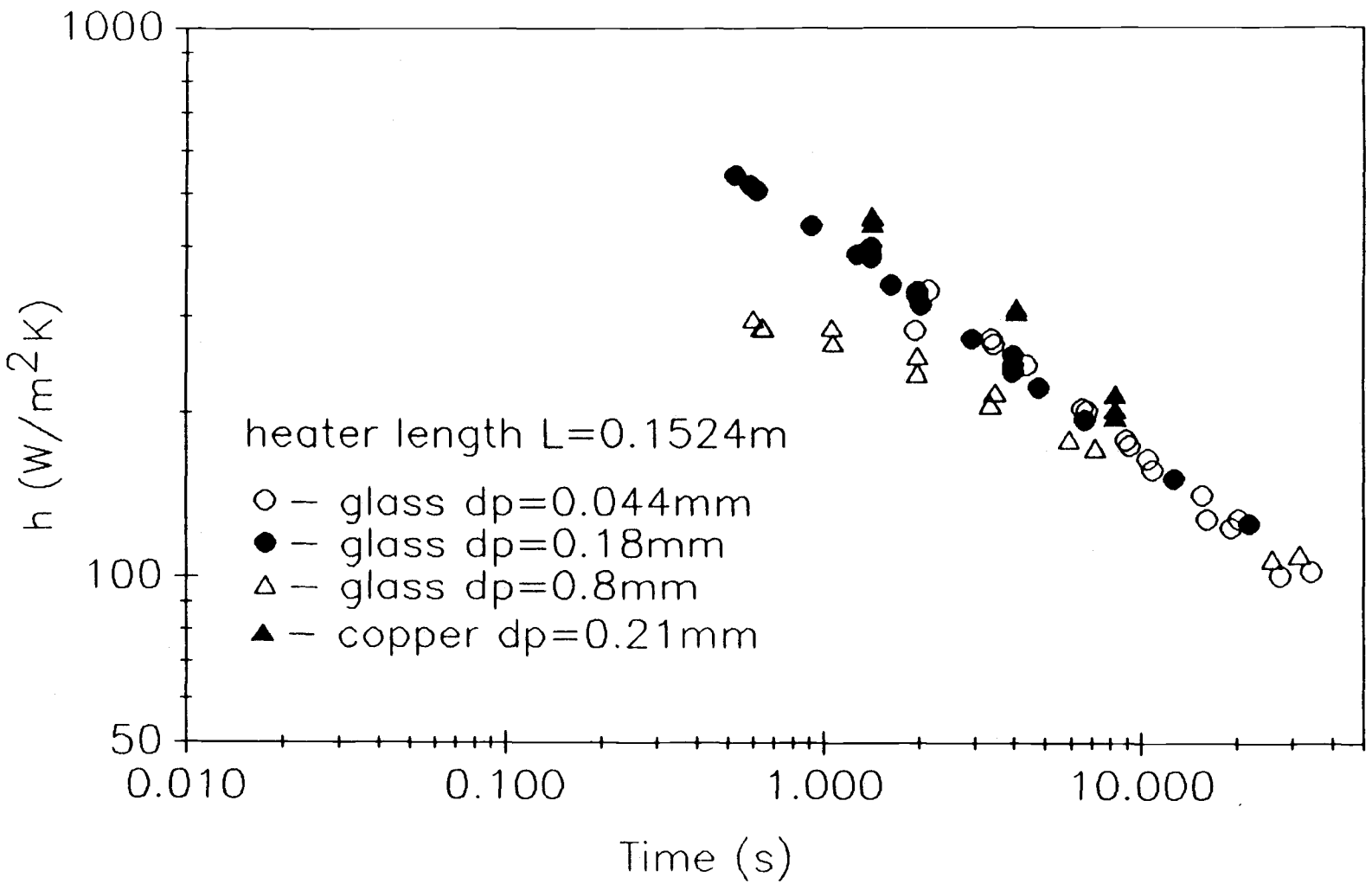

Figure (IV.A.4). Comparison between heat transfer coefficient as a function of contact time with the heated surface for 0.044mm, 0.18mm, 0.8mm glass beads and copper of 0.21mm in diameter.

appears to level off (Figure IV.A.2). Figure (IV.A.3) presents data for silica sand, and Figure (IV.A.4) presents heat transfer to glass beads and copper against time. Figure (IV.A.4) shows moderately higher values in the heat transfer coefficient were obtained for copper than for glass, although the conductivity of copper is 384 times higher than glass.

IV.B. Data Comparison with Other Researchers

Heat exchangers are observed to be more efficient when the fluid flows perpendicular to the heated surface. This phenomenon is often explained by the formation of a thinner laminar boundary layer which forms when the fluid flows normal to the heated surface. Following the same reasoning, a similar behavior for a gas-solid system should be expected.

When the data for sand of 0.8mm diameter flowing past horizontal and vertical heater configurations was plotted jointly in Figures (IV.B.1 and IV.B.2), the horizontal configuration seems to provide higher heat transfer results. Apart from material properties, "time" that solids spend in contact with the heated surface is the second most important parameter when predicting the heat transfer coefficient. Thus, Figures (IV.B.3 and IV.B.4) present the same data in the time

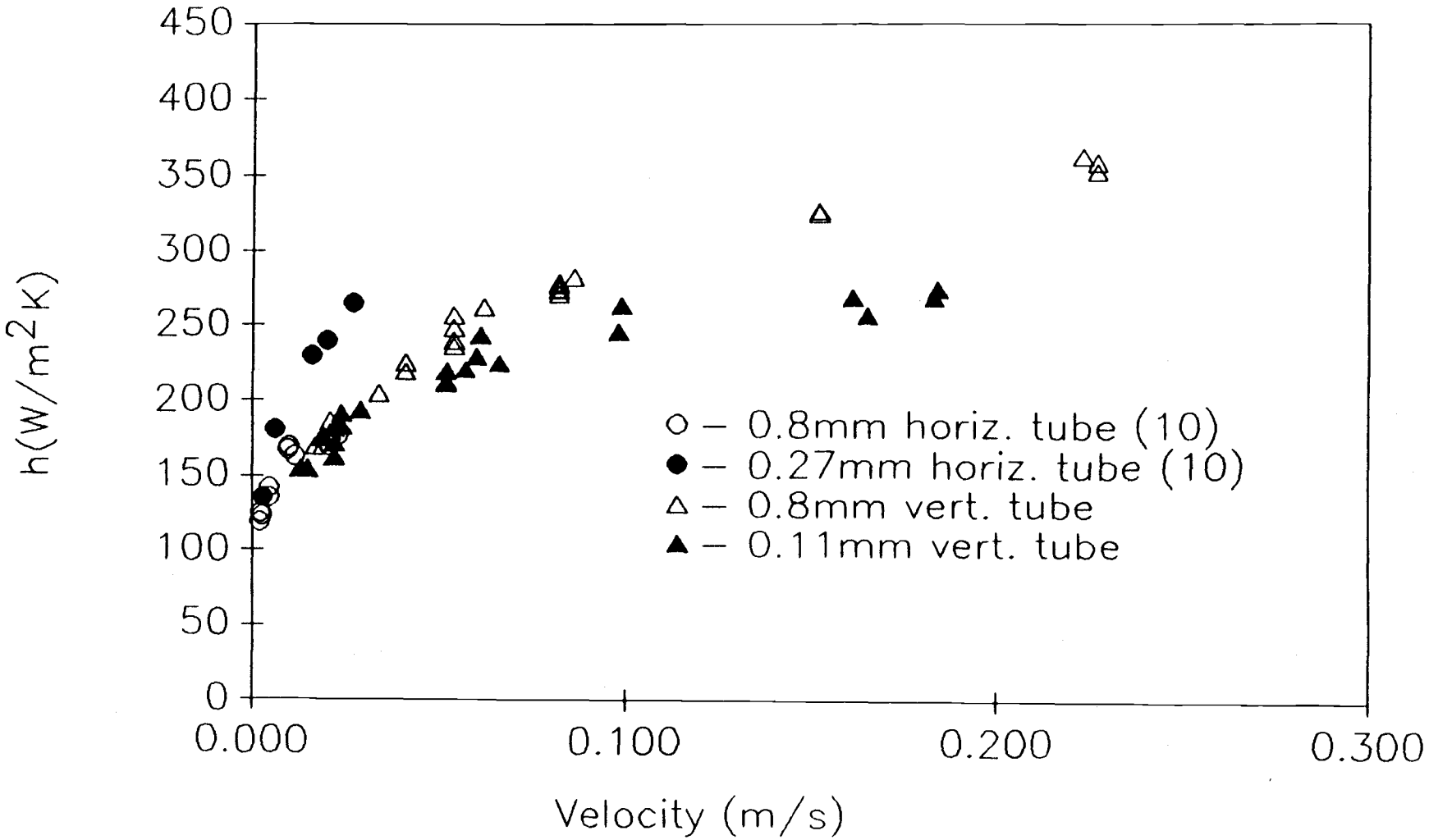

Figure (IV.B.1). Comparison between heat transfer coefficients as a function of the linear solids velocity for Colakyan's (10) data and the present study for 0.11mm, 0.27mm and 0.8mm diameter sand.

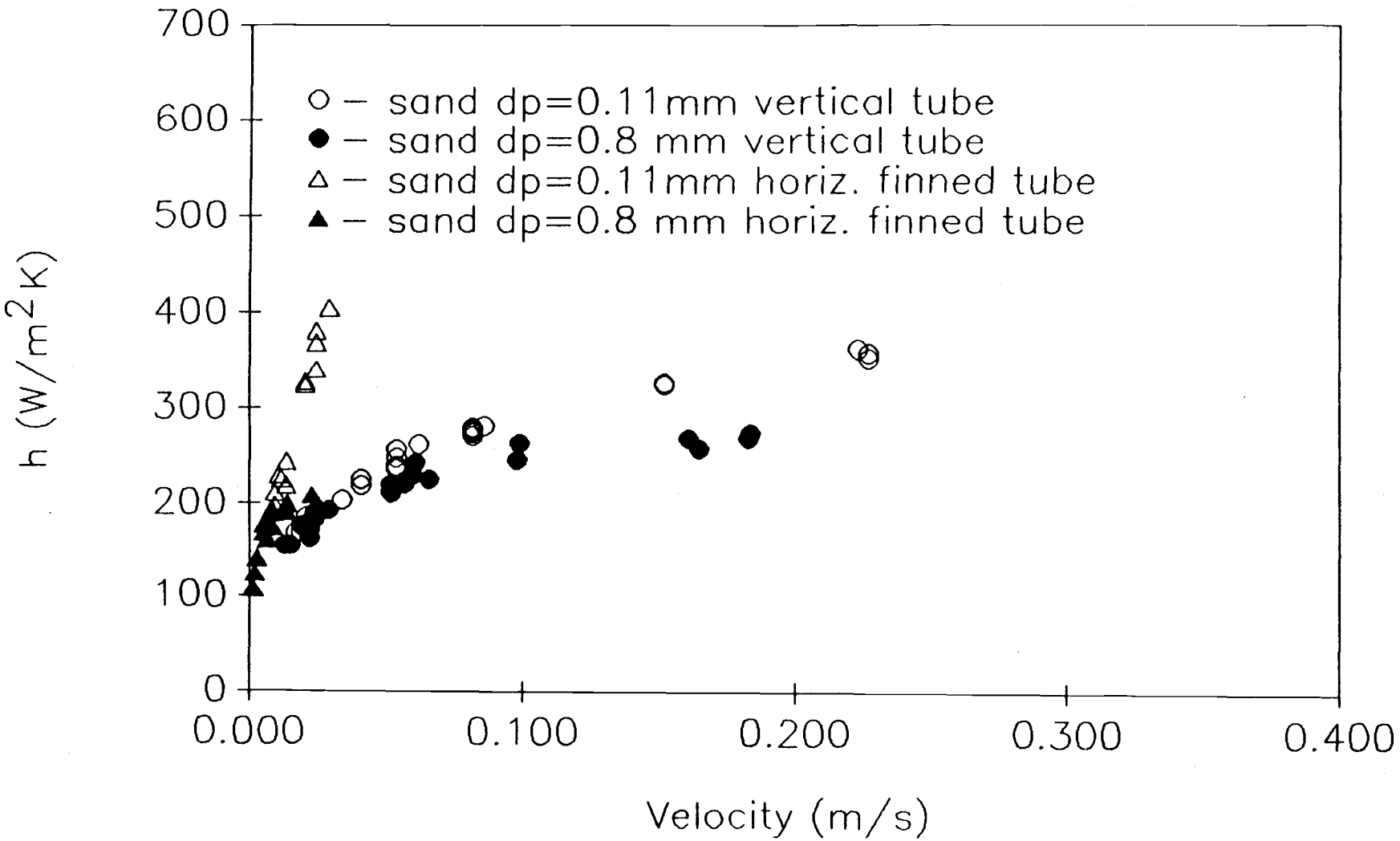

Figure (IV.B.2). Comparison between heat transfer coefficients as a function of the linear solids velocity for horizontal finned (11) and vertical tube for 0.11mm and 0.8mm diameter sand.

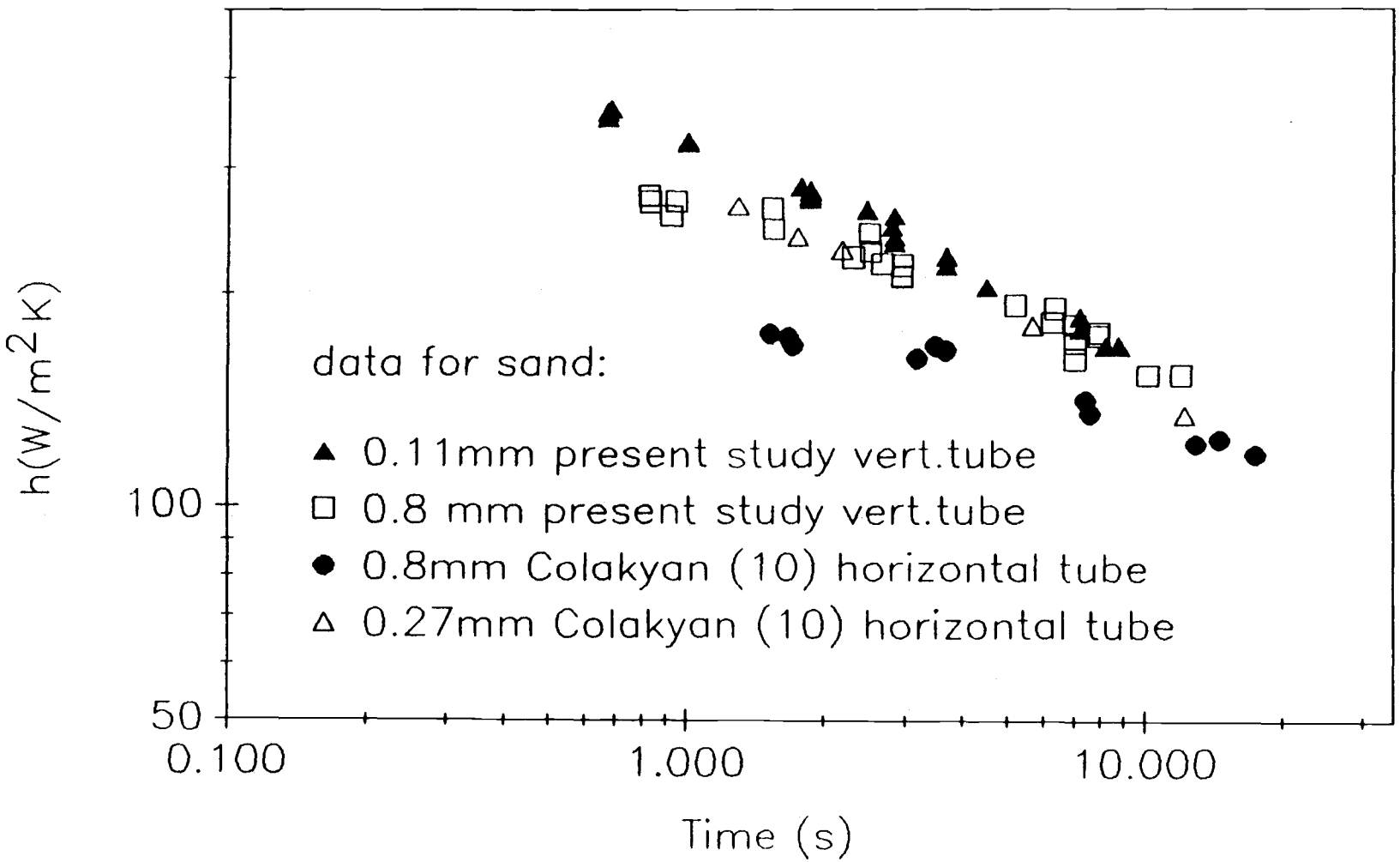

Figure (IV.B.3). Comparison between heat transfer coefficients as a function of contact time for Colakyan's (10) data and the present study for 0.11m, 0.27mm, and 0.8mm diameter sand.

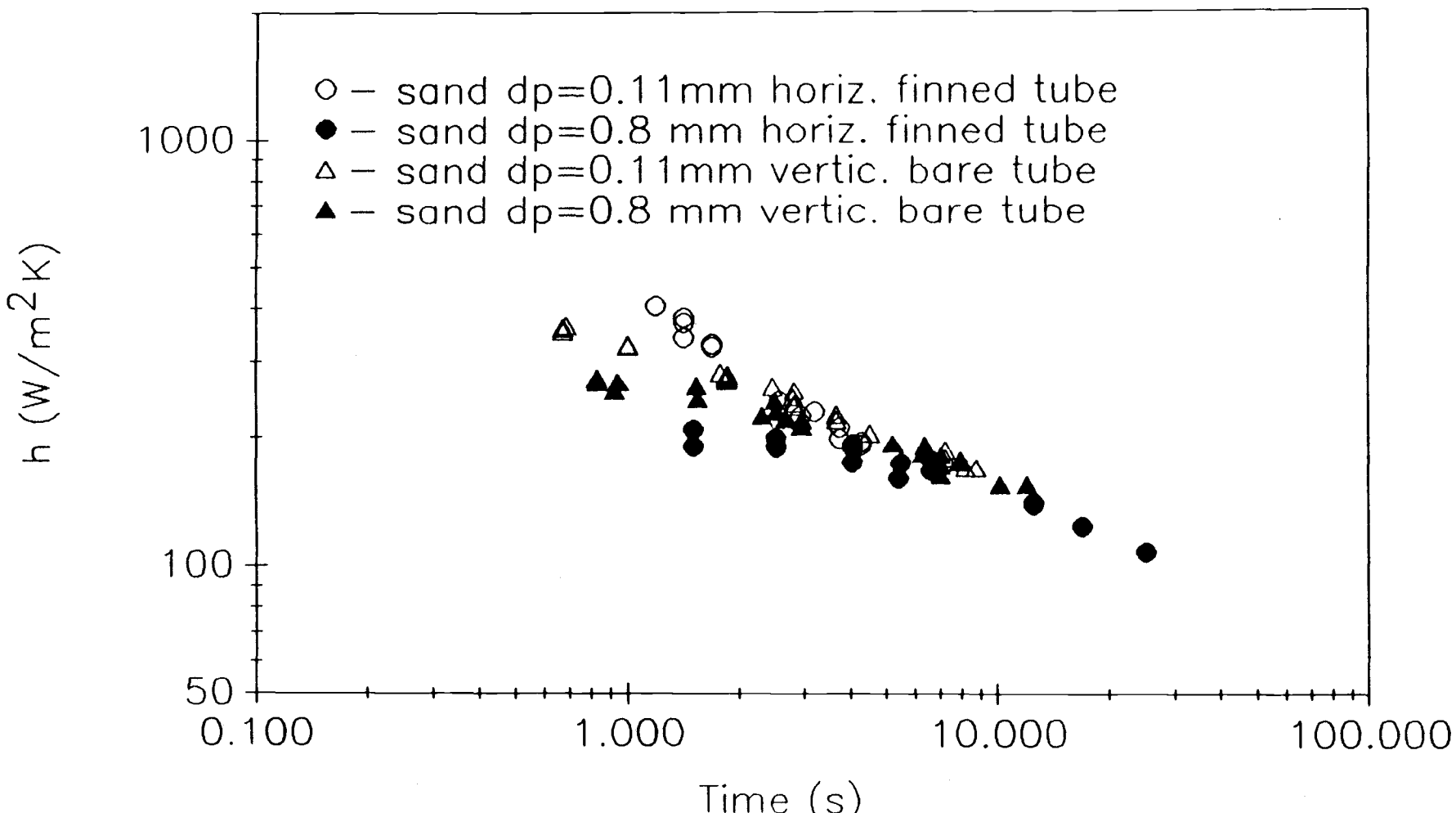

Figure (IV.B.4). Comparison between heat transfer coefficients as a function of contact time for the author's (11) data and the present study for 0.11mm and 0.8mm diameter sand.

domain. The result was "almost" unexpected; vertically oriented heaters showed higher heat transfer results when plotted against velocity. As opposed to horizontal heaters, vertical heaters without external obstructions have an equally distributed flow of solids at the surface without formation of gaps or stagnant zones. Flow patterns about horizontal tubes are characterized by higher particle-wall porosity and results in decreased heat transfer. A detailed explanation of solids flow is given in section V.D.1. Therefore, it is concluded that for vertical and horizontal heaters with equivalent characteristic length higher values of the heat transfer coefficient are expected for vertical configurations.

Experimental results from Ernst (9), Wunschmann (12), and this study are given in Figure (IV.B.5). As shown, they all follow the same line till they level off. The plateau where the maximum heat transfer occurs varies with different heater arrangements.

In Sullivan's (3) study of the heat transfer coefficient characteristic of granular media flowing past a thin vertical plate, moderately lower results were obtained than would be expected (Figure IV.B.6). Uncontrolled heat losses due to their experimental apparatus or even a minor obstruction in the particle flow may produce the results which they obtained.

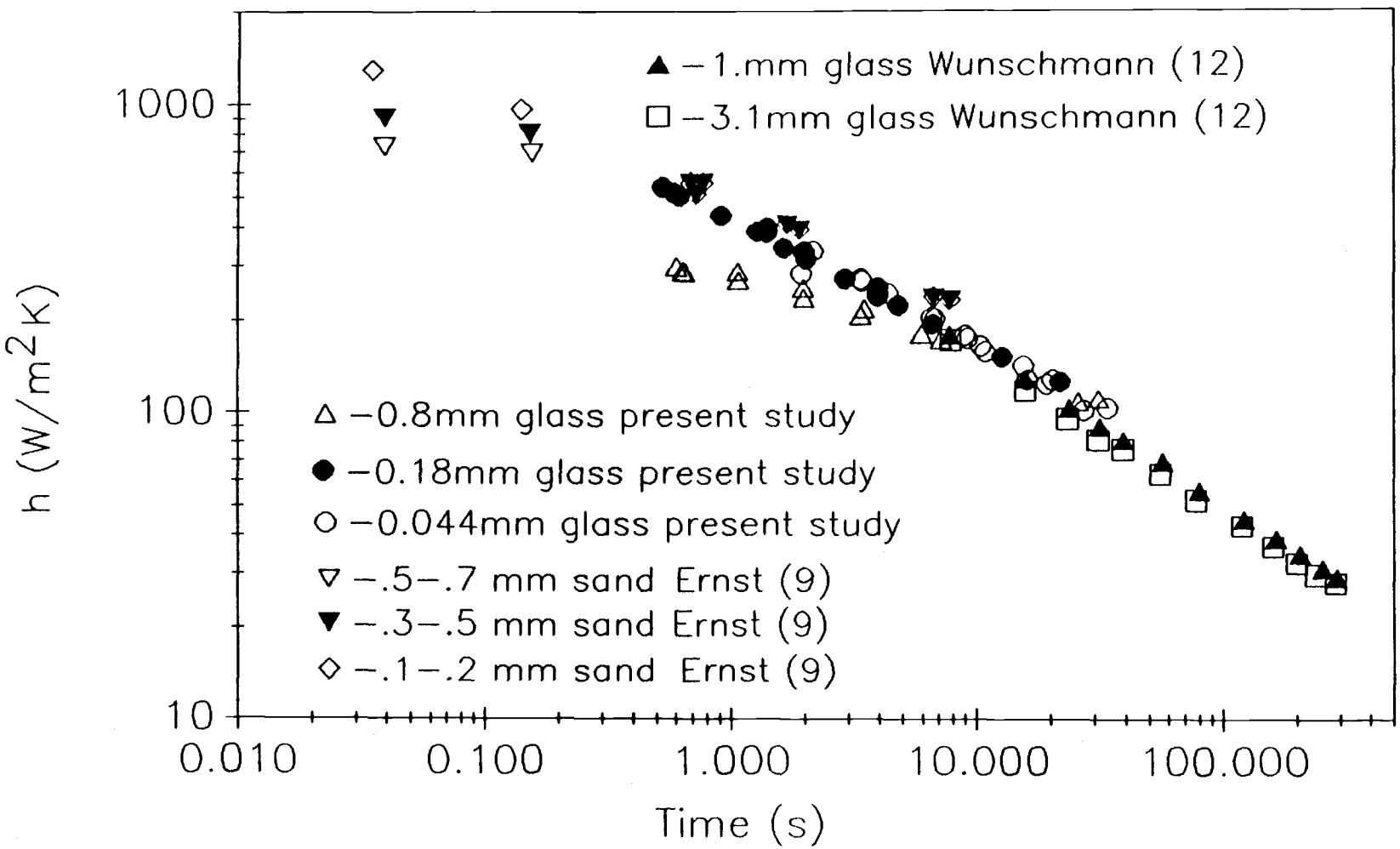

Figure (IV.B.5). Comparison between heat transfer coefficients as a function of contact time with the heated surface for Ernst's (9), Wunschmann's (12), and the present data.

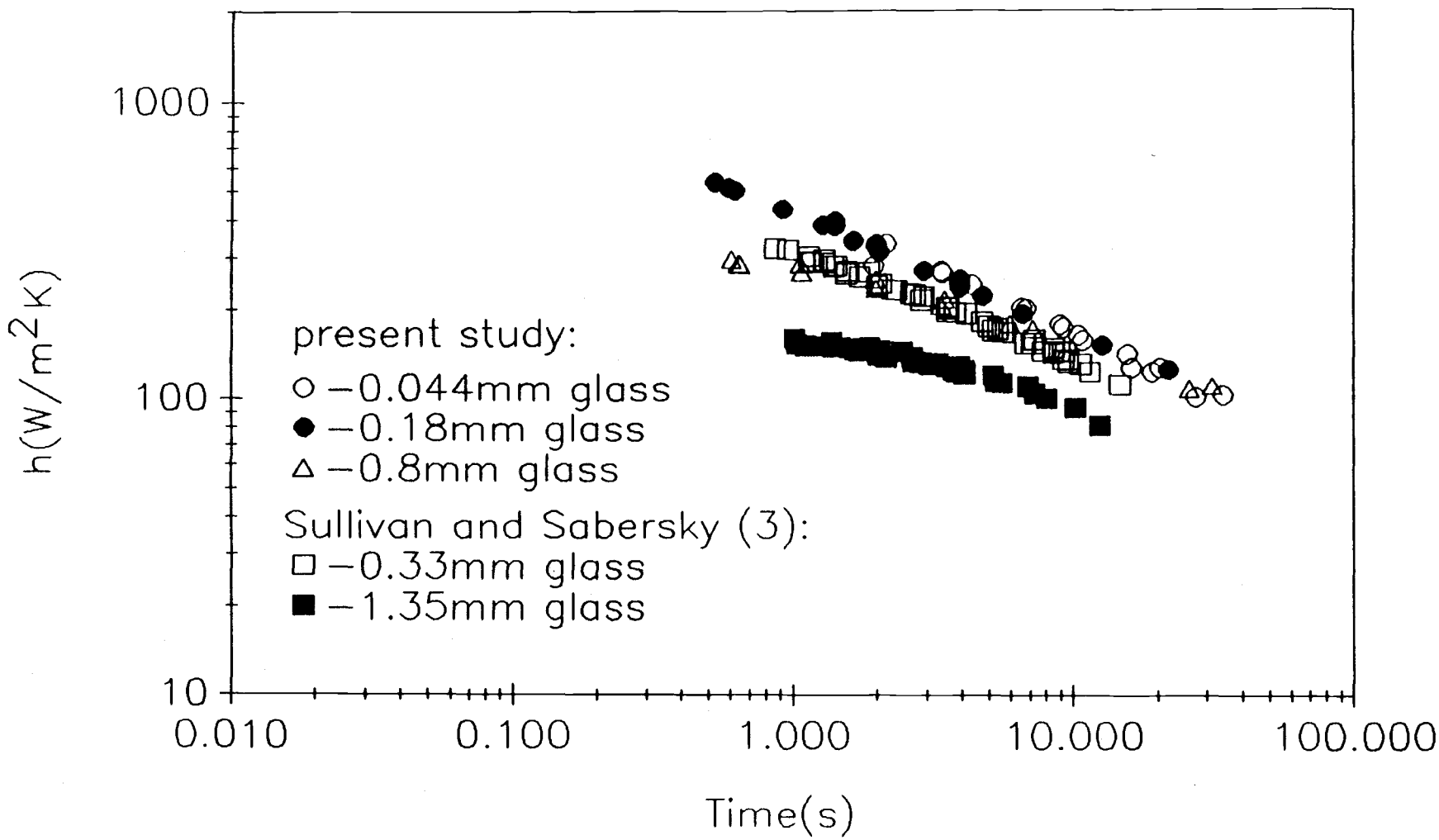

Figure (IV.B.6). Comparison between heat transfer coefficients as a function of contact time with the heated surface for Sullivan's (3) data and the present study.

V. MODEL ASSUMPTIONS

The significance of heat transfer coefficients from a design standpoint has already been emphasized. Therefore the ability to predict this quantity in terms of bed dimensions and properties is of invaluable importance. Two representative theories of particle bed heat transfer exist: (1) the bed may be assumed to comprise of homogeneous properties of solid and gas and modeled as a region with a single property or, (2) a more complex mechanism of separate gas-particle heat transfer interactions. The bed itself cannot be considered homogeneous since heat transfer response is different for solid and gas phases but for long bed heating times this has been shown to be a good approximation. The latter approach is most important as the velocity of the bed increases since heat propagates among too few particles from the heated surface for the bed to be considered homogeneous. Modeling heat transfer discretely between gas and particle is however complicated because of gas movement and particle separation, transitions from the heated surface, and particle contact with the wall are not fully understood.

In this chapter an attempt to explain the simplifying assumptions of the heat transfer mechanism to moving beds of solids will be provided.

V.A. The Role of the Gas Phase

In a moving packed bed of solids, heat is transferred from an immersed surface by particles directly touching the surface and by interstitial gas (air in this study) which is moving with the particles at the same velocity past the heated surface. Since the volumetric heat capacity of the air is quite low in comparison to that of solids it is assumed that heat removed by gas convection is negligible. Most of the heat is absorbed by the solid phase. In spite of this, the gas plays an important role as a heat transfer medium between the heated surface and the first row of particles as well as between the particles themselves. Without the gas, heat removal by only particulate solids would be very poor regardless of the solid properties as demonstrated in some experiments for vacuum conditions (2,12). Figure (V.A.1) shows experimental data reproduced from Wunschmann and Schlünder (12). Some researchers have found that the heat transfer coefficient between the heated surface and granular material increases with an increase of the thermal conductivity and/or thermal capacity of the gas (Harakas & Beatty (2)). The physical property of the interstitial gas has a great influence on the heat transfer coefficient.

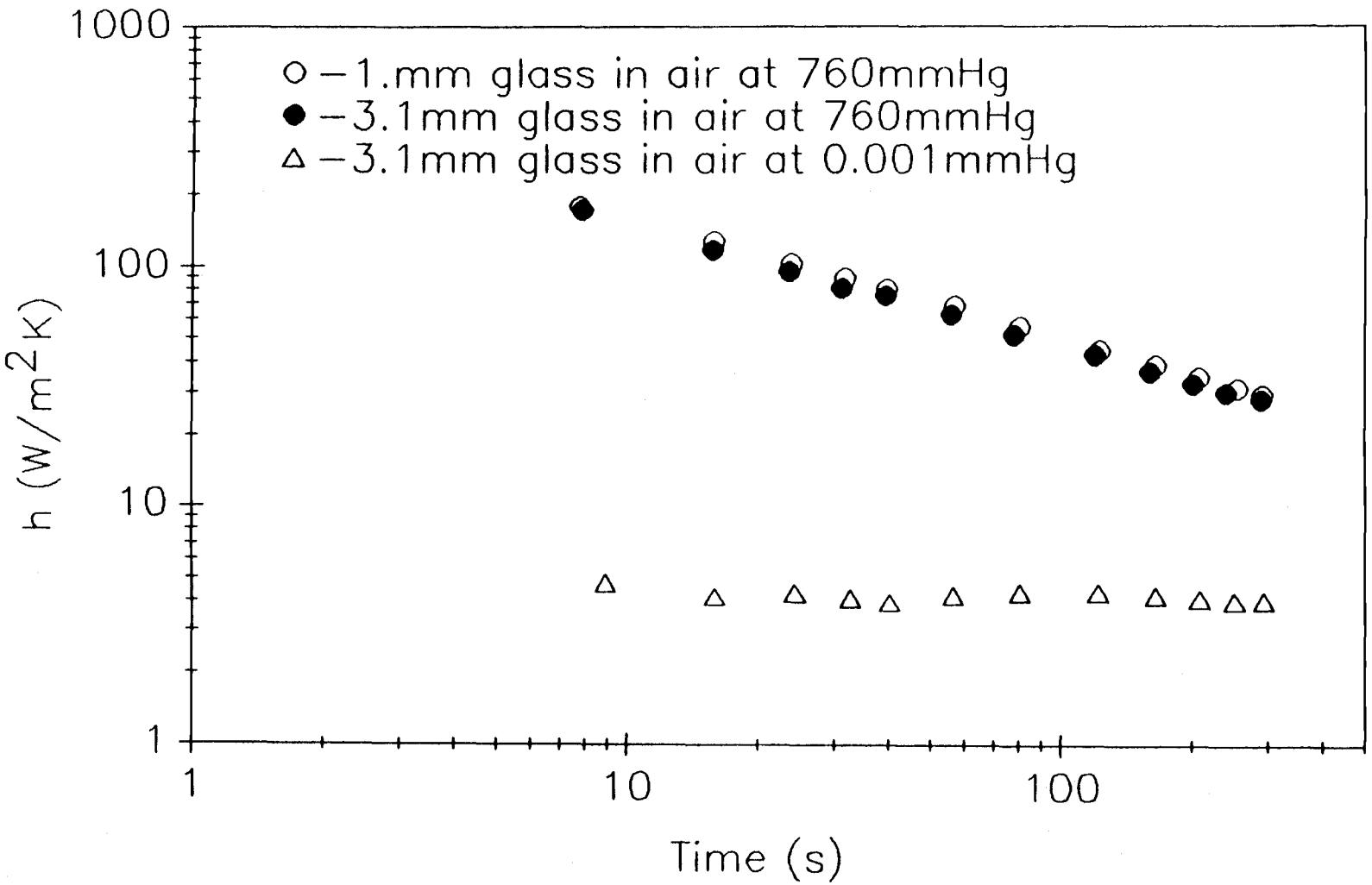

Figure (V.A.1). Comparison between heat transfer coefficients as a function of contact time with the heated surface for glass in air and vacuum conditions (reproduced from Wunschmann (12)).

V.B. Contact Resistance

This important factor must be considered when trying to understand heat transfer between two immobile touching solids. Baskakov (4) was first to introduce the concept of contact resistance to account for the discrepancies between experimental data and the Mickley and Fairbanks model (1). Baskakov's (4) explanation was instrumental in explaining the observed dependence of the heat transfer coefficient on particle size (as d_p increases h decreases). The problem of determining a resistance term for correction with the Mickley and Fairbanks model (1) has been handled in many ways either by defining an appropriate effective thermal conductivity or by introducing an arbitrary set zone of increased voidage close to the surface. Many researchers questioned the physical existance of the gas gap at the contact point although it appeared almost impossible to explain or fit the experimental data without it. Others such as Schlünder (13) or Decker and Glicksman (14) abandoned the use of a gas film separating the surface from the first row of particles. Schlünder (13) suggests that a known formula from the kinetic theory of gases for estimation of reduced gas conductivity should be used to define the gas conductivity in the region where the mean free path of

the gas molecules is larger than the distance between the particle and the wall, namely

$$k_{gs} = \frac{k_g}{1 - 2\frac{\lambda}{\sigma} \cdot \frac{(2 - \gamma)}{\gamma}} \qquad \text{(V.B.1)}$$

where

k_{gs} = reduced thermal conductivity of gas (W/mK).

k_g = thermal conductivity of the gas as a continuum (W/mK).

λ = mean free path of gas molecules (m).

σ = thickness of the gas layer (m).

γ = accommodation coefficient.

The phenomena of the reduced thermal conductivity implies heat transfer is decreased as particle size decreases since the percent of area within one mean free path of the contact wall increases.

The contact resistance can be treated more realistically by considering the microscopic structure of the surface especially at contact of the particle and heater. When viewing the solid surface with even an optical microscope only structures above 0.1μm are visible. Thus a highly rugged structure can exist at the optically smooth surface. The physical properties at the surface interface such as surface energy,

tension, and conductivity arise as a result not only from the bulk atomic structure but also from somewhat different atomic arrangement at the surface. Some properties, such as surface energy which is inversely proportional to the particle size, are instrumental in explaining the phenomena of adhesion and/or agglomeration that is most likely to occur in a bed of fine particulate solids. Due to existing surface forces, the impurity-free surface of a freshly formed solid will be covered by layers of gas molecules in less than a second. Physically adsorbed gas can be removed from the surface either by heating the solid to its melting point or by degassing the surface under high vacuum. Brenner (15) observed that oxygen adsorbtion on iridium surfaces reduces surface free energy. Therefore much larger friction coefficients were measured for flow by surfaces under vacuum than in the presence of air. In the case of nonmetals (e.g. diamond or NaCl) the friction coefficient increases six times when measured under vacuum. All these facts provide support for the long disputed existence of an adsorbed gas layer which is obviously carried along with each particle as its own atmosphere. However the thickness and changes that occur according to experimental conditions are uncertain. Thus for the gas in gas-solid systems the difference should be made between the strongly adsorbed

gas (air) which cannot leave the particle surface freely and acts more like part of the solid, and the bulk gas (air) that moves freely between the particles. When the particle is in contact with another solid surface it is beyond imagination that adsorbed gas can be removed only by particle weight. It is more probable to expect the generation of a "binding force" between the particles and the wall as well as between particles themselves. Also, it has been evident that surface phenomena can be related to the forces between atoms and molecules. In general, interatomic forces are short range but sometimes they can act across or between interfaces (London forces). As particle size decreases the importance of forces like inertia or gravity flow decrease, until the atomic forces become dominant. Adhesion that usually occurs in a bed of fine solids is only one of the examples where the sum of the binding forces between the particles is higher than environmental forces. Apart from the adsorbed gas most solids will pick up moisture from the surrounding air, as observed for glass beads of 0.044mm and iron powders. The adsorption layer is not freely moveable but particles can come closer to each other much easier than when they are clean. Attraction forces between the particles are usually caused by Van der Waals, electrostatic, or magnetic forces. These forces are

considerable when particles are close together and they decrease rapidly with distance. Since the adsorbed layer is thicker around smaller particles and at the same time the roughness peaks are lower than for large particles, the ability of such particles to approach each other closer and with larger surface area is increased.

Therefore it is believed that reduction in particle size can bring some improvement in the heat transfer coefficient since the greater interparticle forces will not allow separation at increased solids velocities as in the case of large particles. On the other hand, when particles become too small and interparticle forces are dominant, most of the gas (air) will be adsorbed at the solid surface while the amount of freely moving gas (air) will decrease leading to a consequent decrease in heat transfer. At this point, the gas conductivity changes since there are very few gas molecules in free motion. Therefore, lower values for the heat transfer coefficient than for air alone are possible.

V.C. Particle Shape

Beds of particles of irregular shape or size should increase heat transfer since surface area in contact with the wall or adjacent particles is minimized for uniform sized spheres. Although particle packings of

extremely irregular shape and size may require individual measurements of heat transfer coefficient, something could be said about what one would expect for a heat transfer coefficient to a packed bed of irregularly shaped particles if each particle closely approximates a sphere. In fact, for randomly packed beds of irregular particles porosity varies proportionally with sphericity (16). Since effective properties of the heat transfer medium are a strong function of porosity, increased porosity at the wall is responsible for lower heat transfer coefficients.

Provided porosity distribution from the heated wall to the bed is understood a computer calculation to simulate heat transfer to the most irregular bed would then appear possible. However, in this research similar or even lower heat transfer coefficients were measured under flow conditions which implies packing at the wall may become poorer with decreased sphericity.

V.D. Flow and Porosity Distribution

The degree of separation between particles either between themselves or the heated wall and their motion relative to the wall may change with bed velocity and particle shape. An increased porosity at the wall can be reasoned to lower the effective conductivity of the flowing medium and in fact a reduced heat transfer

coefficient is normally observed. Also, the amount of heat removed from the wall depends on the nearby particle velocity and exchange of particles in layers streaming adjacent to the wall. Bed velocity may also affect suspension of flowing particles. Therefore, heat transfer prediction is largely influenced by interrelated dynamic properties of the bed and static particle separation within.

V.D.I. Flow Properties

Hiroshi Takahasi and Hiroshi Yanai (17) studied a flow profile and void fraction of granular solids in a moving bed. They observed that in some cases spherical particles flowing down the tube form two regions. In the shear region, which extends 4-8 particle diameters from the wall, particles were observed to flow slower that in the main body of the core or plug flow region. When the ratio of bed height to column diameter approached about 2 to 3 the velocity profile became fully developed. This pattern of velocity variation across the test section was not observed for shallow beds of spherical particles neither for irregularly shaped coal, although the latter was not discussed in their paper. In their experiments the void fraction of the particles was found to be influenced by velocity, and to reach an asymptotic value for higher flow rates.

Also, Sullivan (3) observed that the solids adjacent to the wall slide along with approximately the same speed as the bulk flow. He therefore concluded that no boundary layer exists near smooth walls.

For flow studies perpendicular to a heated tube, Sullivan (3) noticed the formation of a cavity immediately downstream of the cylinder. This gap appeared even for very low solid velocities but its size increased with flow rate. In the same study a triangularly shaped stagnant region of solids at the upstream face of the cylinder was observed but its shape and size was velocity independent.

Unlike a fluidized bed, particles in a packed bed are not suspended and free to wander about but are pinned between their neighbors. Only if a particle is balanced near a void large enough to accommodate it will it move to drop in. Particle propagation may then only extend about one particle diameter at a time. The frequency of particle interchange as well as rolling over the heated length would be an important measure of the degree of increased heat transfer expected.

Using the high speed camera described earlier, motion of 0.8mm diameter glass beads at the heated surface were investigated in detail. The fraction of particles observed to interchange position from all particles viewed in the area of one frame over the

duration between interchanges was noted for each film. About one interchange per 160 particles flowing past the frame was likely to occur at low velocities. At high velocities, an alternating pattern of particle streaming occurred as particles settled into voids left by supporting particles. Few particles were observed to rotate at the wall, while all others were slipping without rotation. For two films, the focus and lighting was set to image particles within the bed more than 1mm away from the wall. In each of these films the particles flowed in a linear pattern and no particle interchange was ever observed. This indicates that the majority of interparticle motion appears to occur at the wall where it may make the most significant change in heat transfer. Despite this, few particles would interchange position at the wall so it is reasonable to assume interparticle motion has a negligible effect on increasing heat transfer.

An investigation into the porosity change at the rod wall with flow velocity was performed using the high speed camera and glass beads. Analysis of the films revealed a small change in porosity occurred up to a velocity of 0.5m/s, the maximum velocity investigated. The porosity change at the wall could not be modeled due to insufficient amount of data. Since the lens' focal length allowed particles within one millimeter of the

wall to appear in focus it was difficult to distinguish a particle separation from the wall. Therefore, it was not possible to conclude if a gap separates a particle from the wall or how this gap changes with velocity. Instead, particle separation between each neighbor was measured. The particle orientation as observed did not depart from an orthorhombic array at velocities of 0 to 0.5m/s; another indication porosity did not change greatly. If a bulk porosity change did occur, the solids velocity measured by weight of the discharge solids would be suspect. However, particle velocity at the rod surface was comparable within experimental error to the bulk solids velocity computed by assuming porosity remains as that of the static randomly packed bed.

V.D.2. Static Properties

The bed porosity for perfect spheres can be taken as 0.4 throughout the entire bed except for the first row of particles touching the wall where voidage is greater than that in the bulk of the bed and can be calculated using the relation

$$\left(\frac{1 - \epsilon_r}{1 - \epsilon_0}\right) = \left(\frac{x}{0.7d_p}\right)^{0.378} \qquad \text{(V.D.2.1)}$$

given by Kimura and Kaneda (18) where

ϵ_r = void fraction at the distance smaller than $0.7d_p$.

ϵ_0 = void fraction at the distance larger than $0.7d_p$.

x = distance from the wall (m).

d_p = particle diameter (m).

If particles form closely a regular array or pattern between themselves an equation for porosity distribution within a packed bed to one particle diameter from a plane wall may be obtained. Random packing of spherical particles normally form an orientation closely approximated by cubic or orthorhombic arrays, the orthorhombic array being most prevalent. When the particle array is divided into its smallest decomposable unit of a single particle and the void surrounding it (Fig. V.D.2.1), this region appears as a sphere inscribed in a 4 or 6 sided prism (rhombohedron). Viewed from the contact point of a side tangent to the sphere, the region is azimuthally symmetric. The apparent particle area heated from the surface of one side may then be represented two dimensionally by a

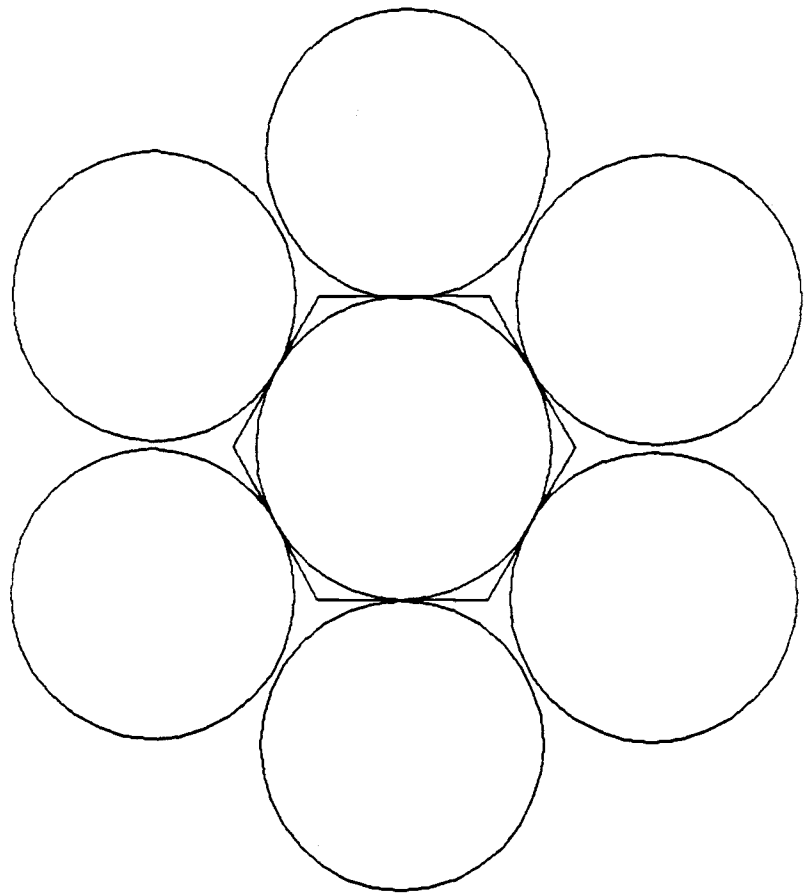

Figure (V.D.2.1). Particles in orthorhombic array.

plane intersecting the region a distance s from the side (Fig. V.D.2.2). This allows an equivalent representation of the temperature gradient between two and three dimensional models of the particle-in-a-prism region. The ratio of void to particle surface area in the intersecting plane at distance s is

$$\epsilon(s) = 1 - \frac{\pi(2(s/r)-(s/r)^2)}{n \tan(\pi/n)} \qquad \text{(V.D.2.2)}$$

where

n = number of sides of polygon represented by intersection the of plane to region.

r = radius of particle.

The porosity of the region based on volume is

$$\epsilon = 1 - \frac{2\pi}{3n \tan(\pi/n)}$$

and, for example, ϵ=.395 for n=6.

Assuming heat transfer through particle contact points is negligible, then, heat transfer may be modeled two dimensionally over the particle-in-a-prism region where the heated surface is located at s=0.

Measurements by researchers such as Benenati et. al. (19) have shown the porosity distribution from the wall into a packed bed of spheres appears as a damped

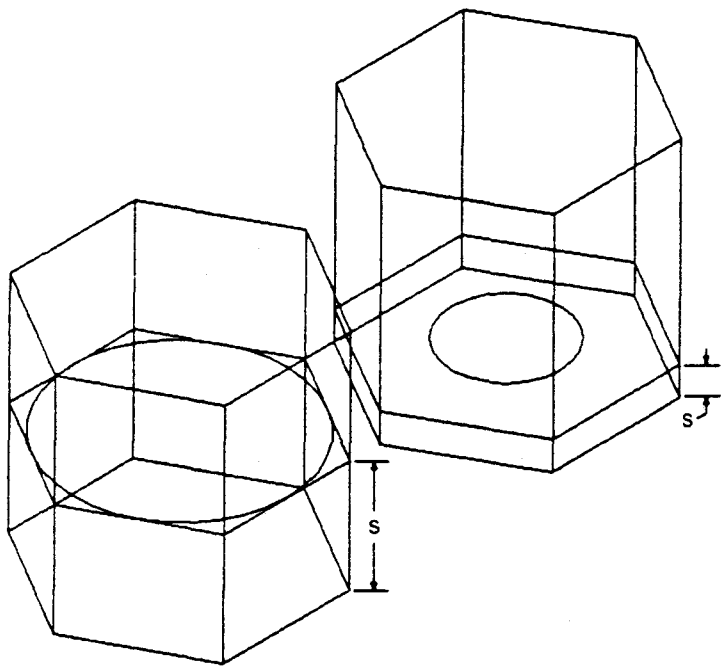

Figure (V.D.2.2). Scheme for porosity calculation by penetration s into orthorhombic array of spheres.

sinusoid asymptotic to a porosity of 0.4. When integrated over distance traversed from the wall, Eq. V.D.2.2 closely approximates their findings. For tube to particle diameter ratios (D/d_p) less than 6, particle size has a significant influence on the bed porosity distribution function and Eq. V.D.2.2 would no longer hold. When this ratio is larger than 6 the porosity distribution function drops from unity to 0.4 within 0.7 particle diameters from the wall (19). The results for voidage at the wall were independent whether the wall was concave or convex.

V.E. Summary

It is obvious that extensive knowledge of all the above mentioned variables and flow behavior of two phase systems is necessary to understand the phenomena of heat transfer between heated surfaces and flowing granular media. The following general assumptions may be made regarding heat transfer to flowing packed beds of solids:

1. Thermal properties of the interstitial gas largely determine heat transfer throughout the bed.

2. The assumption of a contact resistance term between heated wall and particle is necessary

to model experimental data. A definite physical explanation of the resistance is complicated. The complication arises in modeling the gas adsorbed at the solid surface alone or an additional gas gap separating the solid from the wall.

3. Bulk porosity distribution appears independent of bed velocities common to most research with flowing packed beds. The particle rotation and propagation at the wall is too rare an event to significantly enhance heat transfer. However the velocity dependence of a gas film which separates particles from a vertically heated surface is unknown.

4. Porosity of a static bed as a function of distance from the wall varies as defined by Eq. V.D.2.2 for beds of regular spheres provided the ratio of tube to particle diameter is greater than 6.

VI. HEAT TRANSFER COEFFICIENT MODELS

This section reviews the effectiveness of several analytic and numerical models of increasing complexity upon prediction of the heat transfer coefficient given the assumptions of the last section. A unique empirical model is also presented which assumes the departure from the Mickley and Fairbanks (1) model at low residence times is most dependant upon a characteristic change of flow properties.

VI.A. Analytic Models

To date, any experimental apparatus used to record heat transfer to a flowing bed of particles measures steady state temperatures on the heated surface and within the bed once flow of solids has been adjusted to a constant velocity. The heat transfer coefficient is then calculated by the temperature difference from the bed the heated surface finally assumes. To represent heat transfer to a flowing bed of solids mathematically, a moving coordinate system is typically used whereby the point of reference travels with the particle. This representation models the process as an unsteady state heat conduction problem where the bed is assumed to possess some initial temperature and heat is applied from the surface for a time assumed equivalent to that

required by the particle to traverse the length of the heated section in the experimental system. The heat transfer coefficient is then calculated for the amount of heat added to the bed and the temperature of the wall relative to that of the bed initial temperature.

In any experimental system, heat transfer to the bed begins when the gas-solid mixture flows past the heated boundary and continues for the length of the heater. What is measured therefore is a heat transfer coefficient averaged over that length. For comparison, the coefficient predicted by the moving coordinate system corresponds to a single time or point along the heated length and therefore this instantaneous value must be averaged over the time of flow past this length.

The problem of any simple analytic treatment of heat transfer to flowing beds which does not account for contact resistance, such as the Mickley and Fairbanks (1) equation, is that as the simulation time decreases to zero the heat transfer coefficient modeled approaches infinity when actually a maximum value is observed. Nevertheless, the equation is a reasonable model to be used at large residence times. A comparable model applied to rod geometry as opposed to slab geometry was derived and appears in Appendix A. Models applied to both geometries are comparable at low residence times, however the rod model heat transfer coefficient flattens

out for higher time and decreasing radii. Figure (VI.A.1) shows only a small deviation from either geometry model is observed for 0.8mm and 0.18mm glass particles about 30sec. A greater magnitude of heat transfer appears by both analytic models when compared to experimental data due to the effective conductivity calculated by Eq. A.2

The simplest way of accounting for contact resistance analytically is to separate the treatment into a gas gap region and a solid region in order to model unsteady state conduction to a particle adjacent to the wall. A second analytic model was then developed based on a derivation for a composite semi-infinite slab and appears in Appendix B. Unfortunately, because particle size and curvature is not accounted in the method it would not be expected to fit data for different particle sizes.

Once the composite slab model was modified to treat a hemispherical interface at the wall, the model became appropriate to predict the value of the heat transfer coefficient which occurs during heating of the gap. The derivation, which appears in Appendix C, is useful until the heat transfer coefficient becomes equivalent to that of the Mickley and Fairbanks (1) equation based on effective properties. This is an inherent limitation since only half a particle from the wall could be

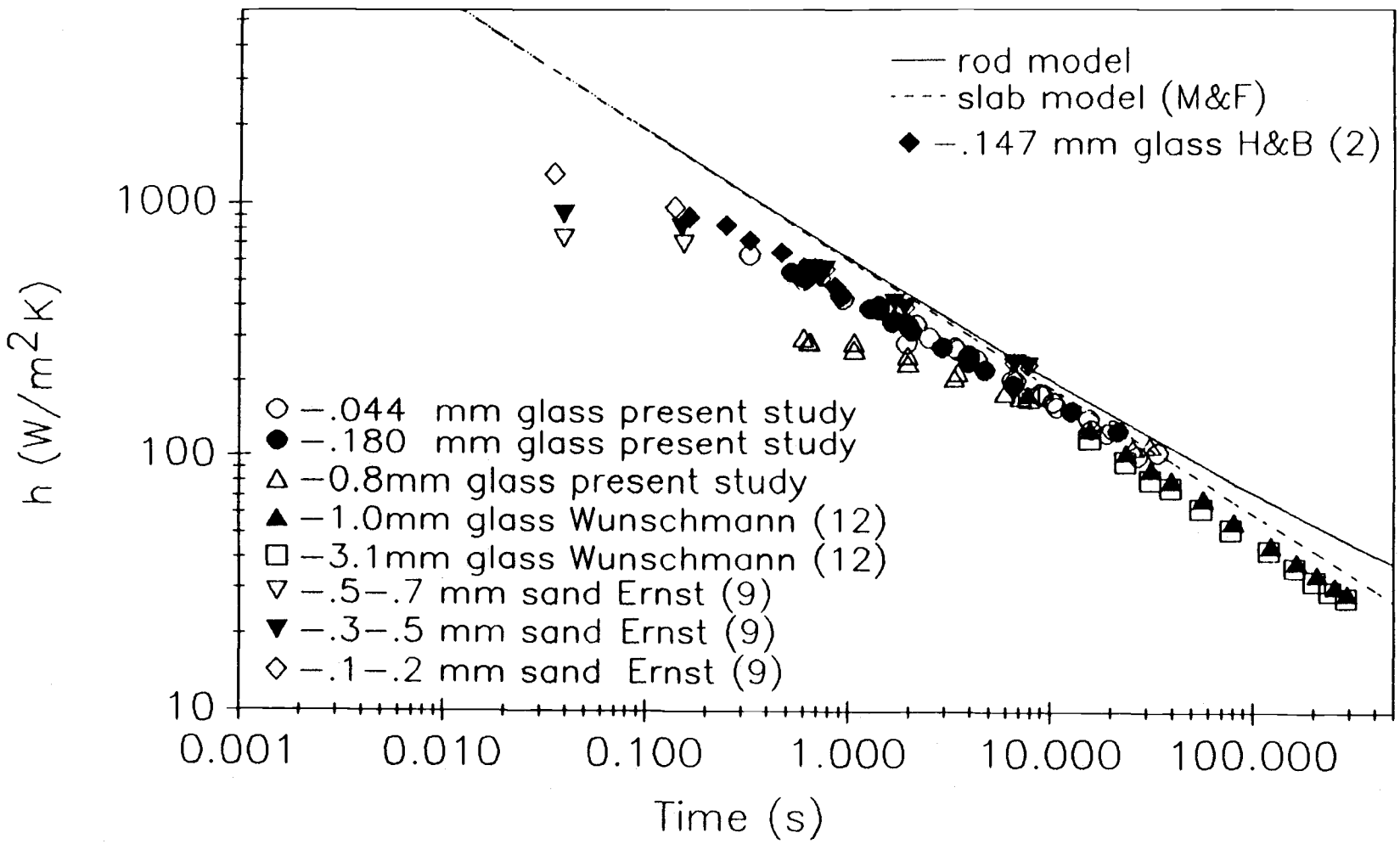

Figure (VI.A.1). Comparison between heat transfer coefficients as a function of contact time with the heated surface for rod and slab analytic models and experimental data.

modeled whereas heat propagation from one to three particle diameters into the bed is necessary before the solution assumes the behavior of the Mickley and Fairbanks equation (1).

The maximum heat transfer coefficient due to gas gap heating predicted by the above model appears as a time independent value particularly for particle diameters less than a millimeter. This maximum is not influenced by solid properties and is given approximately by

$$h = \frac{k_g}{r}\left[\frac{2(\delta+1)}{\delta+2}\sqrt{\frac{\delta+2}{\delta}}\ \mathrm{Arctan}\left(\sqrt{\frac{\delta+2}{\delta}}\right) - \frac{\pi}{2}\right]$$

where

k_g = gas conductivity (W/m^2-K).

r = particle radius (m).

δ = ratio of gap width to particle radius.

Denloye (20) assumed conduction into the bed could be modeled by a high porosity region nearest the wall and a second region which assumes the bulk porosity of the bed. As opposed to the above model, with this treatment he was able to approximate the heat transfer coefficient extending to a time where agreement with the Mickley and Fairbanks equation (1) is possible using appropriate effective properties for each region. However, the multiple use of effective conductivity

correlations which increases the subjectivity of the heat transfer coefficient prediction is to be discouraged when a more direct method to determine the coefficient is possible numerically.

VI.B. Numerical Model

To be able to calculate the heat transfer coefficient to packed beds without use of effective conductivity correlations and to explore the effects of different contact resistance terms and gas-particle orientations, a finite difference method was developed to model two-dimensional heat conduction in slab and cylindrical geometries with spatially dependent properties. Detailed explanation of the equations, assumptions, input preparation, as well as verification of the method is given in Appendix D.

Input to the program was prepared to follow the porosity distribution by distance into the bed given by Eq. V.D.2.2. It was discovered a separation between particles themselves needn't be represented to fit the data once an appropriate gas gap separated the first particle from the wall. Figures (VI.B.1 and VI.B.2) show the comparison between calculated and experimental data for glass beads of 0.8mm and 0.18mm diameter respectively. For this research, an air gap of 21μm for 0.8mm diameter and a gap of 15μm for 0.18mm diameter

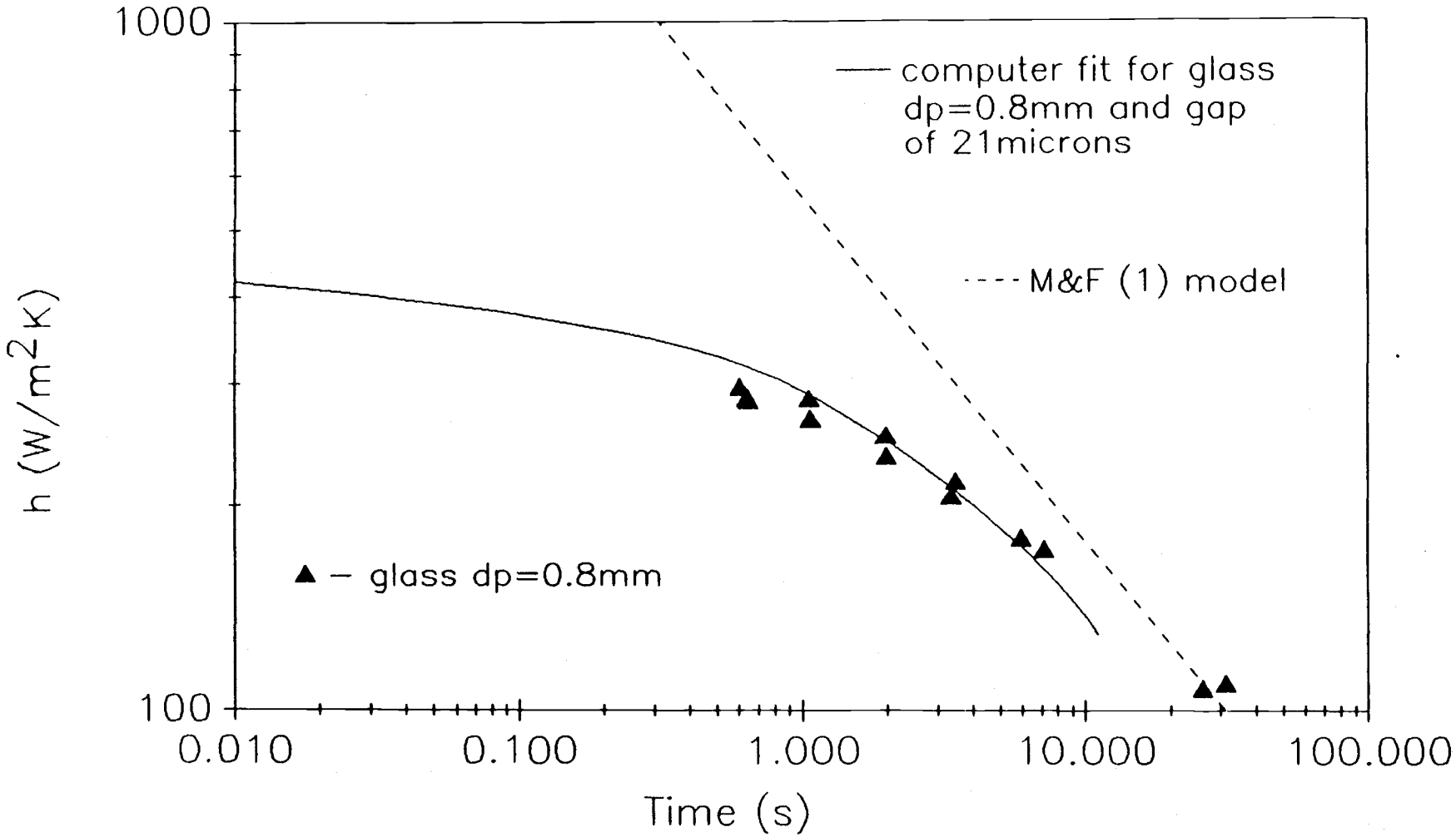

Figure (VI.B.1). Heat transfer coefficient comparison as a function of contact time with the heated surface for the M&F (1) model and the numerical solution for 0.8mm diameter glass beads.

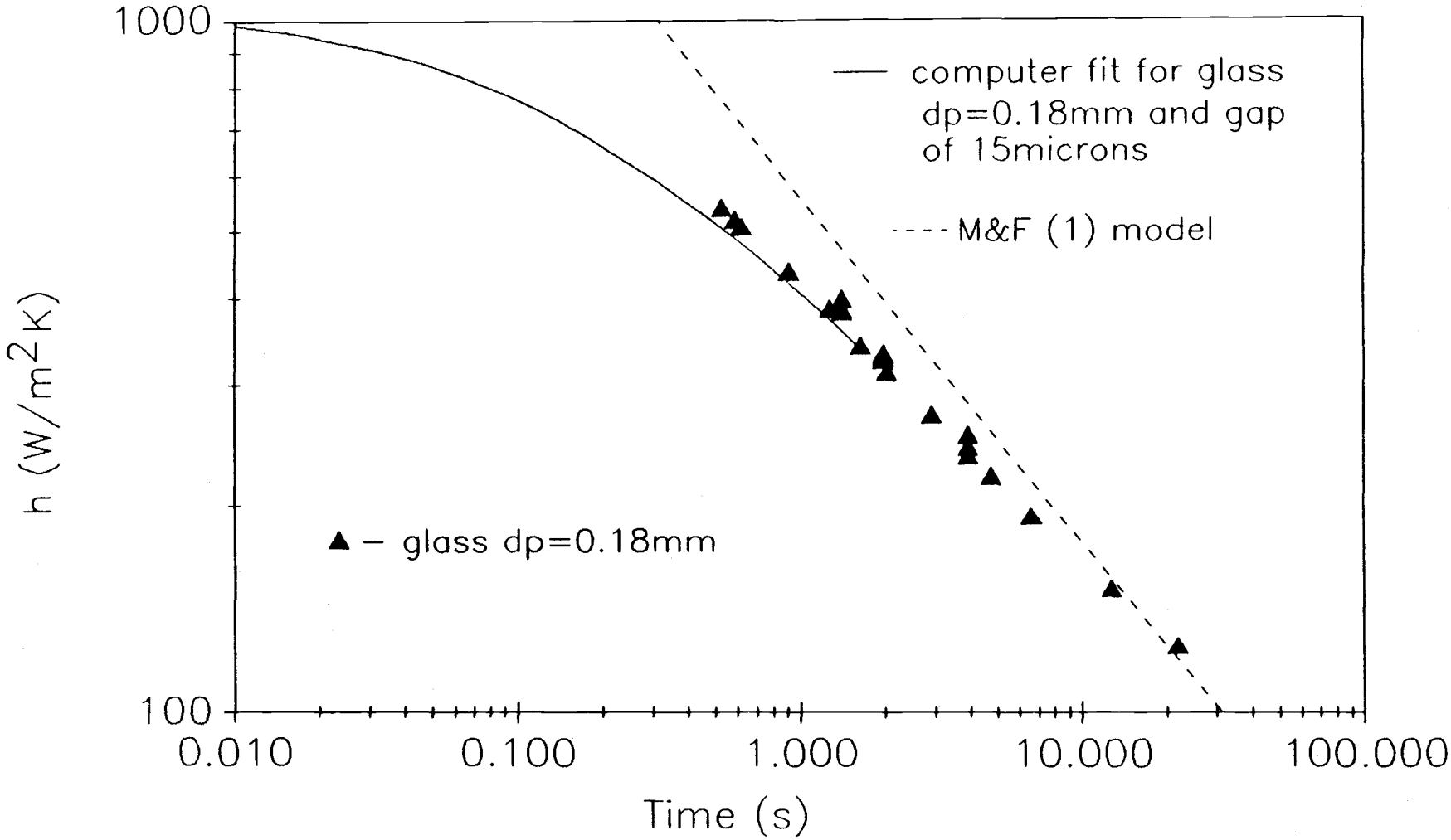

Figure (VI.B.2). Heat transfer coefficient comparison as a function of contact time with the heated surface for the M&F (1) model and the numerical solution for 0.18mm diameter glass beads.

glass was required to fit the experimental findings. Introduction of a greater contact resistance appears necessary for smaller particles since a proportionally thicker gas gap to particle size ratio is needed to fit the data.

As mentioned before, each particle may possess an adsorbed gas layer at its surface and so modeling the solid by a direct contact with the wall would be improper. In order to demonstrate the necessity of contact resistance, then, the number of nodes representing each particle diameter was consecutively increased for several cases so that the area of contact with the wall decreased. The solution appeared to converge gradually with decreasing contact area but an increase in the computed heat transfer coefficient continued beyond the data with a slope of 0.2 on a log-log plot as opposed to 0.5 characteristic of the Mickley and Fairbanks (1) solution. The analytic solution applied from Appendix C without a gas gap confirmed this deviation. The importance of a gas gap, however, was observed only for short contact times since for longer contact times the numerical solution approached the same value with different particle sizes, various gas gaps, and, although poorly, for no gap at all (Figure VI.B.3).

To demonstrate the importance of the concept of reduced gas conductivity as opposed to a gas gap, the

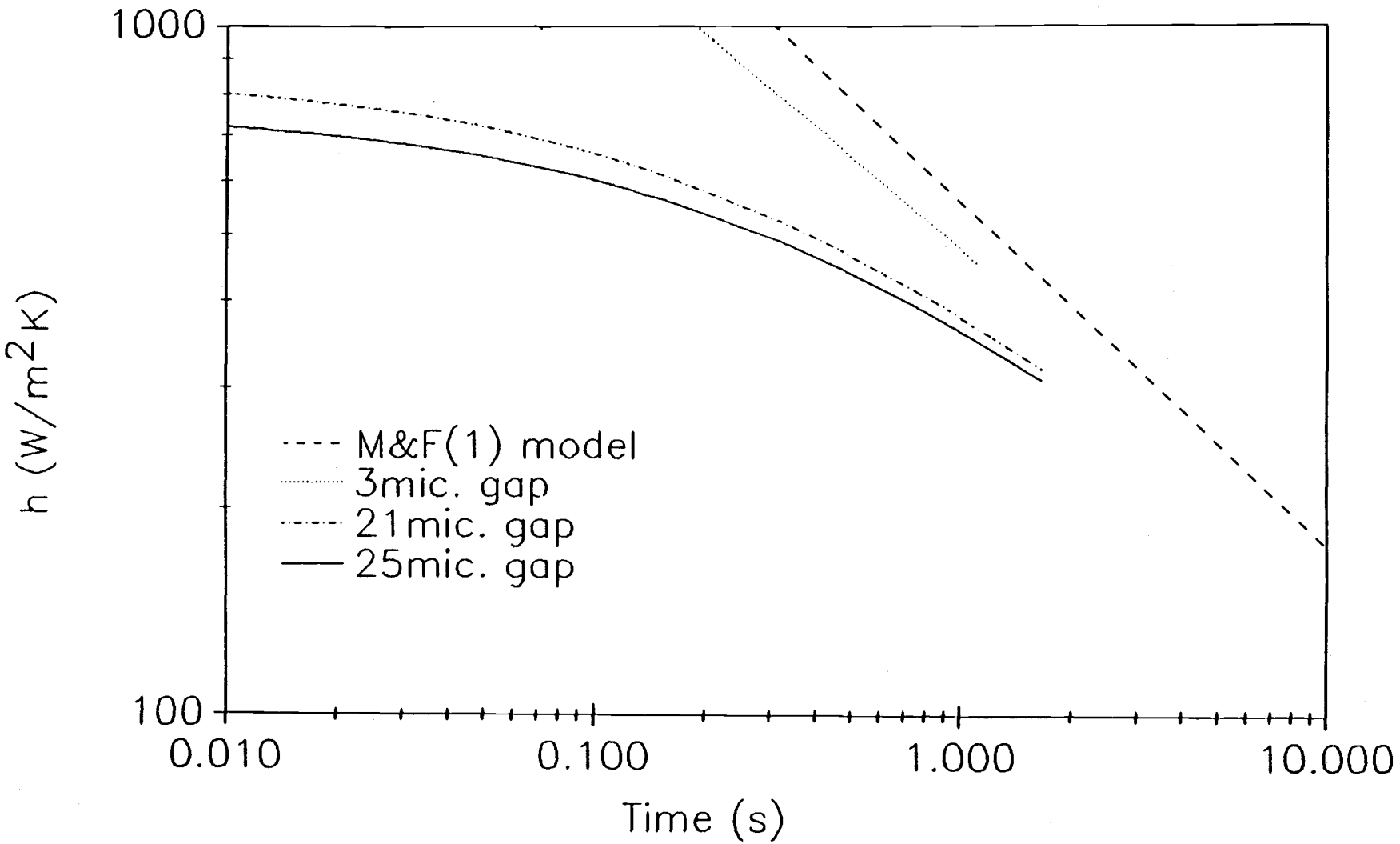

Figure (VI.B.3). Heat transfer coefficient as a function of contact time with the heated surface for M&F (1) model and the numerical solution by gap width for 0.18mm diameter glass beads.

conductivity calculated from Eq. V.B.1 was applied in the vicinity of the contact point by defining a narrow region separating the particle from the wall with reduced gas conductivity. The effect on the solution, however, was insignificant in comparison to implementation of a gas gap of equal width. The additional complexity of modeling reduced gas conduction was therefore judged unnecessary.

VI.C. Empirical Model

The major deficiency of the present analytic and numerical methods as well as solutions from other authors is that no changes in particle separation from the wall influenced by mass flow rate are assumed. If a change in flow properties is responsible for existence of a boundary layer of fluid stagnant at the wall, a maximum heat transfer coefficient is obtained when this fluid film is all that is heated. The importance of the gas gap is negligible once heating extends far into the bed. It is therefore possible to fit data by the present calculational methods assuming a constant width gas gap, or, in the experimental sense, the fluid film at the wall reaches a constant width independent of velocity before heating extends no further than the film itself. Unfortunately, judging by the conflicting results often obtained between independent researchers,

a single criteria does not seem to hold for all experimental setups, and cannot be generally used.

Experimental data show good agreement with the analytic solution for heat transfer by Mickley and Fairbanks (1) at long contact times although the observed slope is somewhat different than predicted by their equation (Figure VI.C.1). Great discrepancy is observed for short contact times where experimental data level off. To know this point of separation is important so that the maximum heat transfer coefficient may be predicted.

In order to obtain some general correlation for the heat transfer coefficient, the existing correlations and experimental data were examined for vertically oriented heating elements provided by Ernst (9), Desai (21), Sullivan (3), and this present study. The experimental equipment used by Wunschmann (12) and Harakas and Beatty (2) was studied. Intuitively one would expect that moving bed coefficients be rather similar when compared in the same system of reference. The difference in heat transfer coefficients observed by various researchers when compared at identical contact times (see Chapter IV) appeared to be influenced from the fluid dynamic behavior specific for each given arrangement.

The choice of parameters that were considered

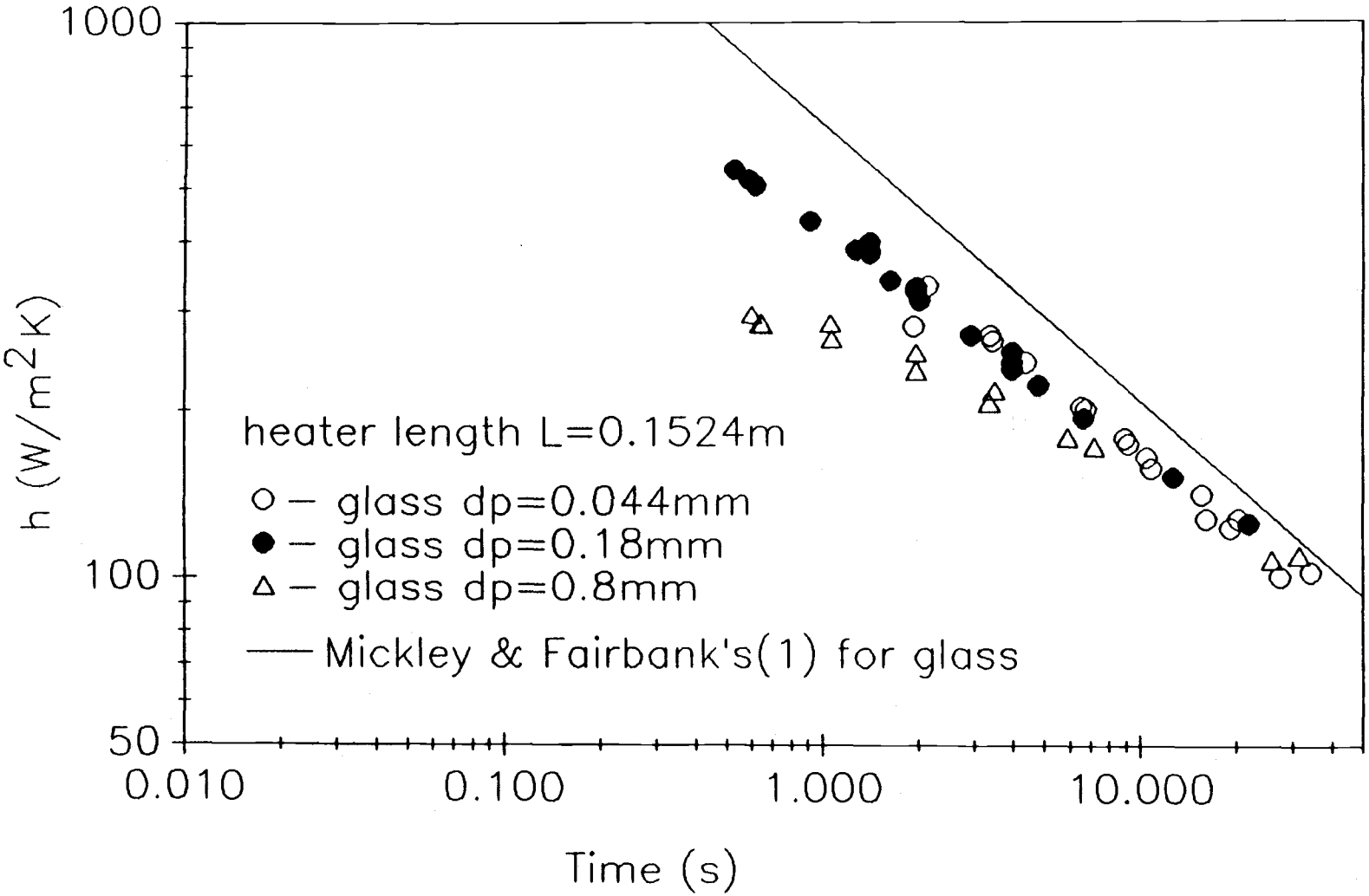

Figure (VI.C.1). Comparison between heat transfer coefficients as a function of contact time with the heated surface for the present data and the M&F (1) model.

important and their combination brought interesting results. It is still not possible to offer the complete analytical solution to this problem, however, and only a simple general technique is proposed for vertically oriented heaters (rods or plates) when gravity flow of solids is not obstructed by either heated or supporting parts. The simple mass flux equation developed predicts empirically the departure point from the Mickley and Fairbanks (1) equation

$$\frac{t_{cr}}{d_p \rho_s} = 0.3622 + 9.691\ L \qquad \text{(VI.C.1)}$$

where

L = heated length (m).

d_p = particle diameter (m).

ρ_s = solid density (kg/m^3).

t_{cr} = critical or separation time (s).

A graphical approximation of the heat transfer coefficient about the inflection point is simple.

1. Calculate the critical time from equation V.C.1.
2. Using this time calculate the maximum heat transfer coefficient from the average Mickley and Fairbanks (M&F) (1) model

$$h_{max} = 2\sqrt{\frac{k_e C_{ps} \rho_b}{\pi t_{cr}}}$$

3. Draw a horizontal line at h_{max} till it intercepts the M&F line.

The heat transfer coefficient curve is expected to follow the M&F line and gradually depart to the value of h_{max}, the curvature about the inflection point increasing with particle radius. A correlation for the time the curve assumes the h_{max} value is given by

$$\frac{t_{max}}{d_p \rho_s} = 0.29087 + 0.0492 \ln(L) \qquad \text{(VI.C.2)}$$

The curve for the heat transfer coefficient appears to level off at t_{max}, but further extrapolation is impossible. It is expected that the heat transfer coefficient decreases at velocities above those now measured due to an increase in porosity when solids flow by gravity. For particle sizes below 0.044mm or smaller, problems with solids flow will occur because of high interparticle forces. The heat transfer coefficient is therefore expected to drop and none of the existing models can predict its value.

A demonstration of the graphical method with experimental data of Ernst (9), Desai (21), and this study are given respectively in Figures (VI.C.2 through VI.C.5) of this chapter.

The results by Harakas and Beatty (2) could not be fitted to the correlations since in their experimental

system solids did not flow by gravity. The maximum value of heat transfer coefficient did not occur, however their data follow the expected trend at lower contact times as presented in Figure (VI.C.6).

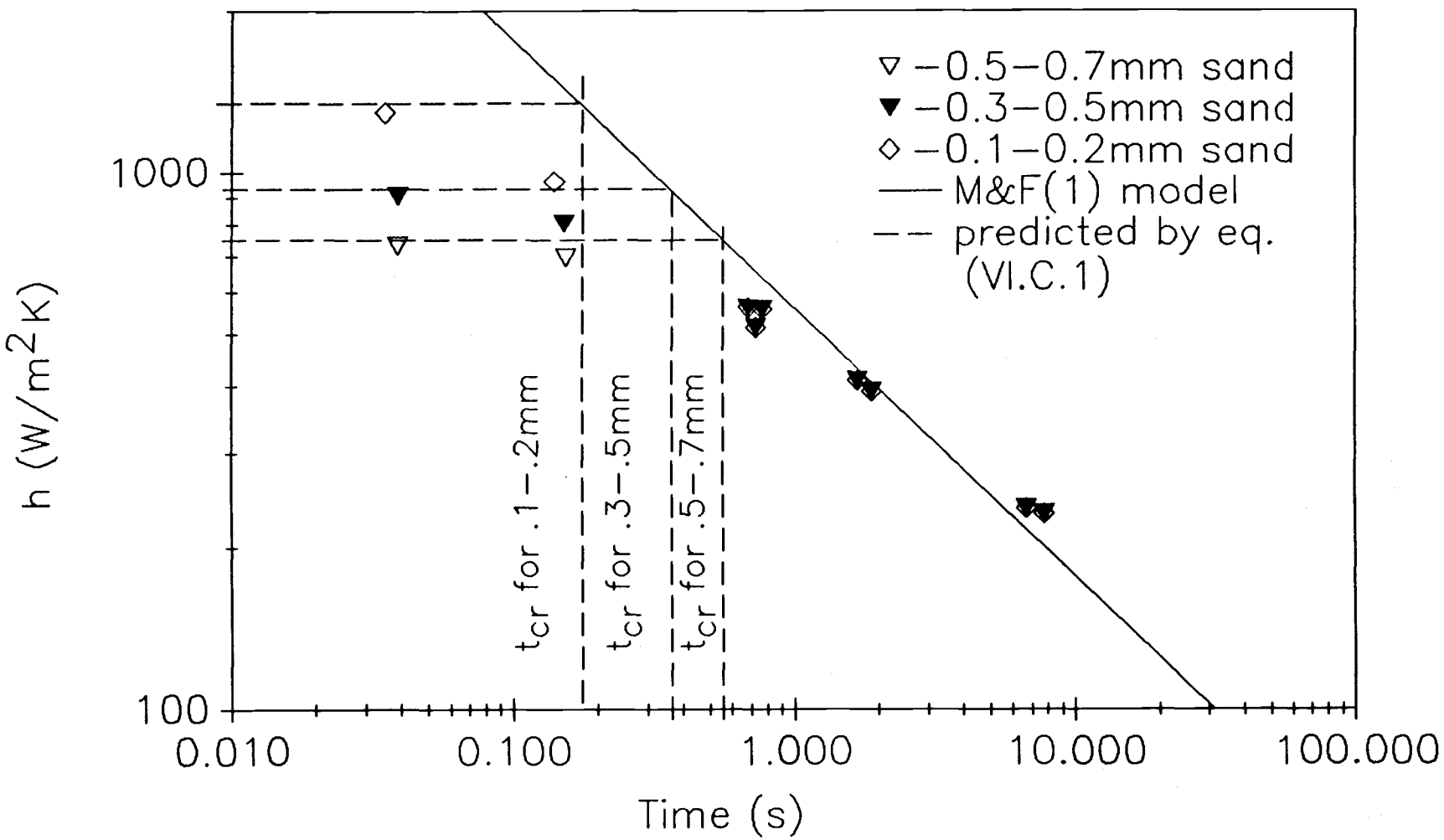

Figure (VI.C.2). Empirical prediction of t_{cr} by Eq. (VI.C.1) and Ernst's (9) data.

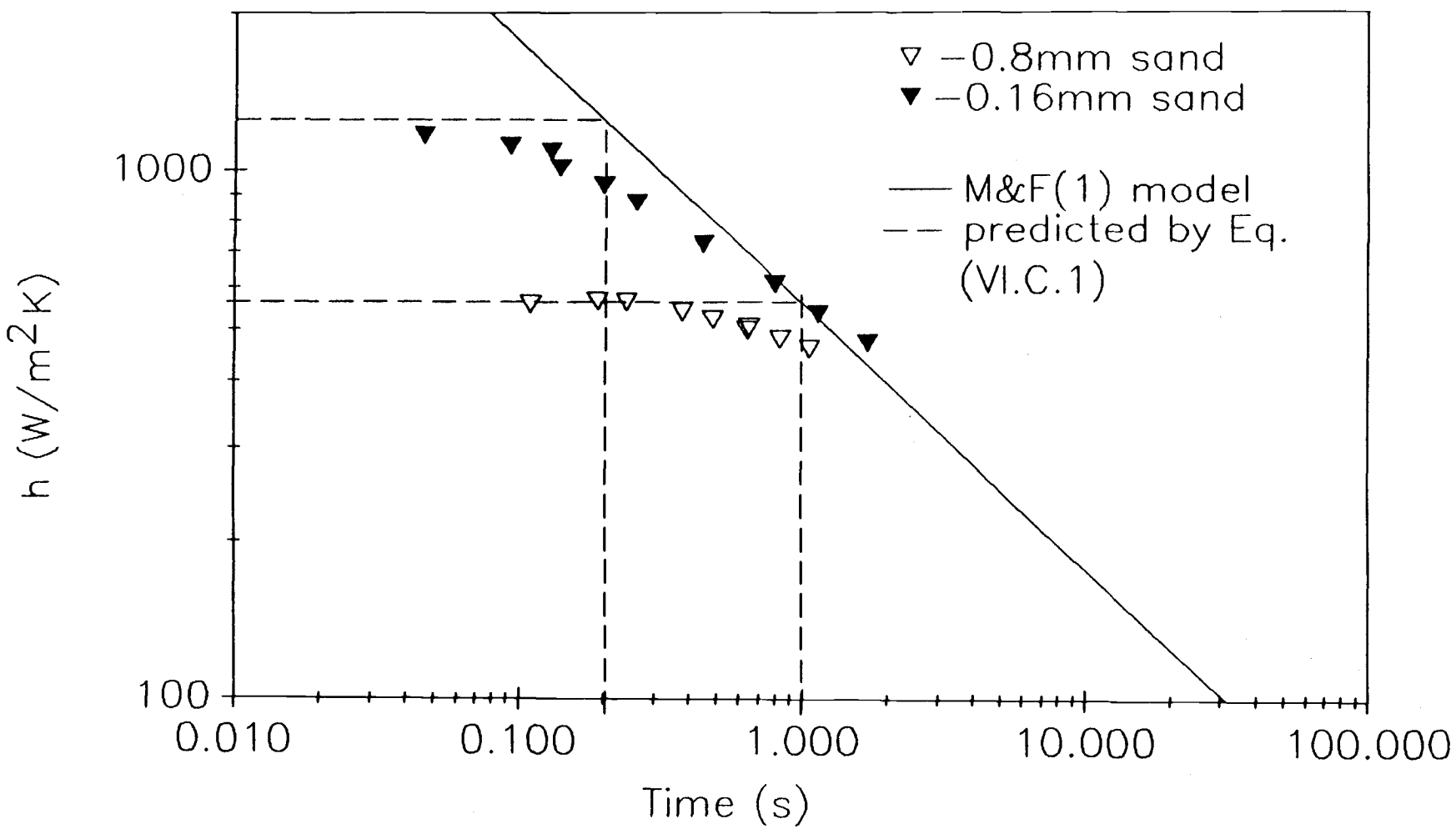

Figure (VI.C.3). Empirical prediction of tcr by Eq. (VI.C.1) and Desai's (21) data for glass.

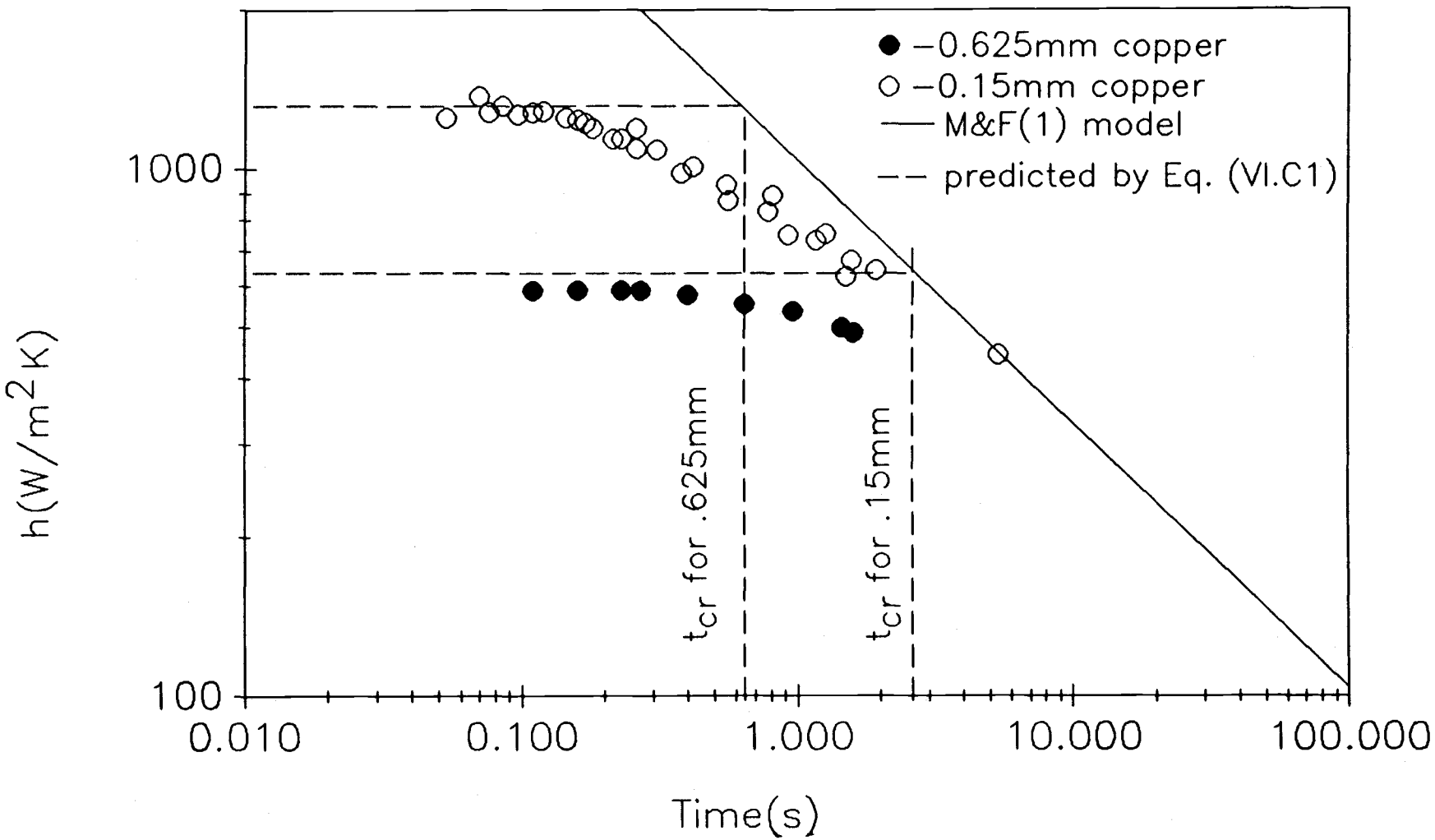

Figure (VI.C.4). Empirical prediction of t_{cr} by Eq. (VI.C.1) and Desai's (21) data for copper.

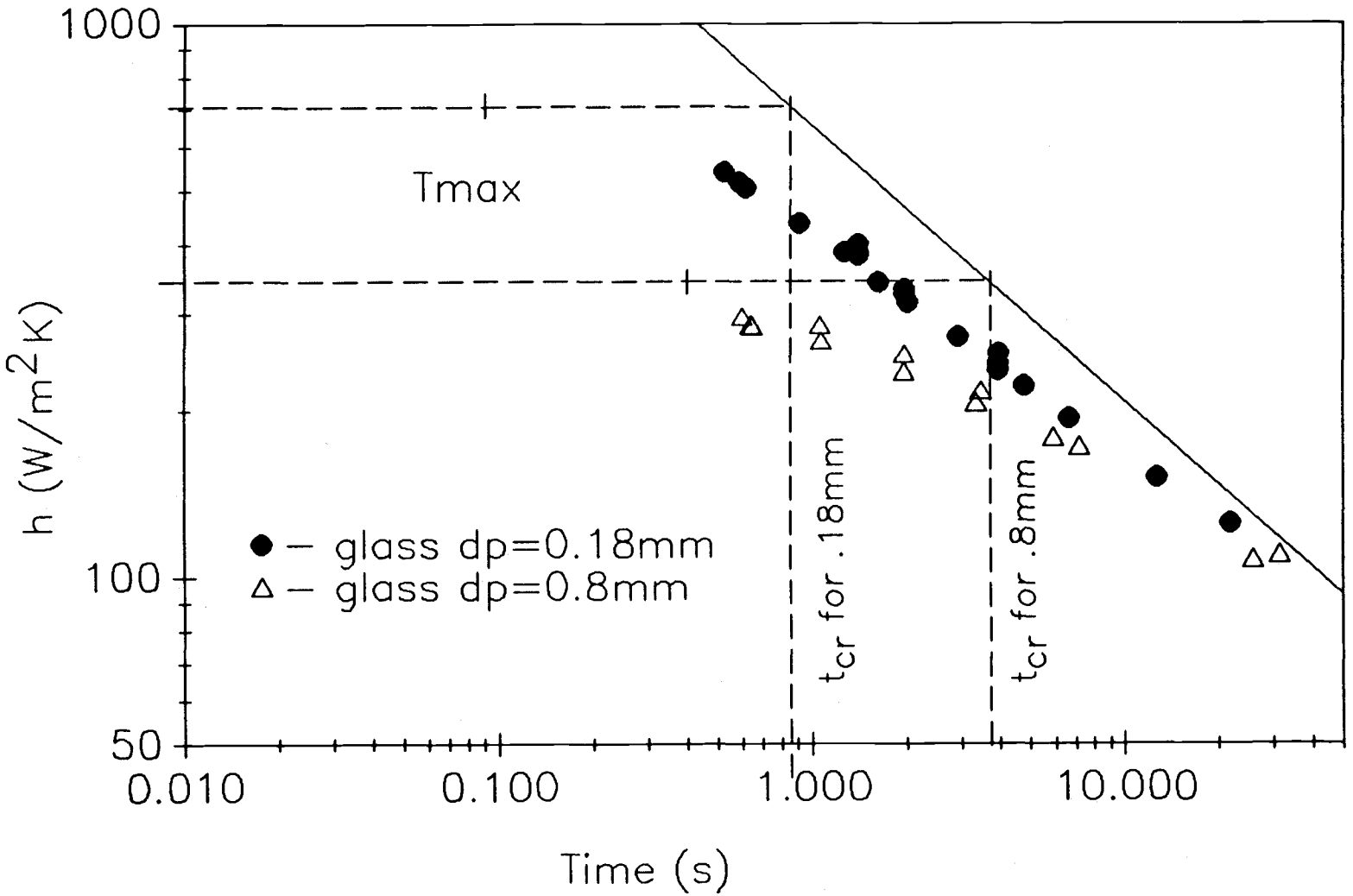

Figure (VI.C.5). Empirical prediction of t_{cr} by Eq. (VI.C.1) and t_{max} by Eq. (VI.C.2) for the present study.

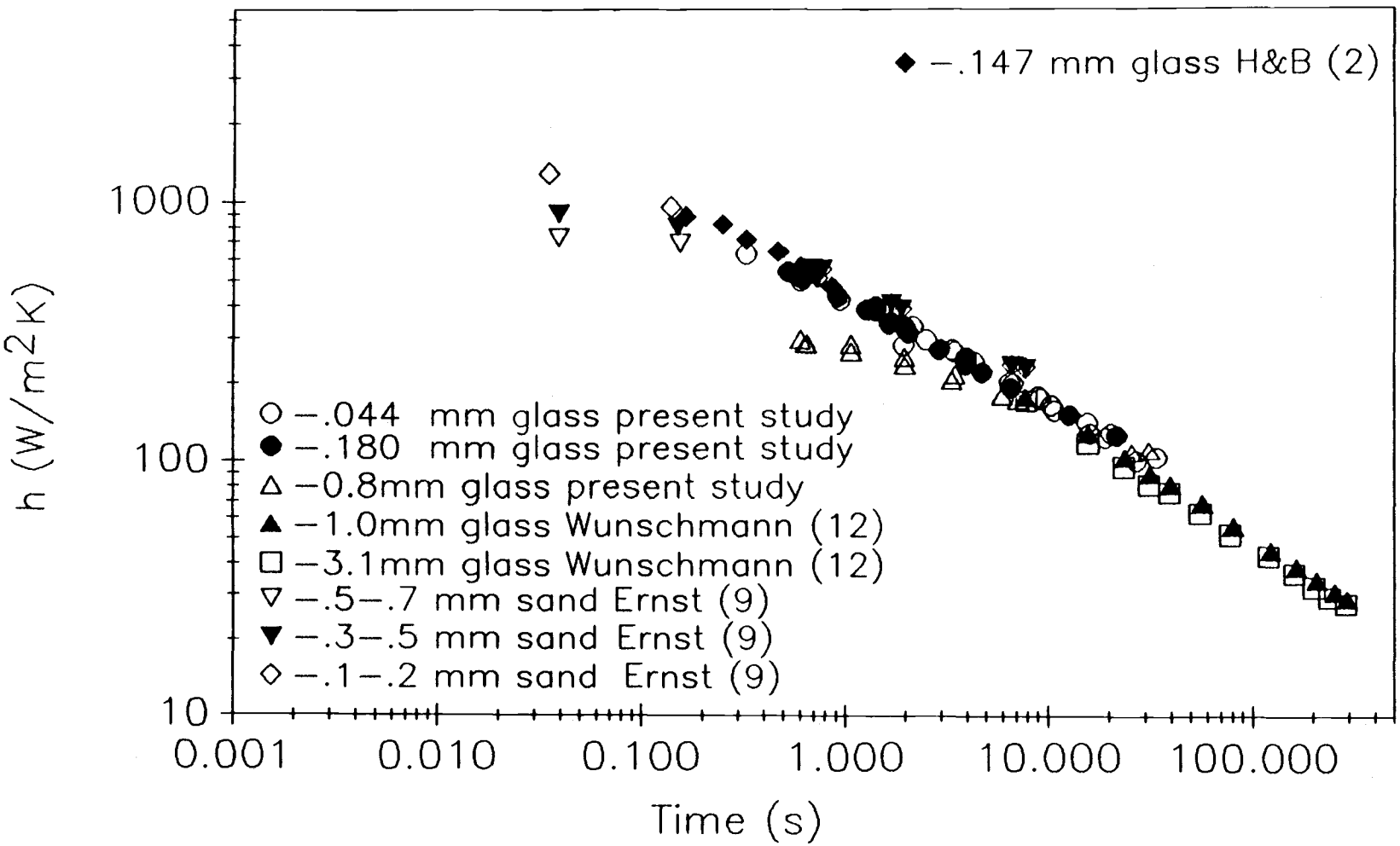

Figure (VI.C.6). Comparison between heat transfer coefficients by contact time with the heated surface for Ernst's (9), Wunschmann's (12), Harakas (2) and the present data.

VII. CONCLUSIONS

VII.A. Summary of Findings

The heat transfer coefficient between a single vertical tube and a moving bed of solids in air at atmospheric pressure was measured and compared to measurements performed by independent researchers characteristic of a number of different experimental configurations. The gas and solid properties, contact time with the heated surface, and experimental configuration were observed to have the greatest influence on the heat transfer coefficient. The distinct improvement of heat transfer from vertically oriented tubes as compared to horizontal tubes could also be explained.

Simple models of heat transfer to packed beds such as the Mickley and Fairbanks (1) model assume the bed may be modeled with effective properties. As particle size increases and residence time decreases, however, the measured heat transfer coefficient gradually assumes a maximum value, contrary to the model. More accurate predictions of the heat transfer coefficient assume a contact resistance exists between the heated surface and the bed. Analytic and numerical models applied in this research confirm this resistance must exist.

A static gas adsorption layer on the particle

surface and a flow dependent particle separation or gas gap from the wall may both contribute to an observed contact resistance. High speed photographic studies of flowing packed beds performed by the author show an insignificant porosity change occurs up to bed velocities of 0.5m/s but a measure of gas gap was impossible. Since inter-particle separation and movement appeared rare, heat transfer at high velocities is most influenced by changes in the wall porosity distribution and thickness of the gas gap layer. Computer simulation of heat transfer to a packed bed showed a steady width gas gap of 21μm for 0.8mm and 15μm for 0.18mm glass beads was capable of fitting experimental data.

On the assumption that the heat transfer coefficient is flow dependent, an empirical correlation was fitted and predicts the time of departure from the Mickley and Fairbanks (1) equation independent of heat transfer properties of the bed.

$$\frac{t_{cr}}{d_p \rho_s} = 0.3622 + 9.691\ L \qquad \text{(VI.C.1)}$$

This correlation is the only of its kind which can predict the departure point from the Mickley and Fairbanks (1) equation to data obtained by the researchers evaluated here for various heated lengths.

VII.B. Further work

To demonstrate the existence of a velocity dependent gas film about the boundary to a flowing packed bed a more refined experiment using high speed photography should be attempted. Since the distance from the wall the particles could remain in focus was much greater than the gas gap expected to fit data by computer solution, a fiber optics plate should be used to couple the image from the surface of a flowing packed bed. The extremely short range of focus characteristic from the optical surface of a fiber optics plate may enable photographic observation of a gas film.

The behavior of the heat transfer coefficient requires further study due the shortage of measurements once a maximum value occurs. Using particle sizes on the order of one half millimeter or more and high conductivity solids such as copper would ensure an observation of early departure from the Mickley and Fairbanks (1) equation. The residence time may also be decreased by increasing the flow rate of the particle bed and decreasing the heated length of the surface. This should allow an opportunity to collect more data to verify theories regarding heat transfer to flowing packed beds for velocities greater than the Mickley and Fairbanks (1) equation applies.

BIBLIOGRAPHY

1. Mickley, H. S. and D. F. Fairbanks. "Mechanisms of heat transfer to fluidized beds", AIChE J., 1 374 (1955).

2. Harakas, N. K. and K. O. Beatty, Jr. "Moving bed heat transfer: effect of interstitial gas with fine particles," Chem. Eng. Prog. Symp. Ser., 59, No. 41, 122-128 (1963).

3. Sullivan, W. N. and R. H. Sabersky. "Heat transfer to flowing granular media," Int. J. Heat and Mass Transfer, 18 97 (1964).

4. Baskakov, A. P. "The mechanism of heat transfer between a fluidized bed and a surface," Int. Chem. Eng., 4 320 (1964).

5. Denloye, A. O. O. and J. S. M. Botterill. "Heat transfer in flowing packed beds," Chem. Eng. Sci., 32 461 (1977).

6. Spelt, Jan Karel. An Experimental Study of Heat Transfer to Flowing Granular Media, M. S. Thesis, California Institute of Technology, Pasadena, CA (1981).

7. Donskov, S. V. Teploenergetika, In Russian, 11 (1958).

8. Kurochkin, Yu P. Inzhenerno-Fizicheskifi Zhuranal, In Russian, 4 76 (158).

9. Rudolf, Enrst. "Wärmeübergang and Wärmeaustaushern im Moving Bed," Chemi. Ing. Techn, in German, 32 17 (Jahrel 1960).

10. Colakyan, Manuk. Moving Bed Heat Transfer and Fluidized Flutriation, PhD Thesis, Oregon State University (1984).

11. Obušković, Nevenka. Heat Transfer Between Moving Beds of Solids and a Transverse Finned Tube, M. S. Thesis, Oregon State University (1985).

12. Wunschmann J. and E. U. Schlünder. "Heat transfer from heated surfaces to spherical packings," Int. Chem. Eng., 20, No. 4, 555 (October 1980).

13. Schlünder, E. U. "Heat transfer to moving packings at short contact times," Int. Chem. Eng., 20, No. 4, 551 (October 1980).

14. Decker, N. and L. R. Glicksmann. "Heat transfer in large particle fluidized beds," Int. J. Heat Mass Transfer, 26, No. 9, 1307 (1983).

15. Brenner, S. S. Surface Sci., 2 496 (1964).

16. Brown, G. G. Unit Operations, J. Wiley, New York, 130 (1966).

17. Takashi, Hiroshi and Hiroshi Yanai. "Flow profile and void fraction of granular solids in a moving bed," Powder Technology, 7 205 (1973).

18. Kimura, M. and T. Kaneda. Chem. Eng. Sci, 23 1147 (1968).

19. Benenati, R. F. and C. B. Brosilow. "Void fraction distribution in beds of spheres," AIChE Journal, 8, No. 3, 359 (1962).

20. Denloye, A. O. O. PhD Thesis, University of Birmingham (1976).

21. Desai, M. PhD Thesis, University of Birmingham (1970).

22. Cumberland, D. J. and R. J. Crawford. The Packing of Particles, Elsevier Science Publishers B. V. (1987).

23. Earle, Kenneth H. Kinetic Theory of Gases, McGraw-Hill Book Company (1938).

24. Patton, J. S., Sabersky R. H., and C. E. Brennen. "Convective heat transfer to rapidly flowing granular materials," Int. J. Heat Mass Transfer, 29 1263-1269 (1986).

25. Overbeek, J. T. and M. J. Sparnaay. "London-Van der Waals attraction between macroscopic objects," Faraday Soci-Discussions, 18 12-23 (1954).

26. Derjaguin, B. V. and I. I. Abrikossova. "Direct measurements of molecular attraction of solids," J. Phys. Chem. Solids, 5 1-10 (1958).

27. Argo, W. B. and J. N. Smith. "Heat transfer in packed beds," Chem. Eng. Progress, 49 443 (1953).

28. Delvosall, C. and J. Vanderschuren. "Gas to particle and particle to particle heat transfer in fluidized beds of large particles," Chem. Eng. Sci., 40 769-779 (1985).

29. Baddour, R. F. and C. Y. Yoon. "Local radial conductivity and the wall effect in packed beds," Chemical Engineering Progress Symposition Series No. 32, 57 35.

30. Borland, D. and D. Geldart. "Electrostatic charging in gas fluidized beds," Powder Technology, 5 289 (1971/72).

31. Bagnold, R. A. "Experiments on a gravity-free dispersion of large solid spheres in a Newtonian fluid under shear," Proc. Roy. Soc. Edin. A, A225 49 (1954).

32. Gabor, John D. "Wall to bed heat transfer in fluidized and packed beds," Chemical Engineering Progress Symposition Series No. 105, 66 76 (1970).

33. Haughey, B. P. and G. S. C. Beveridge. "Local property variations in a randomly packed bed of equal-sized spheres," Chem. Eng. Sci., 22 715 (1967).

34. Savage, Stuart B. "Gravity flow of cohesionless granular materials in chutes and channels," J. Fluid. Mech., 92 53-96 (1979).

35. Levamax, Grummer Milton. "Heat transfer to gases through packed tubes," Ind. Eng. Chem., 40 (1948).

36. Brinn, M. S. et al. "Heat transfer to granular materials," Industrial and Eng. Chemistry, 40 1050 (June 1948).

37. Chandran, R. and Chen J. C. "Influence of the wall on transient conduction into packed media," AIChE Journal, 31 168 (1985).

38. Couderc, J. P., H. Angelino, M. Enjalbert et C. Guiglion, "Echanges themiques en fluidisation gazeuse. II--Etude mathématique à l'aide d'un modéle simple," In French, Chem. Eng. Sci., 22 99-107 (1967).

39. Mickley, H. S., D. F. Hawthorn, and D. F. Fairbanks. Chemical Engineering Progress Symposition Series No. 32, 57 51 (1961).

APPENDICES

Appendix A

Analytic Heat Transfer Coefficient for Rod

Given a heated rod of radius a surrounded by a bed of effective thermal diffusivity α and conductivity k, the heat flux at the surface of the rod is given by

$$q'' = \frac{4kV}{a\pi^2} \int_0^\infty \frac{e^{-\alpha u^2 t}\, du}{u(J_0^2(ua) + Y_0^2(ua))}$$

where $V = T(a,t) - T_\infty$ (1,2).

Since the heat transfer coefficient is given by q''/V we have

$$h(t) = \frac{4k}{a\pi^2} \int_0^\infty \frac{e^{-Fo_a^2 z}\, dz}{z(J_0^2(z) + Y_0^2(z))} \qquad (A.1)$$

where

Fo_a = Fourier number based on rod radius a.

$= \alpha t/a_2$.

When averaged over the interval of 0 to Foa the heat transfer coefficient is

$$h(t) = \frac{4k}{aFoa\pi^2} \int_0^\infty \frac{(1 - e^{-Fo_a^2 z})\, dz}{z^3(J_0^2(z) + Y_0^2(z))} .$$

The indefinite integral above has been solved here using a 15 point Gauss-Legendre numerical integration method summed over progressively larger segments of the integral range until the contribution of the last segment does not change the final sum by an error of

10^{-6}. Answers using this method were comparable within 10% to approximate values tabulated by Jaeger and Clarke (3).

The following program creates a file of heat transfer coefficient values for the cylinder using the numerical method described above and for the Mickley and Fairbanks model for five decades of time values. Material properties are read from a file supplied as input and the heat transfer coefficients are output to a file called GAUSS.OUT. Rod radius A and average gas temperature of the bed TGAVE are entered in a data statement in the program. Effective conductivities of the bed are calculated using Kunii's equation (4).

$$\frac{k_e}{k_g} = \frac{1 - \epsilon}{\frac{k_g}{k_s} + \psi} \qquad (A.2)$$

where

ϵ = porosity of bed.

$\psi = 0.2\ \epsilon^2$.

References

1. Jaeger, J. C. "Heat flow in the region bounded internally by a circular cylinder," Proc. Roy. Soc. Edin. A., 61 223 (1942).

2. Carslaw, H. S. and J. C. Jaeger. Conduction of Heat in Solids, Clarendon Press, 334 (1959).

3. Jaeger, J. C. and Martha Clarke. "A short table of $\int_0^\infty \frac{e^{-xu^2}\,du}{u(J_0^2(u) + Y_0^2(u))}$," Proc. Roy. Soc. Edin. A., 61 229 (1942).

4. Yagi, S. and D. Kunii. "Studies on effective thermal conductivities in packed beds," AIChE J., 3 373 (1957).

GAUSST.FOR

```
      PROGRAM HPLOT
C CONSTRUCTS A PLOT OF AVERAGE HEAT TRANSFER COEFFICIENT VS TIME BY M&F AND
C CYLINDER MODELS
      REAL KE,KS,KG
      CHARACTER TITL*75,FNAME*30
      COMMON FOA
C  ROD RADIUS, A (m)
C  AVERAGE GAS TEMPERATURE, TGAVE (C)
      DATA A,TGAVE /.00635,40./
      PI=ACOS(-1.)
C
      PRINT *,'Enter property file name'
      READ(5,'(A)')FNAME
C
C  READ MATERIAL PROPERTIES
      OPEN(7,FILE=FNAME)
      READ(7,'(A)') TITL
      READ(7,*) ROS,ROE,DP,KS,CP
      CLOSE(7)
C
C  CALCULATE EFFECTIVE ALFA & K
      EPS=1.-ROE/ROS
      PHI=0.197*EPS**1.904
      CPRL=CP*ROE/PI
      KG=(TGAVE+273.)*.0000741+.004038
      KE=KG*(1.-EPS)/(KG/KS+PHI)
      ALFA=KE/(CP*ROE)
C
C  WRITE TIME, AVE CYLINDER H, M&F H TO FILE GAUSS.OUT
      WRITE(6,15)
      OPEN(8,FILE='GAUSS.OUT')
      DO 10 I=1,55
      IF(I.LT.10)              T=.001*I
      IF(I.GE.10.AND.I.LT.20) T=.01+T
      IF(I.GE.20.AND.I.LT.30) T=.1+T
      IF(I.GE.30.AND.I.LT.40) T=1+T
      IF(I.GE.40.AND.I.LT.50) T=10+T
      IF(I.GE.5D)              T=100+T
      FOA=ALFA/A**2*T
      HCYL=(4*KE)/(FOA*A*PI**2)*GAUSS(0.,1E-3,15,1E-4)
      HMF =2*SQRT(KE*CPRL/T)
      WRITE(*,20)T,HCYL,HMF
10    WRITE(8,20)T,HCYL,HMF
15    FORMAT(/'      t     Hcyl-ave  Hmf-ave')
20    FORMAT(3F10.3)
200   END
C
      FUNCTION GAUSS(A1,B1,M,EPS)
C CALCULATES INTEGRAL OF INTEGRAND FUNCTN FROM LIMITS A1 TO INFINITY
C WITHIN ERROR EPS BY ITERATED M POINT GAUSSIAN INTEGRATION
C B1 IS A SEED VALUE FOR INITIAL INTEGRAL
C
C  REFERENCE:
C
C  CARNAHAN, BRICE, H. A. LUTHER, AND JAMES O. WILKES. *APPLIED NUMERICAL
C  METHODS*, JOHN WILEY & SONS, 1969, 1D1-105.
C
      EXTERNAL FUNCTN
      DIMENSION NPOINT(7),KEY(8),Z(24),WGHT(24)
      DATA NPOINT/2,3,4,5,6,10,15/
      DATA KEY/1,2,4,6,9,12,17,25/
      DATA Z              /0.577350269,0.0         ,0.774596669,
     1         0.339981044,0.861136312,0.0         ,0.538469310,
     2         0.906179846,0.238619186,0.661209387,0.932469514,
     3         0.148874339,0.433395394,0.679409568,0.865063367,
```

Print file "gausst.for"

```
     4         0.973906529,0.0        ,0.201194094,0.394151347,
     5         0.570972173,0.724417731,0.848206583,0.937273392,
     6         0.987992518 /
      DATA WGHT           / 1.0       ,0.888888889,0.555555556,
     1         0.652145155,0.347854845,0.568888889,0.478628671,
     2         0.236926885,0.467913935,0.360761573,0.171324493,
     3         0.295524225,0.269266719,0.219086363,0.149451349,
     4         0.066671344,0.202578242,0.198431485,0.186161000,
     5         0.166269206,0.139570678,0.107159221,0.070366047,
     6         0.030753242 /
      B=B1
      A=A1
      DO 1 I=1,7
    1 IF(M.EQ.NPOINT(I))GOTO 2
      GAUSS=0.
      WRITE(*,7)M
    7 FORMAT('ERROR GAUSS: M IS 2,3,4,5,6,10, OR 15 NOT ',I3)
      RETURN
    2 N=0
      SUM1=0.
    3 SUM=0.
      JF=KEY(I)
      JL=KEY(I+1)-1
      C=(B-A)/2.
      D=(B+A)/2.
      DO 6 J=JF,JL
      IF(Z(J).EQ.0)SUM=SUM+WGHT(J)*FUNCTN(D)
    6 IF(Z(J).NE.0)SUM=SUM+WGHT(J)*(FUNCTN(Z(J)*C+D)+FUNCTN(-Z(J)*C+D))
      SUM=C*SUM
      SUM1=SUM1+SUM
      IF(SUM/SUM1.LT.EPS)GOTO 9
      C=B
      N=N+1
      B=B*(1+SUM1/(4*N*SUM))
      A=C
      GOTO 3
    9 GAUSS=SUM1
      RETURN
      END
C
      FUNCTION FUNCTN(U)
C INTEGRAND FUNCTION TO BE USED BY GAUSS FOR AVERAGE H
      COMMON FOA
      REAL J0,J1
      FUNCTN=(1-EXP(-FOA*U**2))/(U**3*(J0(U)**2+Y0(U)**2))
      RETURN
      END
C
C  POLYNOMIAL APPROXIMATIONS TO J0 & Y0 BESSEL FUNCTIONS
C
C  REFERENCE:
C
C  ABRAMOWITZ, M. AND I. E. STEGAN, ED., *HANDBOOK OF MATHMATICAL FUNCTIONS*,
C  US DEPT. OF COMMERCE, AMS 55, 1970, 369-370.
C
      REAL FUNCTION J0(X)
      IF(X.LE.3.0.AND.X.GE.-3.0) THEN
      B=(X/3)**2
      J0=1-2.24999970*B   +1.2656208*B**2-.3163866*B**3+.04444790*B**4
     &    -.003944400*B**5+.00021000*B**6
      ELSEIF(X.GE.3.0) THEN
      J0=F0(X)*COS(PHI0(X))/SQRT(X)
      ELSE
      WRITE(*,*) 'ILLEGAL ARGUMENT CALL TO J0:',X
      ENDIF
```

Print file "gausst.for"

```
      RETURN
      END
C
      FUNCTION YO(X)
      REAL JO
      IF(X.GT.0..AND.X.LE.3.0) THEN
      B=(X/3)**2
      YO=ALOG(X/2)/ACOS(0.)*JO(X)+.36746691
     &    +.605593660*B    -.74350384*B**2+.25300117*B**3-.04261214*B**4
     &    +.004279160*B**5-.00024846*B**6
      ELSEIF(X.GE.3.0) THEN
      YO=FO(X)*SIN(PHIO(X))/SQRT(X)
      ELSE
      WRITE(*,*) 'ILLEGAL ARGUMENT CALL TO YO:',X
      ENDIF
      RETURN
      END
C
      FUNCTION FO(X)
      B=3/X
      FO=  .797884560     -.00000077*B    -.00552740*B**2-.00009512*B**3
     &    +.001372370*B**4-.00072805*B**5+.00014476*B**6
      RETURN
      END
C
      FUNCTION PHIO(X)
      B=3/X
      PHIO=X-.78539816    -.04166397*B    -.00003954*B**2+.00262573*B**3
     &    -.000541250*B**4-.00029333*B**5+.00013558*B**6
      RETURN
      END
```

Appendix B

Heat Transfer Coefficient for Two Region Semi-infinite Slab

Consider the composite semi-infinite slab with constant temperature wall at x=-L and zero initial temperature as shown in Figure (B.1). The temperature gradient at x=-L as a function of time has been listed by Carslaw and Jaeger (1).

$$\left.\frac{\partial T}{\partial x}\right|_{x=-L} = \frac{-V}{\sqrt{\pi\alpha_1 t}}\left[1 + 2\sum_{n=1}^{\infty}\left(\frac{\sigma - 1}{\sigma + 1}\right)^n e^{-(nL)^2/(\alpha_1 t)}\right]$$

where $\sigma = (k_2/k_1)\sqrt{\alpha_1/\alpha_2}$ and V is the temperature difference at the wall. In terms of the heat transfer coefficient at the wall this becomes

$$h(x,t) = \frac{k_1}{\sqrt{\pi\alpha_1 t}}\left[1 + 2\sum_{n=1}^{\infty} c^n\, e^{-n^2/Fo_L}\right] \qquad (B.1)$$

where

$Fo_L = \alpha_1 t/L^2$ and

$$c = \left(\frac{\sigma - 1}{\sigma + 1}\right).$$

For very small or large FoL numbers, the solution may be simplified since

$$\sum_{n=1}^{\infty} c^n\, e^{-n^2/Fo_L} \approx 0 \qquad \Big|_{\text{small FoL}}$$

$$\approx c/(1-c) \Big|_{\text{large FoL}}$$

Two region composite semi-infinite slab

Figure (B.1). Representation of composite slab.

Then

$$h = h_1 \approx \left. \frac{k_1}{\sqrt{\pi \alpha_1 t}} \right|_{\text{small FoL}}$$

$$h = h_2 \approx \left. \frac{k_2}{\sqrt{\pi \alpha_2 t}} \right|_{\text{large FoL}}$$

So that h_1 and h_2 are solutions for the Mickley and Fairbanks equation for region 1 and 2, respectfully. A good approximation for the heat transfer coefficient for moderate values of Fo_L is given by

$$h \approx k_1/L.$$

When B.1 is plotted on a log-log scale against time, the heat transfer coefficient can be identified to form three portions: a linear portion where the coefficient behaves only by heat transfer to region 1, a transition region where heat transfer develops into region 2, and a second linear portion once region 1 completes heating and the temperature gradient in region 2 is most significant.

References

1. Carslaw, H. S. and J. C. Jaeger. Conduction of Heat in Solids, Clarendon Press, 319-322 (1959).

Appendix C

Heat Transfer from Wall to Particle Through Interstitial Fluid

An approximation for heat transfer from a heated wall to a spherical particle for low heating times may be obtained by a special treatment of B.1 over a slab with a hemispherical interface. Assume as usual slab geometry and heat conduction only perpendicular to the wall is significant. Then using B.1 integrate by length l over the hemispherical interface by height z over 0 to r (Fig. C.1) to find the average

$$h = \frac{k_1}{\sqrt{\pi\alpha_1 t}}\left[1+2\sum_{n=1}^{\infty} c^n \int_0^{\pi/2} e^{-n^2(\Delta x+r(1-\cos\theta))^2/\alpha_1 t} \cos\theta d\theta\right]$$

$$= \frac{k_1}{\sqrt{\pi\alpha_1 t}}\left[1+2\sum_{n=1}^{\infty} c^n \int_0^{\pi/2} e^{-n^2(\delta+1-\cos\theta)^2/Fo_r} \cos\theta d\theta\right] \quad (C.1)$$

where $Fo_r = \alpha_1 t/r^2$, $\delta = \Delta x/r$ and c is as defined in Appendix B.

Equation C.1 cannot be integrated further analytically, however a 6 point Gauss-Lengendre numerical integration method obtains a sufficiently accurate solution. Agreement between the equation C.1 and the finite difference treatment described in Appendix D is quite good for short contact times.

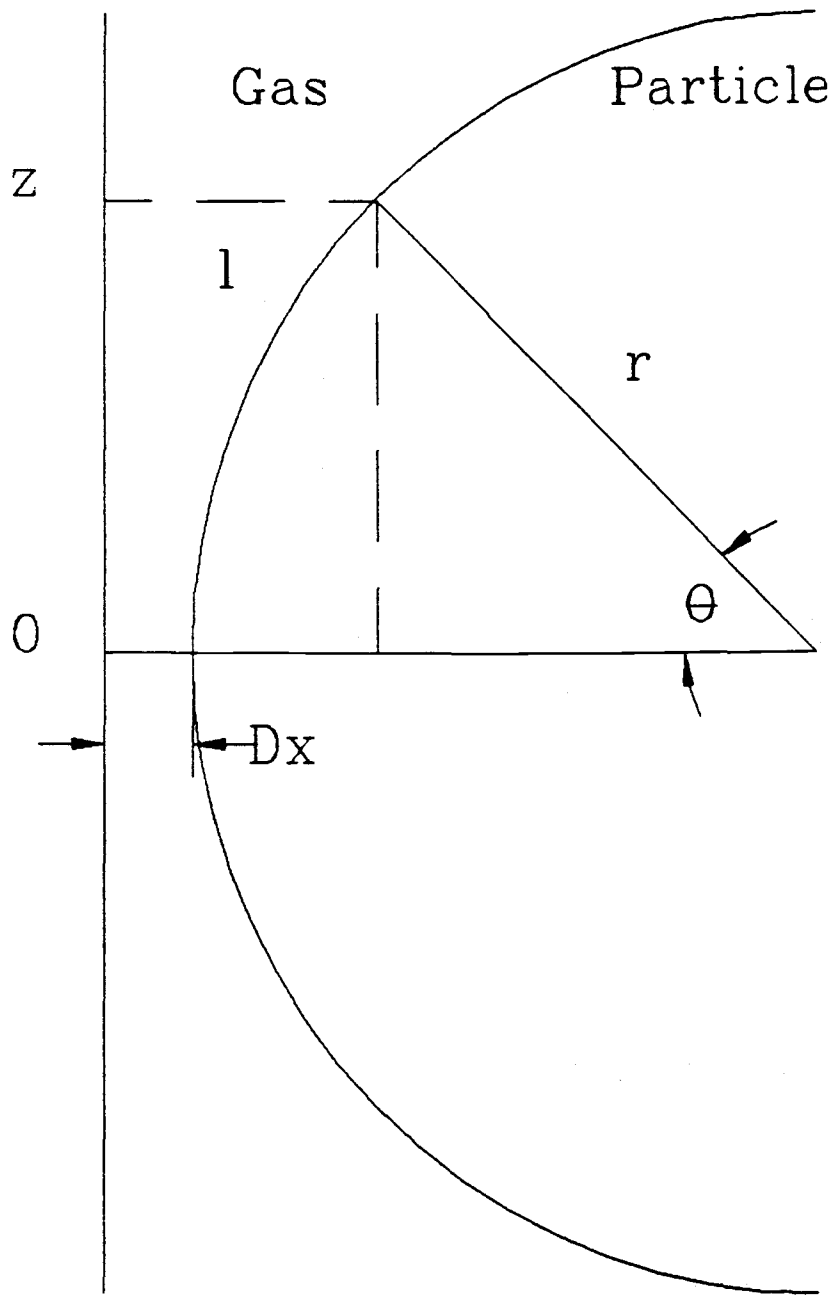

$$l = Dx + r(1 - \cos\theta)$$

Figure (C.1). Representation of separation distance between a spherical particle and wall.

The asymptotic values of h for very low or high Fo_r numbers are the same as for the composite semi-infinite slab. In most cases if not all the gas conductivity is much less than that of the solid and the gas thermal diffusivity is greater than the solid, therefore the value of c is very close to unity. A good approximation for h at moderate values of Fo_r may then be obtained. Assume c = 1 then

$$h/h_1 = 1+2\sum_{n=1}^{\infty} \int_0^{\pi/2} e^{-n^2(\delta+1-\cos\theta)^2/Fo_r} \cos\theta d\theta$$

By use of the Euler-Maclaurin summation formula we can say

$$\sum_{p=1}^{\infty} e^{-p^2} = \int_0^{\infty} e^{-p^2}dp - 1/2 = \frac{\sqrt{\pi} - 1}{2}$$

Then

$$2\sum_{n=1}^{\infty}\int_0^{\pi/2} e^{-n^2(\delta+1-\cos\theta)^2/Fo_r} \cos\theta d\theta =$$

$$2 \int_0^{\pi/2}\int_0^{\infty} e^{-n^2(\delta+1-\cos\theta)^2/Fo_r dn} \cos\theta d\theta =$$

$$2 \int_0^{\pi/2} \left(\frac{\sqrt{Fo_r}}{\delta+1-\cos\theta} \int_0^{\infty} e^{-k^2}dk - 1/2\right) \cos\theta d\theta =$$

$$\sqrt{\pi Fo_r} \int_0^{\pi/2} \frac{\cos\theta d\theta}{\delta+1-\cos\theta} - 1$$

And finally

$$h/h_1 = \sqrt{\pi Fo_r} \left(\frac{2(\delta+1)}{\delta+2}\sqrt{\frac{\delta+2}{\delta}} \operatorname{Arctan}\left(\sqrt{\frac{\delta+2}{\delta}}\right) - \frac{\pi}{2}\right)$$

or

$$h = \frac{k_1}{r}\left[\frac{2(\delta+1)}{\delta+2}\sqrt{\frac{\delta+2}{\delta}}\,\mathrm{Arctan}\left(\sqrt{\frac{\delta+2}{\delta}}\right) - \frac{\pi}{2}\right] \qquad (C.2)$$

This accounts for the plateau value of h for moderate values of Fo_r and is independent of the solid properties (c=1). This equation could be used to account for a gas gap resistance term.

As seen from heat transfer prediction by the finite difference treatment for a particle array from the wall, equation C.1, C.2, and the finite difference treatment agree well at the time required for heat to propagate to one half of the particle diameter.

HCMSG6.FOR

Print file "hcmsg6.for"


```
      PROGRAM HCMPS
      CHARACTER*30 FNAME
C COMPUTES THE HEAT TRANSFER COEFFICIENT TO A COMPOSITE SOLID WITH
C HEMISPHERICAL INTERFACE
      COMMON N,R,ALFAT,WIDTH
      DATA EPS/.0001/
      PI=ACOS(-1.)
C READ INPUT PARAMETERS AND ECHO INPUT
C  CK1   = CONDUCTIVITY OF GAS
C  ALFA1 = THERMAL DIFFUSIVITY OF GAS
C  CK2   = CONDUCTIVITY OF REGION SOLID
C  ALFA2 = THERMAL DIFFUSIVITY OF SOLID
C  WIDTH = WIDTH OF GAP SEPARATING SOLID FROM WALL
C  D     = PARTICLE DIAMETER
C  FNAME = T,H OUTPUT FILE NAME
      READ(5,*)CK1,ALFA1,CK2,ALFA2,WIDTH,D,FNAME
      WRITE(6,45)CK1,ALFA1,CK2,ALFA2,WIDTH,D,FNAME
C PRELIMINARY CALCULATIONS
      SIGMA=CK2/CK1*SQRT(ALFA1/ALFA2)
      C=(SIGMA-1)/(SIGMA+1)
      R=D/2
C COMPUTE & PRINT TIME DECADE VALUES OF THE HEAT TRANSFER COEFFICIENT
      OPEN(8,FILE=FNAME)
      DO 30 I=1,60
      IF(I.LT.10)              T=.00001*I
      IF(I.GE.10.AND.I.LT.20) T=.0001+T
      IF(I.GE.20.AND.I.LT.30) T=.001+T
      IF(I.GE.30.AND.I.LT.40) T=.01+T
      IF(I.GE.40.AND.I.LT.50) T=.1+T
      IF(I.GE.50)              T=1.+T
      ALFAT=ALFA1*T
      N=1
      SUM=C*GAUSS(0.,PI/2,6)
C SUM TERMS UNTIL CONTRIBUTING TERM ADDS LESS THAN EPS TO SUMNEW
   20 N=N+1
      SUMNEW=SUM+C**N*GAUSS(0.,PI/2,6)
      IF(ABS(SUMNEW-SUM).LE.EPS*ABS(SUM)) GOTO 25
      SUM=SUMNEW
      GOTO 20
   25 H=CK1/SQRT(PI*ALFAT)*(1+2*SUMNEW)
      WRITE(8,50) T,H
   30 WRITE(*,50) T,H
      CLOSE(8)
   45 FORMAT('1K1 =    ',1PE12.4,' ALFA1 = ',E12.4/' K2 =    ',E12.4,
     $       ' ALFA2 = ',E12.4/' WIDTH = ',E12.4,' DIAMETER =',E12.4/
     $       ' OUTPUT FILE = ',A)
   50 FORMAT(' ',1P2E12.4)
      END

      FUNCTION FUNCTN(X)
C INTEGRAND TO AVERAGE HEAT TRANSFER OVER FACE OF PARTICLE
      COMMON N,R,ALFAT,WIDTH
      FUNCTN=EXP(-(N*(R*(1-COS(X))+WIDTH))**2/ALFAT)*COS(X)
      RETURN
      END

      FUNCTION GAUSS(A,B,M)
C CALCULATES INTEGRAL OF INTEGRAND FUNCTN FROM LIMITS A TO B
C BY M POINT GAUSSIAN INTEGRATION
C
C  REFERENCE:
C
C  CARNAHAN, BRICE, H. A. LUTHER, AND JAMES O. WILKES. *APPLIED NUMERICAL
C  METHODS*, JOHN WILEY & SONS, 1969, 101-105.
C
```

Print file "hcmsg6.for"

```
      EXTERNAL FUNCTN
      DIMENSION NPOINT(8),KEY(9),Z(40),WGHT(40)
      DATA NPOINT/2,3,4,5,6,10,15,32/
      DATA KEY/1,2,4,6,9,12,17,25,41/
      DATA Z   /0.577350269,0.0         ,0.774596669,0.339981044,
     1          0.861136312,0.0         ,0.538469310,0.906179846,
     2          0.238619186,0.661209387,0.932469514,0.148874339,
     3          0.433395394,0.679409568,0.865063367,0.973906529,
     4          0.0         ,0.201194094,0.394151347,0.570972173,
     5          0.724417731,0.848206583,0.937273392,0.987992518,
     6          .0483076656,.1444719615,.2392873622,.3318686022,
     7          .4213512761,.5068999089,.5877157572,.6630442669,
     8          .7321821187,.7944837959,.8493676137,.8963211557,
     9          .9349060759,.9647622555,.9856115115,.9972638618/
      DATA WGHT /1.0        ,0.888888889,0.555555556,0.652145155,
     1          0.347854845,0.568888889,0.478628671,0.236926885,
     2          0.467913935,0.360761573,0.171324493,0.295524225,
     3          0.269266719,0.219086363,0.149451349,0.066671344,
     4          0.202578242,0.198431485,0.186161000,0.162269206,
     5          0.139570678,0.107159221,0.070366047,0.030753242,
     6          .0965400885,.0956387200,.0938443990,.0911738786,
     7          .0876520930,.0833119242,.0781938957,.0723457941,
     8          .0658222227,.0586840934,.0509980592,.0428358980,
     9          .0342738629,.0253920653,.0162743947,.0070186100/
      DO 1 I=1,8
    1 IF(M.EQ.NPOINT(I))GOTO 2
      WRITE(*,7)M
    7 FORMAT('ERROR GAUSS: M IS 2,3,4,5,6,10,15 OR 32 NOT ',I3)
      RETURN
    2 GAUSS=0.
      JF=KEY(I)
      JL=KEY(I+1)-1
      SUM=0.
      C=(B-A)/2.
      D=(B+A)/2.
      DO 6 J=JF,JL
      IF(Z(J).EQ.0)SUM=SUM+WGHT(J)*FUNCTN(D)
    6 IF(Z(J).NE.0)SUM=SUM+WGHT(J)*(FUNCTN(Z(J)*C+D)+FUNCTN(-Z(J)*C+D))
      GAUSS=C*SUM
      RETURN
      END
```

Appendix D

Finite Difference Calculation of Heat Transfer Coefficient to Packed Beds

D.1. Summary

The programs reviewed in this appendix have advantages over previous moving packed bed heat transfer programs. Similar methods of numerical analysis to determine the heat transfer coefficient to a bed of solids have been used by researchers since Botterill and Williams (2) however these methods incorporate a comparably slow relaxation method of temperature convergence to solve the unsteady state heat transfer equation. Unlike the earlier programs, a simpler and apparently more accurate finite difference representation for the temperature gradient at the heated wall is used to calculate the heat flux. Both programs, one each to treat slab and cylindrical geometries, are unique in that they allow any node in the map to assume a property (i.e. conductivity, density, and specific heat) defined by the user. No particular pattern of node and property arrangement needs to be followed. Finally, the method's speed facilitates longer simulation times and larger map sizes.

D.2 Provisions

1. One of ten individually defined properties may be selected for each node.

2. A choice of ten node dimensions for the axial and radial directions may be separately defined.

3. The time step size and frequency of output summary listings may be changed as the program proceeds.

4. The results of a run may be copied to a binary dump file from which a run may be restarted at a later time.

5. The instantaneous values of the heat transfer coefficient may be saved to a file which may be read by a plotting program.

6. A map size of up to 50x50 node elements may be defined. This is limited only by the maximum array size accommodated by the MS FORTRAN compiler.

7. The implicit alternating direction (IAD) method has been employed with a tridiagonal Gaussian elimination matrix solution to ensure minimum time.

D.3. Model Assumptions

1. Material properties may vary in two dimensions. For the slab material properties may vary in both vertical and horizontal directions whereas for the cylinder materials may vary radially and axially but not azimuthally.

2. Node sizes may vary in two dimensions.

3. Temperature at the heated wall remains constant.

4. The bed configuration is symmetric at the top and bottom boundaries of the map so that its axial temperature distribution has a mirror image about these boundaries. Therefore the temperature gradient is defined as zero here.

5. To model the right hand boundary as if it extended infinitely, the zero temperature gradient is defined there.

6. The transient heat conduction equation is solved for temperatures relative to the initial temperature of the bed and so the bed is represented with a zero temperature difference at

time zero.

7. Material properties do not change with time or temperature.

D.4. Derivation of Finite Difference Equations

A finite difference solution of the transient heat conduction equation requires a discrete representation of temperatures at the intersection points of a grid of nodes, each node interior modeling a different two dimensional position or material property. To each node and its adjacent nodes is applied a finite difference expression of the transient heat conduction equation and boundary condition equations are added to treat nodes at boundaries of the map. Using either a relaxation or matrix solver method the equations are solved simultaneously for all node temperatures at small time increments beginning from an initial temperature state, each time step chosen small enough to ensure convergence of the solution. A heat transfer coefficient local to each node at the "heated" boundary is calculated from the temperature gradient and node conductivity there. The local heat transfer coefficient is then averaged and recorded. The development and programming of the finite difference equations, the coefficients of the IAD solution, and heat transfer coefficient calculation is

presented here.

D.4.1 Representation

Figure (D.1) illustrates the map used to represent position and property in cylindrical or slab geometries. The map has M-1 cells and M interior points radially or horizontally. A node may be distinguished as a cell and a point. Cells outside and adjacent to the zero temperature gradient boundaries are indicated by dashed lines and possess properties identical to their neighbors across the boundaries. At the right hand boundary the temperature gradient is approximated by

$$\frac{\partial T}{\partial x} \approx \frac{T_{kN} - T_{kN+1}}{\Delta x_N}$$

This requires $T_{kN} = T_{kN+1}$ for a zero temperature gradient. The top and bottom boundaries could be treated similarly but a more accurate representation would account for symmetry about the boundary and so we treat temperatures on either side of the boundary as equivalent. The boundary condition equations are then

$$\begin{array}{lll} 1. & \text{Left:} & T_{k0} = T_{wall} \\ 2. & \text{Right:} & T_{kN} = T_{kN+1} \\ 3. & \text{Top:} & T_{M-1j} = T_{M+1j} \\ 4. & \text{Bottom:} & T_{0j} = T_{2j} \end{array} \qquad (D.1)$$

Consider the dashed region at the intersection of four nodes as shown in Figure (D.2). At each one quarter node region adjacent to the intersection

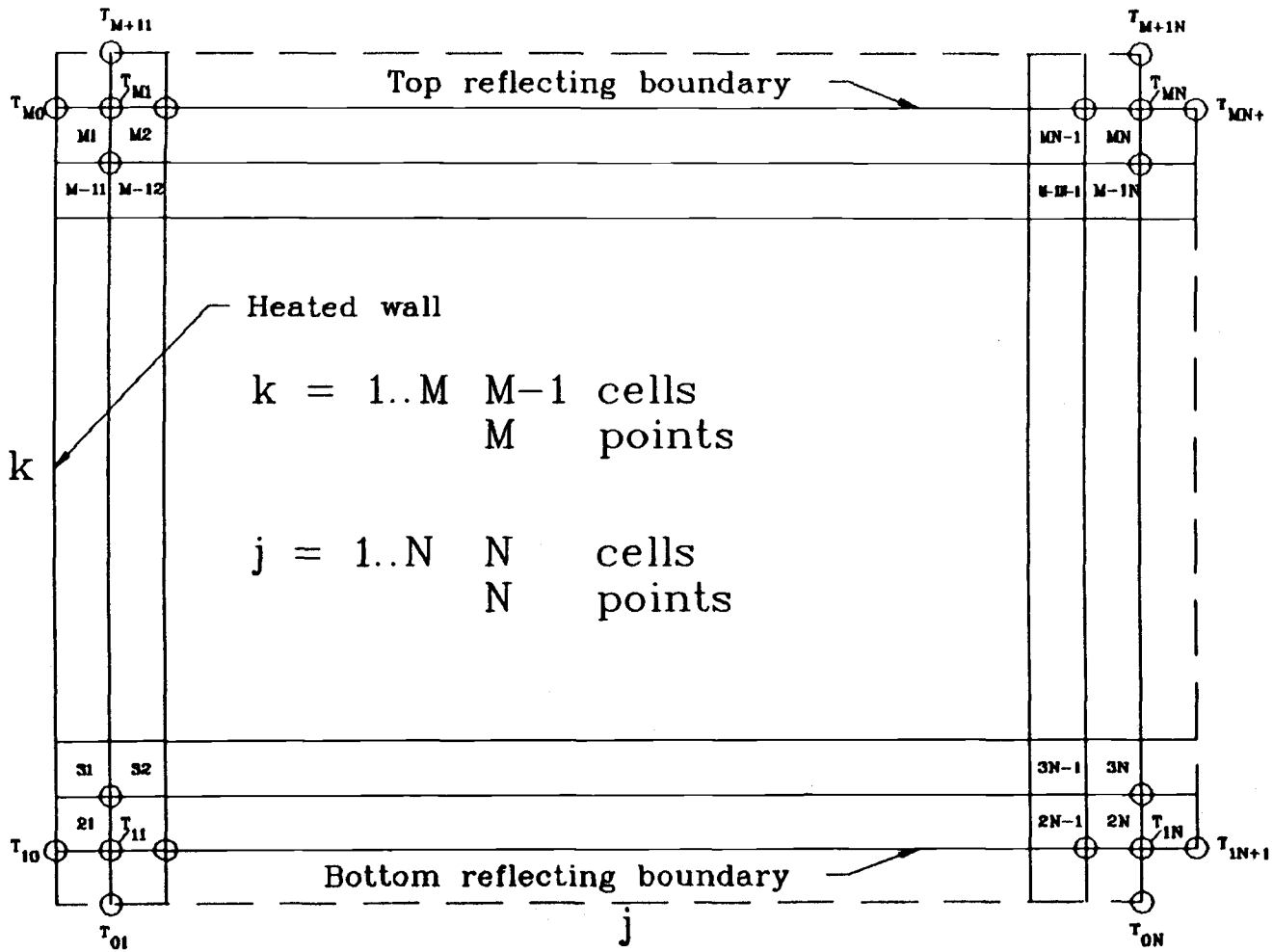

Figure (D.1). Finite difference map to model wall-to-bed heat transfer.

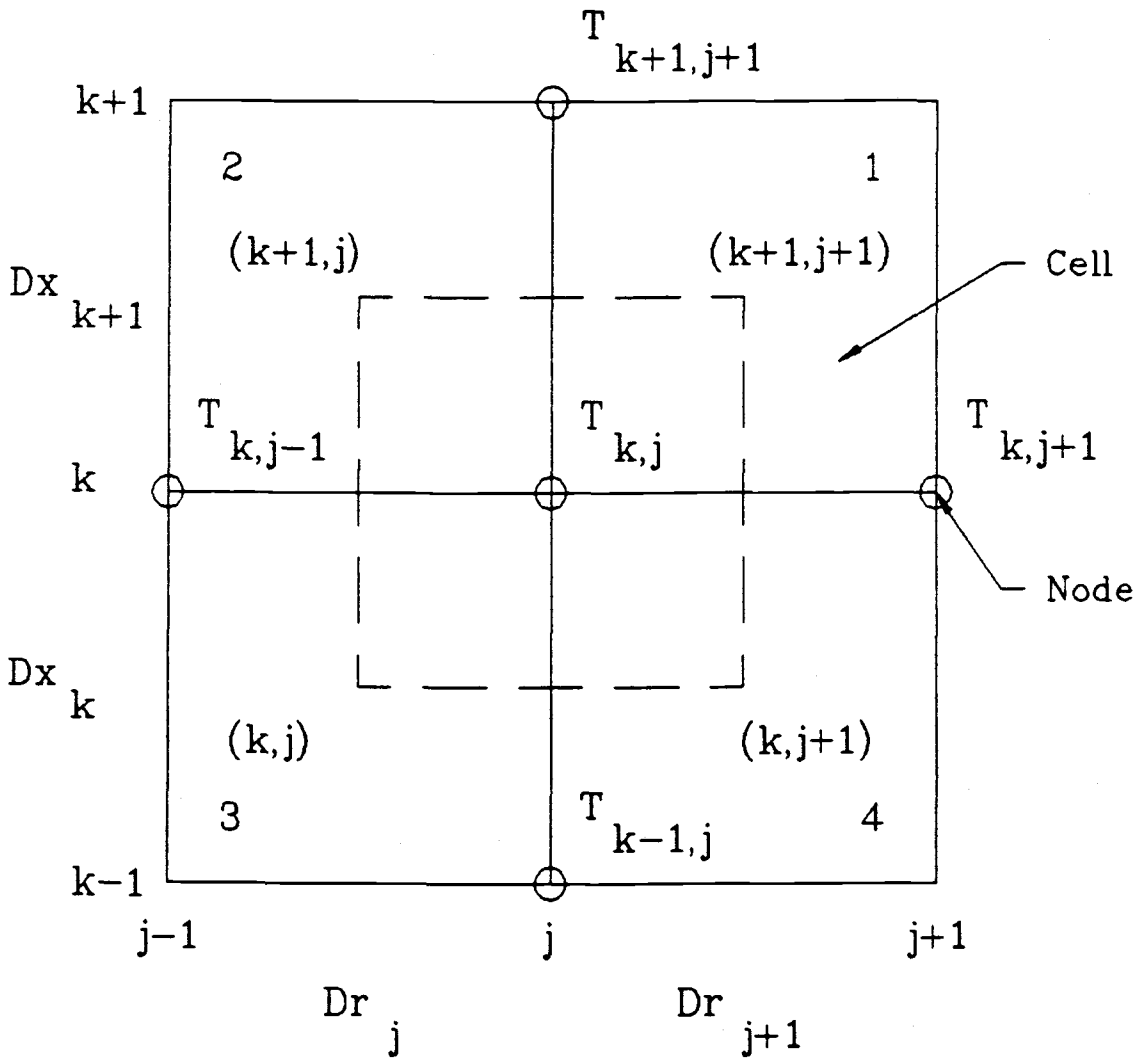

Figure (D.2). Example of cell noding scheme.

temperature is assumed single valued. Each cell and its characteristic property is identified by number or by indices k,j. The transient heat conduction equation

$$\nabla \cdot k\nabla T = \rho Cp\frac{\partial T}{\partial t}$$

will be integrated over the equivalent node volume represented by the dashed region.

$$\int_V \nabla \cdot k\nabla T \, dV = \frac{\partial T}{\partial t}\int_V \rho Cp dV \qquad (D.2)$$

To simplify the analysis, the divergence theorem will be applied to the LHS of D.2.

$$\int_V \nabla \cdot k\nabla T \, dV = \int_S k\nabla T \cdot \mathbf{n} \, dS \qquad (D.3)$$

where **n** is a unit outward normal.

D.4.2. Cylinder

The RHS of D.3 may be separated into radial and axial components

$$\int_S k\nabla T \cdot \mathbf{n} dS = \int_S k\nabla T \cdot \mathbf{e}_r dS + \int_S k\nabla T \cdot \mathbf{e}_x dS \qquad (D.4)$$

where $\mathbf{e}_r$ and $\mathbf{e}_x$ are radial and axial unit vectors, respectfully. Evaluate the integral for the finite difference terms of the LHS of D.2 using D.3 and D.4 as substitutions

$$\int_S k\nabla T\cdot e_r dS = \frac{T_{kj-1}-T_{kj}}{\Delta r_j}\left[k_2\left[\frac{2\pi(r_j-\Delta r_j/2)\Delta x_{k+1}}{2}\right] + k_3\left[\frac{2\pi(r_j-\Delta r_j/2)\Delta x_k}{2}\right]\right]$$

$$+ \frac{T_{kj+1}-T_{kj}}{\Delta r_{j+1}}\left[k_1\left[\frac{2\pi(r_j+\Delta r_{j+1}/2)\Delta x_{k+1}}{2}\right] + k_4\left[\frac{2\pi(r_j+\Delta r_{j+1}/2)\Delta x_k}{2}\right]\right]$$

$$\int_S k\nabla T\cdot e_x dS = \frac{T_{k+1j}-T_{kj}}{\Delta x_{k+1}}\left[k_2\left[\pi r_j^2 - \pi(r_j-\Delta r_j/2)^2\right] + k_1\left[\pi(r_j+\Delta r_{j+1}/2)^2-\pi r_j^2\right]\right]$$

$$+ \frac{T_{k-1j}-T_{kj}}{\Delta x_k}\left[k_3\left[\pi r_j^2 - \pi(r_j-\Delta r_j/2)^2\right] + k_4\left[\pi(r_j+\Delta r_{j+1}/2)^2-\pi r_j^2\right]\right]$$

After some simplification,

$$\int_S k\nabla T\cdot e_r dS = \pi[aT_{kj+1} + bT_{kj-1} - (a+b)T_{kj}]$$

$$\int_S k\nabla T\cdot e_x dS = \pi[cT_{k+1j} + dT_{k-1j} - (c+d)T_{kj}] \qquad (D.5)$$

where

$$a = \frac{(k_1\Delta x_{k+1} + k_4\Delta x_k)(r_j + \Delta r_{j+1}/2)}{\Delta r_{j+1}}$$

$$b = \frac{(k_2\Delta x_{k+1} + k_3\Delta x_k)(r_j - \Delta r_j/2)}{\Delta r_j}$$

$$c = \frac{k_2\Delta r_j(r_j - \Delta r_j/4) + k_1\Delta r_{j+1}(r_j + \Delta r_{j+1}/4)}{\Delta x_{k+1}}$$

$$d = \frac{k_3\Delta r_j(r_j - \Delta r_j/4) + k_4\Delta r_{j+1}(r_j + \Delta r_{j+1}/4)}{\Delta x_k}$$

Evaluate now the integral term on the RHS of D.2.

$$\begin{aligned}\int_V \rho Cp dV = \frac{\pi}{2}(&\rho_1 Cp_1\Delta x_{k+1}\Delta r_{j+1}(r_j + \Delta r_{j+1}/4) + \\ &\rho_2 Cp_2\Delta x_{k+1}\Delta r_j \ (r_j - \Delta r_j/4) + \\ &\rho_4 Cp_4\Delta x_k \ \Delta r_{j+1}(r_j + \Delta r_{j+1}/4) + \\ &\rho_3 Cp_3\Delta x_k \ \Delta r_j \ (r_j - \Delta r_j/4)) \\ = \pi\ &(\Delta t/2)\ e \qquad (D.6)\end{aligned}$$

where

$$e = [(\rho_1 Cp_1\Delta x_{k+1} + \rho_4 Cp_4\Delta x_k)\Delta r_{j+1}(r_j + \Delta r_{j+1}/4) + (\rho_2 Cp_2\Delta x_{k+1} + \rho_3 Cp_3\Delta x_k)\Delta r_j \ (r_j - \Delta r_j/4))]/\Delta t.$$

Combining D.5 and D.6 yields the finite difference equation for the interior nodes of the cylinder

$$\frac{\partial T}{\partial t}(\Delta t/2)e = aT_{kj+1} + bT_{kj-1} - (a+b)T_{kj} + cT_{k+1j} + dT_{k-1j} - (c+d)T_{kj} \qquad (D.7)$$

The same form of equation set D.7 is used at the map boundaries only the constant terms a, b, c, d, and e may be simplified since cells immediately across the boundary have like properties.

Top: $k = M$

$a = 2k_4\Delta x_M(r_j + \Delta r_{j+1}/2)/\Delta r_{j+1}$

$b = 2k_3\Delta x_M(r_j - \Delta r_j/2)/\Delta r_j$

$c = d$

$$d = \frac{k_3 \Delta r_j (r_j - \Delta r_j/4) + k_4 \Delta r_{j+1} (r_j + \Delta r_{j+1}/4)}{\Delta x_k}$$

$$e = 2\Delta x_M (\rho_4 Cp_4 \Delta r_{j+1} (r_j + \Delta r_{j+1}/4) + \rho_3 Cp_3 \Delta r_j (r_j - \Delta r_j/4))/\Delta t$$

Bottom: $k = 2$

$a = 2k_1 \Delta x_2 (r_j + \Delta r_{j+1}/2)/\Delta r_{j+1}$

$b = 2k_2 \Delta x_2 (r_j - \Delta r_j/2)/\Delta r_j$

$$c = \frac{k_2 \Delta r_j (r_j - \Delta r_j/4) + k_1 \Delta r_{j+1} (r_j + \Delta r_{j+1}/4)}{\Delta x_{k+1}}$$

$d = c$

$$e = 2\Delta x_2 (\rho_1 Cp_1 \Delta r_{j+1} (r_j + \Delta r_{j+1}/4) + \rho_2 Cp_2 \Delta r_j (r_j - \Delta r_j/4))/\Delta t$$

Bottom right: $k = 2$, $j = N$

$b = 2k_2 \Delta x_2 (r_N - \Delta r_N/2)/\Delta r_N$

$c = 2k_2 \Delta r_N r_N/\Delta x_2$

$d = c$

$e = 4 r_j \rho_2 Cp_2 \Delta x_2 \Delta r_N/\Delta t$

Top right: $k = M$, $j = N$

$b = 2k_3 \Delta x_M (r_N - \Delta r_N/2)/r_N$

$c = 2k_3 \Delta r_N r_N/\Delta x_M$

$d = c$

$e = 4 r_j \rho_3 Cp_3 \Delta x_M \Delta r_N/\Delta t$

Right: $j = N$

$$b = \frac{(k_2\Delta x_{k+1} + k_3\Delta x_k)(r_j - \Delta r_j/2)}{\Delta r_j}$$

$$c = 2k_2\Delta r_N r_N/\Delta x_{k+1}$$

$$d = 2k_3\Delta r_N r_N/\Delta x_k$$

$$e = 2r_j\Delta r_N[\rho_2 Cp_2\Delta x_{k+1} + \rho_3 Cp_3\Delta x_k]/\Delta t$$

D.4.3. Slab

The derivation of the finite difference equations for the slab is similar. Separate the RHS of D.3 into vertical and horizontal components

$$\int_S k\nabla T\cdot \mathbf{n}dS = \int_S k\nabla T\cdot \mathbf{e}_x dS + \int_S k\nabla T\cdot \mathbf{e}_y dS \qquad (D.8)$$

where $\mathbf{e}_y$ and e_x are vertical and horizontal unit vectors, respectfully. Evaluate each term of D.8

$$\int_S k\nabla T\cdot e_x dS = \frac{T_{kj-1}-T_{kj}}{2\Delta x_j}(k_2\Delta y_{k+1} + k_3\Delta y_k) + \frac{T_{kj+1}-T_{kj}}{2\ x_{j+1}}(k_1\Delta y_{k+1} + k_4\Delta y_k)$$

$$\int_S k\nabla T\cdot \mathbf{e}_y dS = \frac{T_{k+1j}-T_{kj}}{2\Delta y_{k+1}}(k_1\Delta x_{j+1} + k_2\Delta x_j) + \frac{T_{k-1j}-T_{kj}}{2\Delta y_k}(k_4\Delta x_{j+1} + k_3\Delta x_j).$$

After simplification

$$\int_S k\nabla T\cdot e_x dS = [aT_{kj+1} + bT_{kj-1} - (a+b)T_{kj}]/2$$

$$\int_S k\nabla T\cdot e_y dS = [cT_{k+1j} + dT_{k-1j} - (c+d)T_{kj}]/2 \qquad (D.9)$$

where

$$a = (k_1\Delta y_{k+1} + k_4\Delta y_k)/\Delta x_{j+1}$$

$$b = (k_2\Delta y_{k+1} + k_3\Delta y_k)/\Delta x_j$$

$$c = (k_1\Delta x_{j+1} + k_2\Delta x_j)/\Delta y_{k+1}$$

$$d = (k_4\Delta x_{j+1} + k_3\Delta x_j)/\Delta y_k.$$

The LHS of D.2 as applied to slab geometry is

$$\int_V \rho Cp dV = (\rho_1 Cp_1\Delta y_{k+1}\Delta x_{j+1} + \rho_2 Cp_2\Delta y_{k+1}\Delta x_j + \rho_3 Cp_3\Delta y_k\Delta x_j + \rho_4 Cp_4\Delta y_k\Delta x_{j+1})/4$$

$$= (\Delta t/2)e/2 \qquad (D.10)$$

where

$$e = (\rho_1 Cp_1\Delta y_{k+1}\Delta x_{j+1} + \rho_2 Cp_2\Delta y_{k+1}\Delta x_j + \rho_3 Cp_3\Delta y_k\Delta x_j + \rho_4 Cp_4\Delta y_k\Delta x_{j+1})/\Delta t$$

Once D.9 and D.10 are combined for the finite difference approximation for the slab we obtain D.7. Finally, the constant simplifications at the slab boundaries are.

Top: $k = M$

$$a = 2k_4\Delta y_M/\Delta x_{j+1}$$

$$b = 2k_3\Delta y_M/\Delta x_j$$

$$c = d$$

$$d = \frac{k_3\Delta x_j + k_4\Delta x_{j+1}}{\Delta y_M}$$

$e = 2\Delta y_M(\rho_4 Cp_4 \Delta x_{j+1} + \rho_3 Cp_3 \Delta x_j)/\Delta t$

Bottom: $k = 2$

$a = 2k_1 \Delta y_2/\Delta x_{j+1}$

$b = 2k_2 \Delta y_2/\Delta x_j$

$c = (k_1 \Delta x_{j+1} + k_2 \Delta x_j)/\Delta y_2$

$d = c$

$e = 2\Delta y_2(\rho_1 Cp_1 \Delta x_{j+1} + \rho_2 Cp_2 \Delta x_j)/\Delta t$

Bottom right: $k = 2$, $j = N$

$b = 2k_2 \Delta y_2/\Delta x_N$

$c = 2k_2 \Delta x_N/\Delta y_2$

$d = c$

$e = 4\rho_2 Cp_2 \Delta x_N \Delta y_2/\Delta t$

Top right: $k = M$, $j = N$

$b = 2k_3 \Delta y_M/\Delta x_N$

$c = 2k_3 \Delta x_N/\Delta y_2$

$d = c$

$e = 4\rho_3 Cp_3 \Delta x_N \Delta y_M/\Delta t$

Right: $j = N$

$b = (k_2 \Delta y_{k+1} + k_3 \Delta y_k)/\Delta x_N$

$c = 2k_2 \Delta x_N/\Delta y_{k+1}$

$d = 2k_3 \Delta x_N/\Delta y_k$

$e = 2\Delta x_N(\rho_2 Cp_2 \Delta y_{k+1} + \rho_3 Cp_3 \Delta y_k)/\Delta t$

D.5. Implicit Alternating Direction (IAD) Solution Method

To solve the system of five point difference equations defined by D.7 for nodal temperatures the IAD algorithm is employed (1). The IAD method requires significantly less computation time and array size than Gaussian elimination or Gauss-Siedel methods of matrix inversion. The method uses two difference equations to represent temperatures in a single dimension. The equation for each dimension applies for one half a time step, which the method repeatedly applies for a solution of all successive time steps. This enables tridiagonal matrix solutions separately implicit by row (k) or column (j). The finite difference equations for the IAD method applied to heat conduction in a cylinder originate from

$$\frac{T_{kji+1} - T_{kj*}}{\Delta t/2} \int_V \rho C p dV =$$

$$\int_S k\nabla T_{kj*} \cdot e_r dS + \int_S k\nabla T_{kji+1} \cdot e_x dS$$

$$\frac{T_{kj*} - T_{kji}}{\Delta t/2} \int_V \rho C p dV =$$

$$\int_S k\nabla T_{kj*} \cdot e_r dS + \int_S k\nabla T_{kji} \cdot e_x dS$$

where time step subscript i indicates temperatures prior

a time step, i+1 indicates temperatures following a full time step, and * references temperatures at one half a time step.

This becomes, after use of D.7,

$$-aT_{kj+1*}-bT_{kj-1*}+(a+b+e)T_{kj*} = [cT_{k+1j}+dT_{k-1j}-(c+d-e)T_{kj}]_i \quad \text{(D.11a)}$$

$$-aT_{kj+1*}-bT_{kj-1*}+(a+b-e)T_{kj*} = [cT_{k+1j}+dT_{k-1j}-(c+d+e)T_{kj}]_{i+1} \quad \text{(D.11b)}.$$

The method first solves the map for temperatures at one half time step (LHS of D.11a) from initial temperatures (RHS of D.11a), then temperatures are solved at the full time step (RHS of D.11b) from the half time step temperature map. The coefficients of D.11 may be generalized into the upper, lower, and diagonal terms of a tridiagonal matrix.

$$U_kT_{kj+1*}+L_kT_{kj-1*}+D_{k1}T_{kj*} = [U_jT_{k+1j}+L_jT_{k-1j}+D_{j1}T_{kj}]_i \quad \text{(D.12a)}$$

$$U_kT_{kj+1*}+L_kT_{kj-1*}+D_{k2}T_{kj*} = [U_jT_{k+1j}+L_jT_{k-1j}+D_{j2}T_{kj}]_{i+1} \quad \text{(D.12b)}$$

where

$U_k = -a, \qquad D_{k1} = a + b + e$

$U_j = c, \qquad D_{j1} = -(c + d - e)$

$L_k = -b, \qquad D_{k2} = a + b - e$

$L_j = d, \qquad D_{j2} = -(c + d + e)$

At the map boundaries, use of boundary equations D.1 into D.12 requires modification of these constants.

Top: $k = M$

$U_k = -a, \qquad D_{k1} = a + b + e$

$U_j = 0, \qquad D_{j1} = -(c + d - e)$

$L_k = -b, \qquad D_{k2} = a + b - e$

$L_j = c + d, \qquad D_{j2} = -(c + d + e)$

Bottom: $k = 2$

$U_k = -a, \qquad D_{k1} = a + b + e$

$U_j = c + d, \qquad D_{j1} = -(c + d - e)$

$L_k = -b, \qquad D_{k2} = a + b - e$

$L_j = 0, \qquad D_{j2} = -(c + d + e)$

Bottom right: $k = 2$, $j = N$

$U_k = 0, \qquad D_{k1} = b + e$

$U_j = c + d, \qquad D_{j1} = -(c + d - e)$

$L_k = -b, \qquad D_{k2} = b - e$

$L_j = 0, \qquad D_{j2} = -(c + d + e)$

Top right: $k = M$, $j = N$

$U_k = 0, \qquad D_{k1} = b + e$

$U_j = 0, \qquad D_{j1} = -(c + d - e)$

$L_k = -b, \qquad D_{k2} = b - e$

$L_j = c + d, \qquad D_{j2} = -(c + d + e)$

Right: $j = N$

$U_k = 0, \qquad D_{k1} = b + e$

$U_j = c, \qquad D_{j1} = -(c + d - e)$

$L_k = -b, \qquad D_{k2} = b - e$

$L_j = d, \qquad D_{j2} = -(c + d + e)$

D.6. Heat Transfer Coefficient Calculation

The previous sections covered finite difference formulation of the transient heat conduction equation, boundary conditions representation, and coefficient definition. This section will explain calculation of the local and average heat transfer coefficient at the heated wall from the temperature solution. As with the assumptions outlined earlier, both properties and axial or radial step size may vary in this solution.

The local heat transfer coefficient is given by $h_k = q''_k/V_0$ where V_0 is the temperature difference from the wall to the initial bed temperature and q''_k is the heat flux at the wall for cell k. Refer to Figure (D.3) which is a representation of axial nodes and cells adjacent to the heated wall. If

$$q''_k = -k\frac{\partial T}{\partial r} \approx k\,\frac{(T_{k0} - T_{k1})}{\Delta r_1}$$

where conductivity k is an average for the properties of the cell separating T_{k0} and T_{k1}, then the heat flux term at the wall is

$$q''_k = \left(\frac{T_{k0} - T_{k1}}{\Delta r_1}\right)\left(\frac{k_{k+1,1}\Delta x_{k+1} + k_{k,1}\Delta x_k}{\Delta x_{k+1} + \Delta x_k}\right)$$

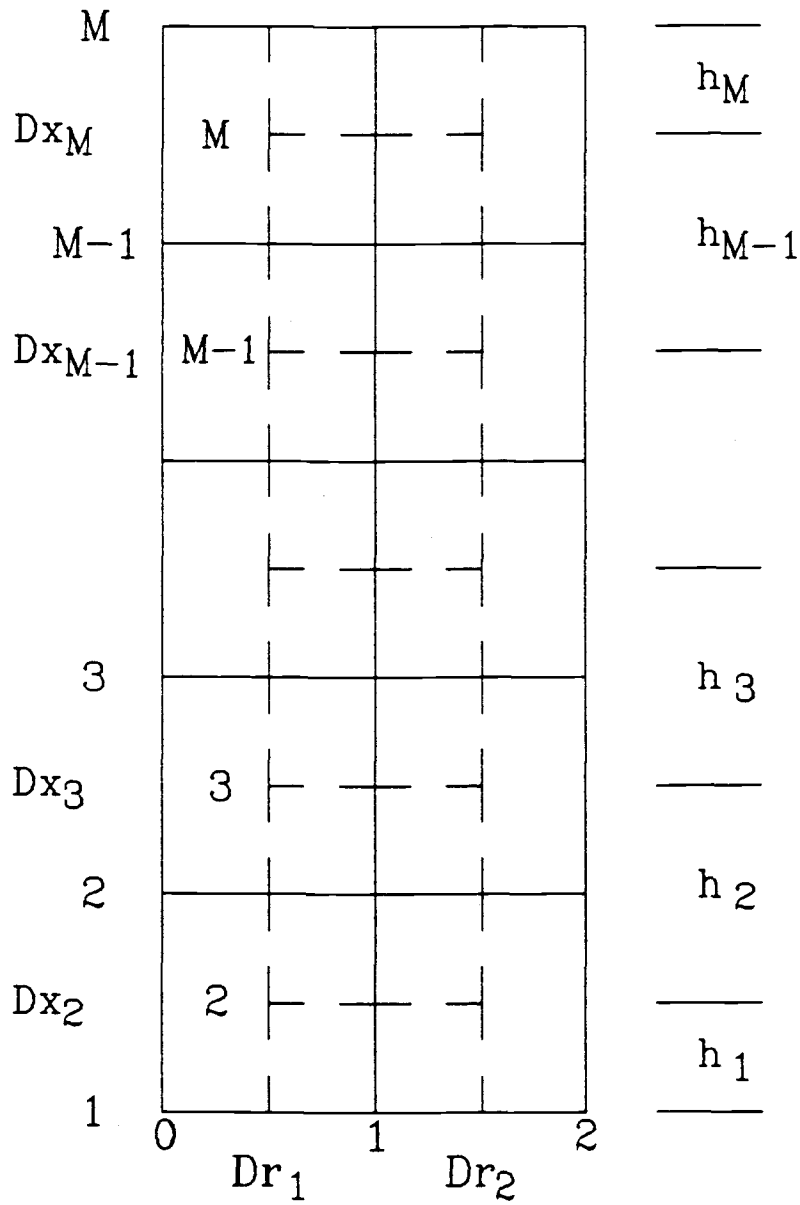

Figure (D.3). Finite difference scheme at wall to obtain axial average heat transfer coefficient.

Since half height cells lie at the top and bottom of the map and these have a constant conductivity, the heat flux there is

$$q''_1 = k_{21} \frac{(T_{10} - T_{11})}{\Delta r_1}$$

$$q''_M = k_{M1} \frac{(T_{M0} - T_{M1})}{\Delta r_1}$$

For an average h about the map height we use

$$h_{ave} = (\int_L h \, dx)/L \approx \frac{\sum_{k=1}^{M} h_k \, (\Delta x_k + \Delta x_{k+1})/2}{L}$$

where

$$L = \sum_{k=2}^{M} \Delta x$$

and for the symmetric top and bottom boundary cells $\Delta x_1 = \Delta x_2$ and $\Delta x_M = \Delta x_{M+1}$.

D.7. Verification

Both slab and cylinder geometry codes were verified repeatedly for temperature and/or heat transfer coefficient calculation with the following analytic methods:

1. Homogeneous properties for slab and cylinder with large inner radius specified.

2. Cylinder with homogeneous properties (Eq. A.1).

3. Two region composite slab for slab and cylinder with large inner radius (Eq. B.1, C.1).

4. Steady state solutions for slab and cylinder chosen for large time solutions and mixed materials.

D.8. Input Selection

This section introduces constraints which when applied to input selection ensure the numerical model performs well under finite node size and region length assumptions. This treatment is subjective but has demonstrated to be effective.

D.8.1. Length of Region

The numerical solution assumes a satisfactory result for the heat transfer coefficient may be obtained by considering a region of finite width with the temperature gradient set to zero at the boundary. As shown previously, the temperature gradient at the boundary will eventually be non-zero. The question then arises to what accuracy would we expect the numerical solution to have for the region length as a function of

time. Consider the region to have homogeneous properties, then the temperature gradient at the heated surface for the semi-infinite slab is

$$\left.\frac{\partial T}{\partial x}\right|_{x=0} = \frac{-V}{\sqrt{\pi\alpha t}} = \frac{-V}{L\sqrt{\pi Fo_L}}$$

where

L = radial length of region.

$Fo_L = \alpha t/L^2$.

t = total time of solution.

The temperature gradient at the heated wall for a finite slab with insulated boundary is

$$\left.\frac{\partial T}{\partial x}\right|_{x=0} = -\frac{2V}{L}\sum_{n=0}^{\infty} e^{-\alpha t[(2n+1)\pi/(2L)]^2}$$

$$= -\frac{2V}{L}\sum_{n=0}^{\infty} e^{-\alpha t[Fo_L((2n+1)\pi/2)^2]}$$

To calculate a heat flux equivalent to either model we would like these temperature gradients equal, or as close as possible with a relative error ϵ so

$$\epsilon = 1 - w\sum_{n=0}^{\infty} e^{-\pi[w(2n+1)/4)^2]}$$

where $w = 2\sqrt{\pi Fo_L}$. This function has been plotted and appears in Figure (D.4). For an error of at most 10%, then, we would choose $Fo_L = .33$ or less. Our criteria is then to choose an Fo_L so that $Fo_L < Fo_L(\epsilon)$ where $Fo_L(\epsilon)$ was calculated with the equation above for error ϵ.

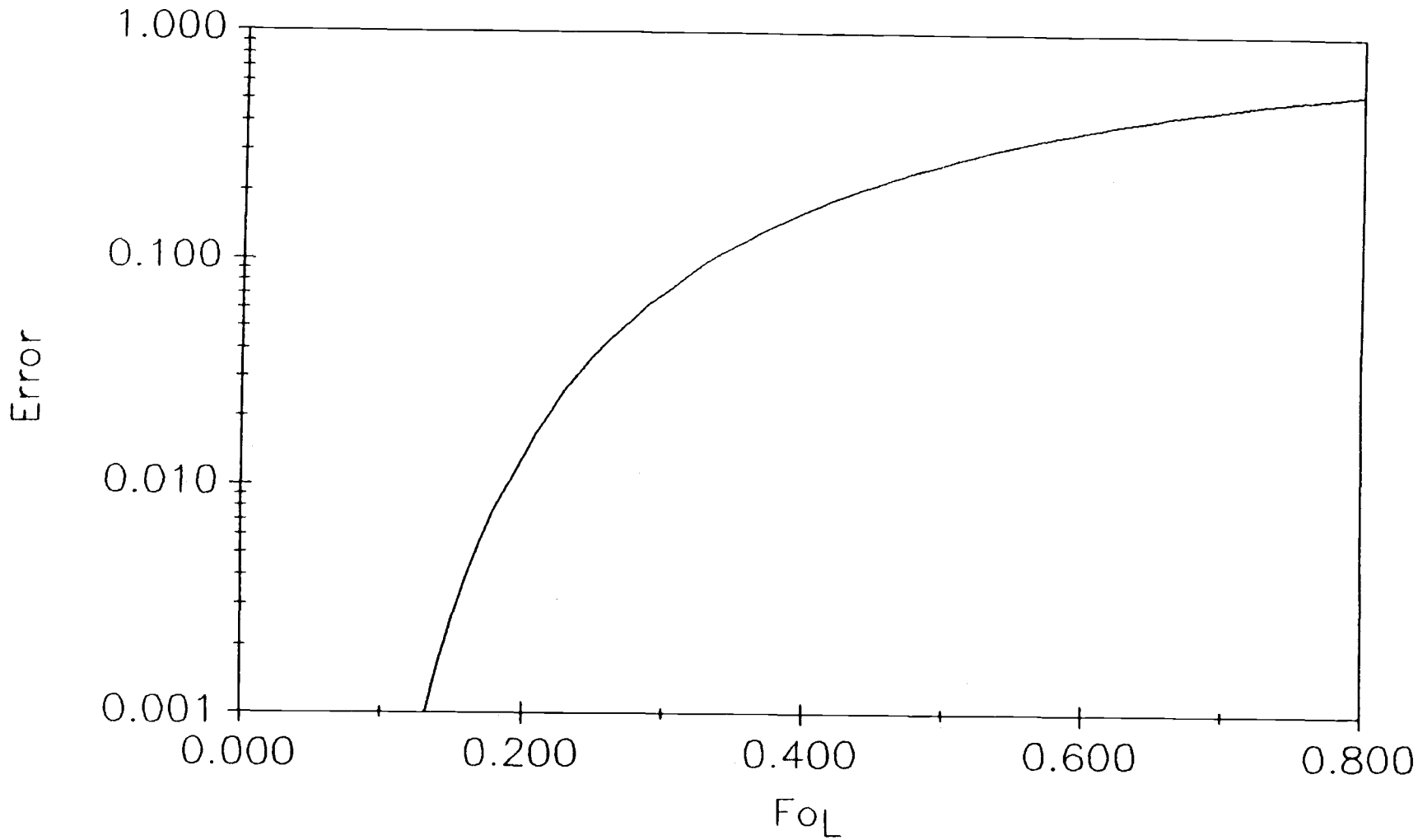

Figure (D.4). Error introduced by modeling a semi-infinite slab as a finite slab.

If the region is not homogeneous (as all numerical solutions of interest for h will be) then the region's effective properties are used and the above criteria is still a good assumption since it is known that as the region is heated it becomes increasingly accurate to model it with effective properties (hence the assumption that by heating three particle diameters from the heated surface the region may be treated as effective).

D.8.2. Choice of Step Size and Simulation Time

The numerical treatment of the transient heat conduction equation depends upon dividing the heat conducting region into cells small enough such that the temperature gradients may be reasonably approximated as the slope of temperature points separated by a cell. Due to the thermal diffusivity characteristic of a heat conducting material, heat requires a finite time to propagate. Cell size should be chosen for some length less than the distance heat will propagate over one time step otherwise temperature gradients will not be calculated correctly. With regard to the temperature gradient at the heated surface, there is some time and cell size for which the temperature gradient cannot be calculated correctly once the solution begins from initial state. If the first cell is small compared to the entire region we could assume the temperature

gradient as the node begins to heat is given by

$$\left.\frac{\partial T}{\partial x}\right|_{x=0} = \frac{-V}{\sqrt{\pi \alpha t}}$$

which is that of the semi-infinite slab. Numerically, the temperature gradient could be represented as

$$\left.\frac{\partial T}{\partial x}\right|_{x} \approx \frac{-V}{\Delta x}$$

however an improved numerical approximation for the derivative is:

$$\left.\frac{\partial T}{\partial x}\right|_{x} \approx \frac{-V}{2\Delta x}$$

Set the analytic and numerical derivative together as

$$\frac{-V}{\sqrt{\pi \alpha t_d}} = \frac{-V}{2\Delta x}$$

and solve

$$4/\pi = Fo_d$$

where $Fo_d = \alpha t_d/\Delta x^2$. Since smaller Δx values lead to a better representation for the gradient our criteria is $Fo_d \leq 4/\pi$. This criteria should be applied to the cell with the smallest size and largest thermal diffusivity to determine t_d, the maximum time step of the solution. A time step less than t_d should be chosen to ensure accuracy of the solution. An increase in time step is however a possibility once cells of minimum t_d value

have been heated long enough such that the temperature difference across them has become negligible.

If the time step size is significantly less than the minimum t_d value of all cells adjacent to the heated wall then this characteristic value represents the minimum simulation time whereafter the solution first becomes correct. To demonstrate this criteria, the numerical method was applied to calculate h for a semi-infinite slab with constant material properties--a solution which is known analytically. When arranged in the following non-dimensional form

$$h\Delta x/k = 1/(\sqrt{\pi Fo_d})$$

the Mickley and Fairbanks equation should appear as a straight line when the LHS is plotted log-log against Fo_d. Figure (D.5) shows both numerical and analytic results agree well only when Fo_d is greater than 1, or near the criteria value of $4/\pi$. When Fo_d is less than the criteria value h approaches the constant value of $k/\Delta x$. The numerical solution may also be shown to depart significantly from the analytic result upon this figure when the Fo_L number is not satisfied.

D.8.3. Selection of Cell Number

Since porosity contour is only approximated by position of block shaped cells, the smaller the cell size and the larger the number of cells used to

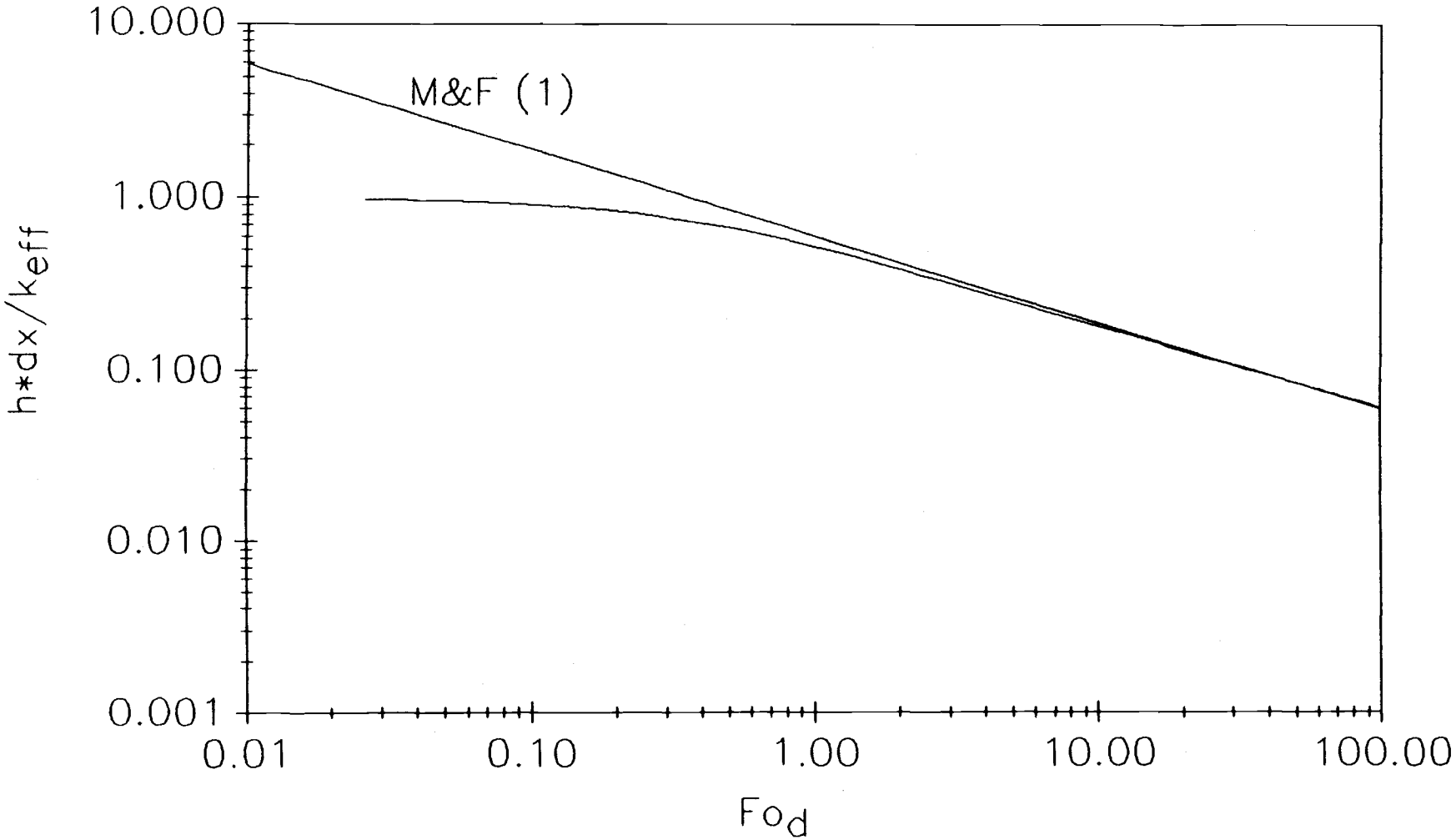

Figure (D.5). Accurary of heat transfer solution to a semi-infinite slab on Fo_d value.

represent the curve should improve the approximation. This approximation to curvature may lead to an exaggeration of particle surface in contact with the wall and therefore a corresponding increase in heat transfer coefficient should be observed. The number of cells per particle radius was increased from 5 to 10, 20, 40, 60, and 80, and the heat transfer curves were compared. When no gap was introduced, the descent of the heat transfer curve from a plateau value occurred at progressively earlier times as cell number increased. The data could be made to fit well this manner but usually with an inordinately large map size. Once a gap was introduced, then for as small a gap as $.001d_p$ a cell number of 5 to 10 per particle radius produced less than 20% difference in heat transfer.

Because the curvature of boundaries separating curved regions of unlike properties can only be approximated by placement of box-like cells, for cells that intersect the boundary an attempt to weight by cell area on either side of the boundary was made. A difference in heat transfer solutions with and without curvature correction was 1% or less for particle representations of 5 cells per radius. It therefore appears the additional complexity for curvature correction in programs by previous researchers including finite element modeling is unjustified (2,3). For the

degree of particle heating required to compare calculations of the heat transfer coefficient to data obtained for as short as 0.1s a number greater than 10 cells per particle radius does not appear to be required.

D.9. Program Utilities

To ease the chore of preparing an input map representative of porosity change with distance from the heated wall, the program MAKMAP was devised. This program produces a map of equally dimensioned square cells with property indices of 0 (void) and 1 (solid) for an array of particles. The number of cells used to represent a particle, the number of contact points to a particle, and the number of particles extending in the radial direction is selected on input. MAKMAP writes its completed map to the file MAKMAP.OUT which is later appended to an input file for the heat transfer calculation codes.

Since the porosity by distance formulation (Eq. V.D.1) is to be used to select a discrete number of void or solid cells in the input map, an average porosity for cell width Δu is

$$\epsilon(u) = 1 - \frac{\pi[1-\Delta u((u-1)+\Delta u/3)-(u-1)^2]}{n \tan(\pi/n)}.$$

where an n of 6 was chosen to model orthorhombic arrays

of particles.

MAKMAP displays the number of cells chosen for void and solid using the cell average porosity defined above as well as the solid fraction apportioned to a cell when the number of solid cells does not divide equally into a column.

D.10. Sample Run

The following input file, 385-21.txt, was prepared to compute the heat transfer coefficient to a packed bed of 0.8mm glass spheres in air through a 21μm gap. This solution applied the program for cylindrical geometry with a rod radius of 6.35mm. The input map was generated by the MAKMAP utility for five nodes per particle radius and an orthorhombic configuration. For a simulation time to 10s the criteria on Fo_L (section D.8.1) required a total radial length of 2.24mm and the Fo_d criteria (section D.8.2) required a t_d no greater than 20μs limited by the gap and a 50ms time step limited by the 80μm node size beyond the gap. A gradual increase in time step from 10μs to 20ms while the gap heated was chosen to maintain stability. The output listing is presented as 385-21.out and a plot file h185-21 and binary restart file b185-21 was also generated. A solution time of about 5min was required on an IBM AT.

D.11. Program Listings

Two versions of the heat transfer coefficient program BLAUSIS appear here to treat cylindrical and slab geometries for compilation on an IBM AT with MS FORTRAN. Source files with increased array sizes to treat a 130 x 130 node map for compilation on a high level workstation or mainframe were used but are not listed here. The program utility MAKMAP follows these listings.

References

1. Carnahan, Brice, H. A. Luther, and James O. Wilkes. Applied Numerical Methods, John Wiley & Sons, 452-453 (1969).

2. Botterill, J. S. M. and J. R. Williams. "The mechanism of heat transfer to gas-fluidised beds," Trans. Instn. Chem. Engrs., 41 217 (1963).

3. Opaliński, Irenenz and Andrezej Wolny. "Discontinuity of particle contact with the surface and heat transfer in fluidized beds," Int. J. Heat Mass Transfer, 30 589-599 (1987).

385-21.TXT

```
Print file "385-21.txt"

  Glass: 0.8mm diameter (21micron gap, 6 contacting particles)
4,' ','h185-21','b185-21'
100.,0.00635,6,31,1,2,2
1,80e-6
8,80e-6
9,21e-6
1,1.04,27E5
0,2.9282E-2,1.047E3
  100,1E-5,100,1,5
  100,1E-4, 50,1,5
  100,1E-2, 20,1,5
  500,2E-2, 50,1,5
1111111111111111111111
988888888888888888888888888888
000000000000000000000000000000
000011110000001111000000111100 0
000111111000001111111000011111100
001111111100111111111001111111110
011111111111111111111111111111111
```

385-21.OUT

```
Print file "385-21.out"

1  Glass: 0.8mm diameter (21micron gap, 6 contacting particles)
 INPUT REVIEW

 CENTER TEMPERATURE                  1.000000E+02
 INNER RADIUS                        6.350000E-03
 NUMBER OF AXIAL NODES                 6
 NUMBER OF RADIAL NODES               31
 NUMBER OF AXIAL STEP CARDS READ       1
 NUMBER OF RADIAL STEP CARDS READ      2
 NUMBER OF PROPERTY CARDS READ         2
 NUMBER OF TIME STEP CARDS READ        4
 H PLOT FILE NAME                    h185-21
 DUMP FILE NAME                      b185-21

 AXIAL STEP CARDS
 ID          DX
  1   8.000000E-05


 RADIAL STEP CARDS
 ID          DR
  8   8.000000E-05
  9   2.100000E-05


 PROPERTY CARDS
 ID          K            RHO*CP
  1   1.040000E+00   2.700000E+06
  0   2.928200E-02   1.047000E+03


 TIME STEP CARDS
 NUMBER        DT         NPRT    MSKP   NSKP
    100   1.00000E-05    100      1      5
    100   1.00000E-04     50      1      5
    100   1.00000E-02     20      1      5
    500   2.00000E-02     50      1      5


 AXIAL  NODE SIZE (RIGHT=TOPMOST)
 LOCATION MAP (BY ID)


 11111


 RADIAL NODE SIZE
 LOCATION MAP (BY ID)

 ´.........´.........´.........
 988888888888888888888888888888


 PROPERTY
 LOCATION MAP (BY ID)

 ´.........´.........´.........
 000000000000000000000000000000
 000011110000001111000000111100 0
 00011111100001111110000111111100
 0011111111001111111100111111110
 011111111111111111111111111111


 TOTAL RADIAL LENGTH          2.421000E-03
```

```
Print file "385-21.out"

 TOTAL AXIAL LENGTH          4.000000E-04

 H SOLUTION FOR 0.000000E+00 TO 9.999999E-04 SECONDS


 PRINT TEMPERATURE MAP EVERY  100  1.00000E-05 SECOND TIME STEPS FOR EVERY   5 RADIAL NODE

 TEMPERATURE MAP AT  1.00000E-03 SECONDS
      5           10           15           20           25           30
 0.163523E+01 0.291312E-02 0.446713E-05 0.126211E-08 0.219265E-12 0.119535E-16
 0.530756E-02 0.143233E-02 0.311287E-08 0.433062E-09 0.669578E-16 0.304987E-17
 0.185718E-03 0.372636E-03 0.336079E-10 0.752225E-10 0.369566E-18 0.392623E-18
 0.733127E-05 0.631582E-06 0.356047E-12 0.467077E-13 0.220466E-20 0.139556E-21
 0.384397E-06 0.440424E-08 0.338205E-14 0.149723E-15 0.126558E-22 0.274069E-24
 0.139207E-06 0.727768E-10 0.555285E-16 0.127009E-17 0.131883E-24 0.148844E-26

     HEAT FLUX        H
  6 1.44204E+04 1.44204E+02
  5 1.58051E+04 1.58051E+02
  4 2.11873E+04 2.11873E+02
  3 3.93284E+04 3.93284E+02
  2 1.35841E+05 1.35841E+03
  1 1.37648E+05 1.37648E+03

 AVERAGE H @  1.00000E-03 SECONDS:  5.76392E+02



 TOTAL RADIAL LENGTH         2.421000E-03
 TOTAL AXIAL LENGTH          4.000000E-04

 H SOLUTION FOR 1.000001E-03 TO 1.100000E-02 SECONDS


 PRINT TEMPERATURE MAP EVERY   50  1.00000E-04 SECOND TIME STEPS FOR EVERY   5 RADIAL NODE

 TEMPERATURE MAP AT  6.00000E-03 SECONDS
      5           10           15           20           25           30
 0.182894E+01 0.540537E-02 0.421630E-04 0.119690E-06 0.899429E-09 0.284641E-11
 0.942900E-01 0.317573E-02 0.147280E-05 0.694811E-07 0.221190E-10 0.173407E-11
 0.256942E-01 0.106132E-02 0.288327E-06 0.229563E-07 0.345031E-11 0.635835E-12
 0.615280E-02 0.244420E-04 0.415443E-07 0.429799E-09 0.403584E-12 0.103282E-13
 0.164876E-02 0.213678E-05 0.449349E-08 0.304368E-10 0.358686E-13 0.583607E-15
 0.913877E-03 0.404577E-06 0.749565E-09 0.473469E-11 0.498381E-14 0.749022E-16

     HEAT FLUX        H
  6 1.42125E+04 1.42125E+02
  5 1.55701E+04 1.55701E+02
  4 2.07618E+04 2.07618E+02
  3 3.77074E+04 3.77074E+02
  2 1.25058E+05 1.25058E+03
  1 1.29893E+05 1.29893E+03

 AVERAGE H @  6.00000E-03 SECONDS:  5.42299E+02


 TEMPERATURE MAP AT  1.10000E-02 SECONDS
      5           10           15           20           25           30
 0.194243E+01 0.654737E-02 0.542806E-04 0.168729E-06 0.134212E-08 0.462154E-11
 0.193550E+00 0.400456E-02 0.381001E-05 0.100923E-06 0.761917E-10 0.288512E-11
 0.871689E-01 0.139218E-02 0.133204E-05 0.343168E-07 0.237566E-10 0.108248E-11
 0.363011E-01 0.498395E-04 0.356513E-06 0.102372E-08 0.570343E-11 0.309104E-13
 0.172559E-01 0.733603E-05 0.741354E-07 0.132179E-09 0.106355E-11 0.368455E-14
 0.126157E-01 0.234188E-05 0.233500E-07 0.380641E-10 0.303402E-12 0.102026E-14
```

```
Print file "385-21.out"

     HEAT FLUX        H
  6 1.41404E+04 1.41404E+02
  5 1.54730E+04 1.54730E+02
  4 2.05379E+04 2.05379E+02
  3 3.68349E+04 3.68349E+02
  2 1.19558E+05 1.19558E+03
  1 1.24556E+05 1.24556E+03

AVERAGE H @  1.10000E-02 SECONDS:  5.23503E+02



TOTAL RADIAL LENGTH          2.421000E-03
TOTAL AXIAL LENGTH           4.000000E-04

H SOLUTION FOR 1.099999E-02 TO 1.011000E+00 SECONDS


PRINT TEMPERATURE MAP EVERY   20  1.00000E-02 SECOND TIME STEPS FOR EVERY   5 RADIAL NODE

TEMPERATURE MAP AT  2.11000E-01 SECONDS
      5            10            15            20            25            30
 0.839442E+01 0.213273E+01 0.706441E-01 0.645534E-02 0.127650E-03 0.320485E-04
 0.682873E+01 0.211021E+01 0.392352E-01 0.565404E-02 0.378581E-04 0.212877E-04
 0.704141E+01 0.203370E+01 0.420421E-01 0.470824E-02 0.339188E-04 0.115880E-04
 0.751188E+01 0.192834E+01 0.499976E-01 0.377332E-02 0.355434E-04 0.265703E-05
 0.792600E+01 0.162199E+01 0.582741E-01 0.295621E-02 0.397742E-04 0.199767E-05
 0.808665E+01 0.149063E+01 0.617622E-01 0.262738E-02 0.418705E-04 0.180481E-05

     HEAT FLUX        H
  6 1.30884E+04 1.30884E+02
  5 1.39466E+04 1.39466E+02
  4 1.68068E+04 1.68068E+02
  3 2.62980E+04 2.62980E+02
  2 9.17444E+04 9.17444E+02
  1 9.50055E+04 9.50055E+02

AVERAGE H @  2.11000E-01 SECONDS:  4.05685E+02


TEMPERATURE MAP AT  4.11000E-01 SECONDS
      5            10            15            20            25            30
 0.143643E+02 0.603602E+01 0.544655E+00 0.142961E+00 0.586427E-02 0.103238E-02
 0.129852E+02 0.607037E+01 0.461220E+00 0.141221E+00 0.374912E-02 0.945396E-03
 0.132070E+02 0.615719E+01 0.487548E+00 0.136749E+00 0.399892E-02 0.801009E-03
 0.136732E+02 0.631815E+01 0.541364E+00 0.131102E+00 0.463995E-02 0.625992E-03
 0.140757E+02 0.561624E+01 0.591694E+00 0.111346E+00 0.528709E-02 0.531744E-03
 0.142306E+02 0.530060E+01 0.612065E+00 0.102810E+00 0.555674E-02 0.495032E-03

     HEAT FLUX        H
  6 1.17613E+04 1.17613E+02
  5 1.27768E+04 1.27768E+02
  4 1.61496E+04 1.61496E+02
  3 2.56405E+04 2.56405E+02
  2 8.48541E+04 8.48541E+02
  1 8.78371E+04 8.78371E+02

AVERAGE H @  4.11000E-01 SECONDS:  3.78440E+02


TEMPERATURE MAP AT  6.11000E-01 SECONDS
      5            10            15            20            25            30
 0.192658E+02 0.967169E+01 0.146836E+01 0.561026E+00 0.436791E-01 0.147317E-01
```

Print file "385-21.out"

```
 0.179964E+02 0.975233E+01 0.135292E+01 0.561731E+00 0.357365E-01 0.142605E-01
 0.182098E+02 0.999791E+01 0.140437E+01 0.563035E+00 0.377593E-01 0.130657E-01
 0.186498E+02 0.104637E+02 0.150454E+01 0.567931E+00 0.420459E-01 0.113504E-01
 0.190263E+02 0.948774E+01 0.159610E+01 0.499322E+00 0.461113E-01 0.102599E-01
 0.191705E+02 0.904117E+01 0.163279E+01 0.468805E+00 0.477660E-01 0.982647E-02

     HEAT FLUX        H
  6 1.10059E+04 1.10059E+02
  5 1.19468E+04 1.19468E+02
  4 1.52399E+04 1.52399E+02
  3 2.45926E+04 2.45926E+02
  2 7.97041E+04 7.97041E+02
  1 8.24954E+04 8.24954E+02

AVERAGE H @  6.11000E-01 SECONDS:  3.56468E+02


TEMPERATURE MAP AT  8.11000E-01 SECONDS
      5           10           15           20           25           30
 0.233939E+02 0.129212E+02 0.268311E+01 0.122671E+01 0.147306E+00 0.698999E-01
 0.222066E+02 0.130374E+02 0.254887E+01 0.123357E+01 0.131264E+00 0.685382E-01
 0.224113E+02 0.134019E+02 0.262021E+01 0.125325E+01 0.136888E+00 0.646679E-01
 0.228279E+02 0.141094E+02 0.275619E+01 0.129216E+01 0.148198E+00 0.587605E-01
 0.231816E+02 0.129358E+02 0.287917E+01 0.115711E+01 0.158692E+00 0.549348E-01
 0.233167E+02 0.123944E+02 0.292823E+01 0.109608E+01 0.162924E+00 0.534048E-01

     HEAT FLUX        H
  6 1.04433E+04 1.04433E+02
  5 1.13070E+04 1.13070E+02
  4 1.44284E+04 1.44284E+02
  3 2.35220E+04 2.35220E+02
  2 7.54326E+04 7.54326E+02
  1 7.80682E+04 7.80682E+02

AVERAGE H @  8.11000E-01 SECONDS:  3.37892E+02


TEMPERATURE MAP AT  1.01100E+00 SECONDS
      5           10           15           20           25           30
 0.269205E+02 0.158291E+02 0.406690E+01 0.206824E+01 0.337267E+00 0.194580E+00
 0.258003E+02 0.159730E+02 0.392109E+01 0.208339E+01 0.312461E+00 0.191920E+00
 0.259973E+02 0.164271E+02 0.400763E+01 0.212910E+01 0.322863E+00 0.184044E+00
 0.263938E+02 0.173190E+02 0.417048E+01 0.221787E+01 0.343298E+00 0.171618E+00
 0.267285E+02 0.160009E+02 0.431674E+01 0.200937E+01 0.362052E+00 0.163561E+00
 0.268559E+02 0.153899E+02 0.437492E+01 0.191423E+01 0.369581E+00 0.160329E+00

     HEAT FLUX        H
  6 9.96644E+03 9.96644E+01
  5 1.07758E+04 1.07758E+02
  4 1.37409E+04 1.37409E+02
  3 2.25446E+04 2.25446E+02
  2 7.18070E+04 7.18070E+02
  1 7.43116E+04 7.43116E+02

AVERAGE H @  1.01100E+00 SECONDS:  3.22015E+02



TOTAL RADIAL LENGTH          2.421000E-03
TOTAL AXIAL LENGTH           4.000000E-04

H SOLUTION FOR 1.010999E+00 TO 1.101100E+01 SECONDS
```

```
Print file "385-21.out"

 PRINT TEMPERATURE MAP EVERY   50  2.00000E-02 SECOND TIME STEPS FOR EVERY   5 RADIAL NODE

 TEMPERATURE MAP AT  2.01100E+00 SECONDS
       5           10           15           20           25           30
  0.389641E+02 0.267877E+02 0.115123E+02 0.741560E+01 0.265672E+01 0.215755E+01
  0.380884E+02 0.270066E+02 0.113426E+02 0.748026E+01 0.258900E+01 0.214728E+01
  0.382581E+02 0.276903E+02 0.114659E+02 0.767136E+01 0.262429E+01 0.211608E+01
  0.385873E+02 0.290002E+02 0.116906E+02 0.801383E+01 0.269160E+01 0.206633E+01
  0.388597E+02 0.273695E+02 0.118888E+02 0.748211E+01 0.275242E+01 0.203295E+01
  0.389623E+02 0.266068E+02 0.119670E+02 0.723538E+01 0.277667E+01 0.201951E+01

      HEAT FLUX        H
   6 8.32472E+03 8.32472E+01
   5 8.91588E+03 8.91588E+01
   4 1.10315E+04 1.10315E+02
   3 1.75859E+04 1.75859E+02
   2 5.95000E+04 5.95000E+02
   1 6.15820E+04 6.15820E+02

 AVERAGE H @  2.01100E+00 SECONDS:  2.63973E+02


 TEMPERATURE MAP AT  3.01100E+00 SECONDS
       5           10           15           20           25           30
  0.461754E+02 0.341275E+02 0.181977E+02 0.130701E+02 0.664325E+01 0.593733E+01
  0.454156E+02 0.343585E+02 0.180384E+02 0.131585E+02 0.655788E+01 0.592252E+01
  0.455668E+02 0.350907E+02 0.181705E+02 0.134343E+02 0.660805E+01 0.587667E+01
  0.458557E+02 0.365294E+02 0.184077E+02 0.139588E+02 0.670289E+01 0.580091E+01
  0.460924E+02 0.348587E+02 0.186151E+02 0.132531E+02 0.678825E+01 0.575142E+01
  0.461812E+02 0.340749E+02 0.186967E+02 0.129239E+02 0.682222E+01 0.573149E+01

      HEAT FLUX        H
   6 7.31152E+03 7.31152E+01
   5 7.89236E+03 7.89236E+01
   4 9.91509E+03 9.91509E+01
   3 1.57515E+04 1.57515E+02
   2 5.23076E+04 5.23076E+02
   1 5.41314E+04 5.41314E+02

 AVERAGE H @  3.01100E+00 SECONDS:  2.33176E+02


 TEMPERATURE MAP AT  4.01100E+00 SECONDS
       5           10           15           20           25           30
  0.511833E+02 0.396173E+02 0.239617E+02 0.184888E+02 0.114184E+02 0.106307E+02
  0.504964E+02 0.398468E+02 0.238147E+02 0.185860E+02 0.113290E+02 0.106140E+02
  0.506343E+02 0.405729E+02 0.239460E+02 0.188936E+02 0.113852E+02 0.105622E+02
  0.508956E+02 0.420162E+02 0.241801E+02 0.194982E+02 0.114912E+02 0.104751E+02
  0.511085E+02 0.403882E+02 0.243840E+02 0.187274E+02 0.115864E+02 0.104188E+02
  0.511882E+02 0.396234E+02 0.244640E+02 0.183671E+02 0.116242E+02 0.103962E+02

      HEAT FLUX        H
   6 6.61235E+03 6.61235E+01
   5 7.14761E+03 7.14761E+01
   4 9.05122E+03 9.05122E+01
   3 1.45222E+04 1.45222E+02
   2 4.73704E+04 4.73704E+02
   1 4.90177E+04 4.90177E+02

 AVERAGE H @  4.01100E+00 SECONDS:  2.11813E+02


 TEMPERATURE MAP AT  5.01100E+00 SECONDS
       5           10           15           20           25           30
  0.550495E+02 0.440793E+02 0.290579E+02 0.235920E+02 0.164337E+02 0.156318E+02
```

```
Print file "385-21.out"

  0.544175E+02 0.443010E+02 0.289215E+02 0.236907E+02 0.163457E+02 0.156146E+02
  0.545448E+02 0.450008E+02 0.290482E+02 0.240034E+02 0.164031E+02 0.155616E+02
  0.547850E+02 0.463990E+02 0.292732E+02 0.246282E+02 0.165110E+02 0.154717E+02
  0.549802E+02 0.448436E+02 0.294688E+02 0.238504E+02 0.166080E+02 0.154139E+02
  0.550531E+02 0.441125E+02 0.295454E+02 0.234864E+02 0.166465E+02 0.153906E+02

      HEAT FLUX        H
   6 6.08847E+03 6.08847E+01
   5 6.57637E+03 6.57637E+01
   4 8.34536E+03 8.34536E+01
   3 1.35163E+04 1.35163E+02
   2 4.35852E+04 4.35852E+02
   1 4.50984E+04 4.50984E+02

 AVERAGE H @  5.01100E+00 SECONDS:  1.95233E+02


 TEMPERATURE MAP AT  6.01099E+00 SECONDS
       5            10            15            20            25            30
  0.582683E+02 0.479229E+02 0.336729E+02 0.283819E+02 0.214066E+02 0.206232E+02
  0.576817E+02 0.481340E+02 0.335457E+02 0.284784E+02 0.213221E+02 0.206064E+02
  0.578000E+02 0.487995E+02 0.336663E+02 0.287834E+02 0.213783E+02 0.205545E+02
  0.580229E+02 0.501321E+02 0.338799E+02 0.293982E+02 0.214838E+02 0.204660E+02
  0.582036E+02 0.486598E+02 0.340654E+02 0.286415E+02 0.215785E+02 0.204093E+02
  0.582711E+02 0.479675E+02 0.341381E+02 0.282873E+02 0.216162E+02 0.203865E+02

      HEAT FLUX        H
   6 5.65474E+03 5.65474E+01
   5 6.10378E+03 6.10378E+01
   4 7.74608E+03 7.74608E+01
   3 1.26274E+04 1.26274E+02
   2 4.04476E+04 4.04476E+02
   1 4.18506E+04 4.18506E+02

 AVERAGE H @  6.01099E+00 SECONDS:  1.81355E+02


 TEMPERATURE MAP AT  7.01099E+00 SECONDS
       5            10            15            20            25            30
  0.610848E+02 0.513571E+02 0.379165E+02 0.328738E+02 0.262035E+02 0.254535E+02
  0.605378E+02 0.515567E+02 0.377977E+02 0.329662E+02 0.261234E+02 0.254373E+02
  0.606483E+02 0.521851E+02 0.379116E+02 0.332581E+02 0.261772E+02 0.253876E+02
  0.608560E+02 0.534451E+02 0.381132E+02 0.338489E+02 0.262783E+02 0.253026E+02
  0.610243E+02 0.520581E+02 0.382881E+02 0.331259E+02 0.263690E+02 0.252482E+02
  0.610872E+02 0.514058E+02 0.383566E+02 0.327874E+02 0.264051E+02 0.252263E+02

      HEAT FLUX        H
   6 5.27496E+03 5.27496E+01
   5 5.69189E+03 5.69189E+01
   4 7.22031E+03 7.22031E+01
   3 1.18170E+04 1.18170E+02
   2 3.77096E+04 3.77096E+02
   1 3.90169E+04 3.90169E+02

 AVERAGE H @  7.01099E+00 SECONDS:  1.69169E+02


 TEMPERATURE MAP AT  8.01099E+00 SECONDS
       5            10            15            20            25            30
  0.636252E+02 0.544923E+02 0.418530E+02 0.370849E+02 0.307673E+02 0.300564E+02
  0.631139E+02 0.546802E+02 0.417418E+02 0.371726E+02 0.306917E+02 0.300411E+02
  0.632172E+02 0.552715E+02 0.418489E+02 0.374491E+02 0.307427E+02 0.299939E+02
  0.634113E+02 0.564579E+02 0.420386E+02 0.380102E+02 0.308385E+02 0.299133E+02
  0.635686E+02 0.551544E+02 0.422031E+02 0.373256E+02 0.309245E+02 0.298616E+02
  0.636272E+02 0.545412E+02 0.422675E+02 0.370051E+02 0.309587E+02 0.298408E+02
```

Print file "385-21.out"

```
     HEAT FLUX        H
  6 4.93126E+03 4.93126E+01
  5 5.32038E+03 5.32038E+01
  4 6.74636E+03 6.74636E+01
  3 1.10672E+04 1.10672E+02
  2 3.52439E+04 3.52439E+02
  1 3.64653E+04 3.64653E+02

AVERAGE H @  8.01099E+00 SECONDS:  1.58152E+02


TEMPERATURE MAP AT  9.01102E+00 SECONDS
      5           10           15           20           25           30
 0.659567E+02 0.573892E+02 0.455220E+02 0.410324E+02 0.350784E+02 0.344082E+02
 0.654782E+02 0.575656E+02 0.454179E+02 0.411151E+02 0.350073E+02 0.343937E+02
 0.655749E+02 0.581210E+02 0.455185E+02 0.413757E+02 0.350554E+02 0.343493E+02
 0.657565E+02 0.592357E+02 0.456966E+02 0.419052E+02 0.351457E+02 0.342732E+02
 0.659037E+02 0.580122E+02 0.458510E+02 0.412602E+02 0.352268E+02 0.342244E+02
 0.659585E+02 0.574367E+02 0.459115E+02 0.409582E+02 0.352591E+02 0.342048E+02

     HEAT FLUX        H
  6 4.61579E+03 4.61579E+01
  5 4.97985E+03 4.97985E+01
  4 6.31271E+03 6.31271E+01
  3 1.03692E+04 1.03692E+02
  2 3.29828E+04 3.29828E+02
  1 3.41258E+04 3.41258E+02

AVERAGE H @  9.01102E+00 SECONDS:  1.48031E+02


TEMPERATURE MAP AT  1.00110E+01 SECONDS
      5           10           15           20           25           30
 0.681174E+02 0.600835E+02 0.489507E+02 0.447326E+02 0.391357E+02 0.385057E+02
 0.676692E+02 0.602491E+02 0.488531E+02 0.448103E+02 0.390690E+02 0.384920E+02
 0.677598E+02 0.607703E+02 0.489476E+02 0.450553E+02 0.391143E+02 0.384503E+02
 0.679299E+02 0.618164E+02 0.491147E+02 0.455533E+02 0.391992E+02 0.383787E+02
 0.680676E+02 0.606688E+02 0.492595E+02 0.449471E+02 0.392754E+02 0.383329E+02
 0.681190E+02 0.601289E+02 0.493163E+02 0.446632E+02 0.393057E+02 0.383144E+02

     HEAT FLUX        H
  6 4.32272E+03 4.32272E+01
  5 4.66393E+03 4.66393E+01
  4 5.91110E+03 5.91110E+01
  3 9.71654E+03 9.71654E+01
  2 3.08885E+04 3.08885E+02
  1 3.19588E+04 3.19588E+02

AVERAGE H @  1.00110E+01 SECONDS:  1.38642E+02


TEMPERATURE MAP AT  1.10111E+01 SECONDS
      5           10           15           20           25           30
 0.701302E+02 0.625986E+02 0.521592E+02 0.482006E+02 0.429469E+02 0.423554E+02
 0.697103E+02 0.627539E+02 0.520678E+02 0.482736E+02 0.428843E+02 0.423425E+02
 0.697952E+02 0.632426E+02 0.521563E+02 0.485036E+02 0.429268E+02 0.423033E+02
 0.699545E+02 0.642237E+02 0.523130E+02 0.489713E+02 0.430065E+02 0.422361E+02
 0.700836E+02 0.631477E+02 0.524488E+02 0.484022E+02 0.430780E+02 0.421931E+02
 0.701317E+02 0.626416E+02 0.525020E+02 0.481357E+02 0.431065E+02 0.421758E+02

     HEAT FLUX        H
  6 4.05065E+03 4.05065E+01
  5 4.36997E+03 4.36997E+01
  4 5.53763E+03 5.53763E+01
```

```
Print file "385-21.out"

   3 9.10601E+03 9.10601E+01
   2 2.89379E+04 2.89379E+02
   1 2.99406E+04 2.99406E+02

 AVERAGE H @  1.10111E+01 SECONDS:  1.29894E+02


Fortran STOP
```

HSLB4PC.FOR

```
      PROGRAM BLAUSIS
C  CALCULATES TEMPERATURES AND HEAT TRANSFER COEFFICIENTS FOR TWO DIMENSIONAL SLAB
C  VARIABLE NODE SIZE AND PROPERTIES ALLOWED
C  PC VERSION
      REAL LJ,LK
      DIMENSION T(50,50),ITYPE(50,50),DK1(50,50),DJ2(50,50),
     $         TS(50,50),Q2P(50),H(50),IXSZ(50),IYSZ(50),
     $IXDX(10),DY(10),DX(10),NSTEP(10),CK(10),ROCP(10),DT(10),NPRT(10),
     $NSKP(10),MSKP(10),INDX(10),IYDX(10)
      COMMON UK(50,50),LK(50,50),DK2(50,50),UJ(50,50),
     $LJ(50,50),DJ1(50,50),F,M,N
      CHARACTER TITLE*80,HNAME*40,DNAME*40,RNAME*40
C INPUT PREPARATION
C  RECORD 1:
C    TITLE - 80 CHARACTER PROBLEM DESCRIPTION
C  RECORD 2:
C    NTM   - NUMBER OF TIME STEP CARDS TO BE READ
C    RNAME - RESTART FILE NAME.  IF PRESENT READ ONLY TIME STEP CARDS AFTER THIS CARD
C    HNAME - H PLOT FILE NAME.  IF PRESENT WRITE T,HAVE(T) TO HNAME.
C    DNAME - DUMP FILE NAME.  IF PRESENT WRITE DUMP FILE TO DNAME.
C  RECORD 3:
C    CENT  - TEMPERATURE @ X=0
C    A     - NOT USED.  PRESENT FOR COMPATIBILITY OF CYLINDER INPUT FILES
C    M     - TOTAL NUMBER OF VERTICAL NODE ENDPOINTS (=TOTAL NODES - 1)
C    N     - TOTAL NUMBER OF HORIZONTAL NODES
C    NYSZ  - NUMBER OF VERT  NODE SIZE CARDS TO BE READ
C    NXSZ  - NUMBER OF HORIZ NODE SIZE CARDS TO BE READ
C    NPROP - NUMBER OF PROPERTY CARDS TO BE READ
C  READ NYSZ VERT NODE SIZE CARDS:
C    IYDX  - INDEX OF NODE SIZE (0-9)
C    DY    - NODE SIZE
C  READ NXSZ HORIZ NODE SIZE CARDS:
C    IXDX  - INDEX OF NODE SIZE (0-9)
C    DX    - NODE SIZE
C  READ NPROP PROPERTY CARDS:
C    INDX  - INDEX OF PROPERTY (0-9)
C    CK    - THERMAL CONDUCTIVITY
C    ROCP  - DENSITY*SPECIFIC HEAT
C  READ NTM TIME STEP CARDS:
C    NSTEP - TOTAL NUMBER OF TIME STEPS ACTIVE FOR THIS CARD
C    DT    - TIME STEP SIZE
C    NPRT  - NUMBER OF TIME STEPS A TEMPERATURE/H COEFF SUMMARY IS PRINTED
C    MSKP  - PRINT FOR EACH MSKP VERT  NODES
C    NSKP  - PRINT FOR EACH NSKP HORIZ NODES
C  READ VERT  NODE SIZE MAP FOR M-1 NODES FROM TOP MOST POSITION (1 CARD)
C  READ HORIZ NODE SIZE MAP FOR N NODES FROM RIGHT MOST POSITION (1 CARD)
C  READ PROPERTY LOCATION MAP (M-1 ROWS WITH N COLUMNS)
C END OF INPUT
C  READ DATA
      READ(5,1) TITLE
      WRITE(6,2)TITLE
      READ(5,*) NTM,RNAME,HNAME,DNAME
      IF(RNAME.EQ.' ')THEN
        READ(5,*) CENT,A,M,N,NYSZ,NXSZ,NPROP
        WRITE(6,5)CENT,  M,N,NYSZ,NXSZ,NPROP,NTM,HNAME,DNAME
C  READ AXIAL STEP SIZE CARDS
        DO 31 I=1,NYSZ
        READ(5,*) IYDX(I),DY(IYDX(I)+1)
  31    WRITE(6,7)IYDX(I),DY(IYDX(I)+1)
        WRITE(6,32)
C  READ RADIAL STEP SIZE CARDS
        DO 34 I=1,NXSZ
        READ(5,*) IXDX(I),DX(IXDX(I)+1)
  34    WRITE(6,7)IXDX(I),DX(IXDX(I)+1)
        WRITE(6,36)
```

Print file "hslb4pc.for"

```
C  READ PROPERTY CARDS
        DO 3 I=1,NPROP
        READ(5,*) INDX(I),CK(INDX(I)+1),ROCP(INDX(I)+1)
   3    WRITE(6,7)INDX(I),CK(INDX(I)+1),ROCP(INDX(I)+1)
C  READ TIME STEP CARDS
        WRITE(6,8)
        DO 4 I=1,NTM
        READ(5,*) NSTEP(I),DT(I),NPRT(I),MSKP(I),NSKP(I)
   4    WRITE(6,9)NSTEP(I),DT(I),NPRT(I),MSKP(I),NSKP(I)
C  READ VERTICAL  STEP SIZE LOCATION MAP
        WRITE(6,37)
        CALL WRTHD(M)
        READ(5,20) (IYSZ(K),K=M,2,-1)
        WRITE(6,21)(IYSZ(K),K=M,2,-1)
C  READ RADIAL STEP SIZE LOCATION MAP
        WRITE(6,38)
        CALL WRTHD(N)
        READ(5,20) (IXSZ(J),J=1,N)
        WRITE(6,21)(IXSZ(J),J=1,N)
C  READ PROPERTY LOCATION MAP
        WRITE(6,39)
        CALL WRTHD(N)
        DO 10 K=M,2,-1
        READ(5,20) (ITYPE(K,J),J=1,N)
  10    WRITE(6,21)(ITYPE(K,J),J=1,N)
C  ADJUST SIZE AND TYPE ID TO AVOID ZERO ARRAY INDEX
        DO 11 K=2,M
        IYSZ(K)=IYSZ(K)+1
        DO 11 J=1,N
  11    ITYPE(K,J)=ITYPE(K,J)+1
        DO 41 J=1,N
  41    IXSZ(J)=IXSZ(J)+1
        TME=0.
      ELSE
C PERFORM RESTART FROM FILE RNAME
        OPEN(8,FILE=RNAME,FORM='UNFORMATTED')
        READ(8)CENT,A,M,N,NXSZ,NYSZ,NPROP,IXDX,IYDX,DX,DY,CK,ROCP,INDX,
     $          ITYPE,IXSZ,IYSZ,T,TS,TME
        CLOSE(8)
        WRITE(6,18) RNAME
        WRITE(6,5)CENT,M,N,NYSZ,NXSZ,NPROP,NTM,HNAME,DNAME
        DO 42 I=1,NYSZ
  42    WRITE(6,7)IYDX(I),DY(IYDX(I)+1)
        DO 43 I=1,NXSZ
  43    WRITE(6,7)IXDX(I),DX(IXDX(I)+1)
        WRITE(6,36)
        DO 13 I=1,NPROP
  13    WRITE(6,7)INDX(I),CK(INDX(I)+1),ROCP(INDX(I)+1)
        WRITE(6,8)
        DO 14 I=1,NTM
        READ(5,*) NSTEP(I),DT(I),NPRT(I),MSKP(I)
  14    WRITE(6,9)NSTEP(I),DT(I),NPRT(I),MSKP(I)
        WRITE(6,37)
        CALL WRTHD(M)
        WRITE(6,21)(IYSZ(K)-1,K=M,2,-1)
        WRITE(6,38)
        CALL WRTHD(N)
        WRITE(6,21)(IXSZ(J)-1,J=1,N)
        WRITE(6,39)
        CALL WRTHD(N)
        DO 16 K=M,2,-1
  16    WRITE(6,21)(ITYPE(K,J)-1,J=1,N)
      ENDIF
      F=CENT
C  SUM INTERVALS TO FIND TOTAL LENGTH
```

Print file "hslb4pc.for"

```
      YLEN=0
      DO 17 K=2,M
   17 YLEN=YLEN+DY(IYSZ(K))
      XLEN=0
      DO 19 J=1,N
   19 XLEN=XLEN+DX(IXSZ(J))
      IF(HNAME.NE.' ') OPEN(7,FILE=HNAME)
      DO 200 L=1,NTM
      WRITE(6,23)XLEN,YLEN,TME,DT(L)*NSTEP(L)+TME
      WRITE(6,24)NPRT(L),DT(L),NSKP(L),MSKP(L)
C  PREPARE TRIDIAGONAL COEFFICIENT MATRIXES
C  TREAT WALL AS INSULATED BOUNDARY
C  CENTER CONDITIONS FOR CONSTANT TEMPERATURE
      DO 40 J=1,N
      DO 40 K=1,M
      IF(K.EQ.M)THEN
C  TREAT TOP CONDITIONS
        IF(J.EQ.N)THEN
C    TREAT TOP WALL
          B=2*CK(ITYPE(M,N))*DY(IYSZ(M))/DX(IXSZ(N))
          C=2*CK(ITYPE(M,N))*DX(IXSZ(N))/DY(IYSZ(M))
          D=C
          E=4*ROCP(ITYPE(M,N))*DX(IXSZ(N))*DY(IYSZ(M))/DT(L)
          UJ (M,N)=0
          LJ (M,N)=C+D
          DJ1(M,N)=-(C+D-E)
          DJ2(M,N)=-(C+D+E)
          UK (M,N)=0
          LK (M,N)=-B
          DK1(M,N)=B+E
          DK2(M,N)=B-E
        ELSE
C    TREAT TOP INTERIOR AND CENTER
          A=2*CK(ITYPE(M,J+1))*DY(IYSZ(M))/DX(IXSZ(J+1))
          B=2*CK(ITYPE(M,J  ))*DY(IYSZ(M))/DX(IXSZ(J  ))
          C=(CK(ITYPE(M  ,J  ))*DX(IXSZ(J  ))+
     $       CK(ITYPE(M  ,J+1))*DX(IXSZ(J+1)))/DY(IYSZ(M  ))
          D=C
          E=2*DY(IYSZ(M))*
     $      (ROCP(ITYPE(M  ,J+1))*DX(IXSZ(J+1))+
     $       ROCP(ITYPE(M  ,J  ))*DX(IXSZ(J  )))/DT(L)
          UJ (M,J)=0
          LJ (M,J)=C+D
          DJ1(M,J)=-(C+D-E)
          DJ2(M,J)=-(C+D+E)
          UK (K,J)=-A
          LK (K,J)=-B
          DK1(K,J)=A+B+E
          DK2(K,J)=A+B-E
        ENDIF
      ELSEIF(K.EQ.1)THEN
C   TREAT BOTTOM CONDITIONS
        IF(J.EQ.N)THEN
C     TREAT BOTTOM WALL
          B=2*CK(ITYPE(2,N))*DY(IYSZ(2))/DX(IXSZ(N))
          C=2*CK(ITYPE(2,N))*DX(IXSZ(N))/DY(IYSZ(2))
          D=C
          E=4*ROCP(ITYPE(2,N))*DX(IXSZ(N))*DY(IYSZ(2))/DT(L)
          UJ (1,J)=C+D
          LJ (1,J)=0
          DJ1(1,J)=-(C+D-E)
          DJ2(1,J)=-(C+D+E)
          UK (K,N)=0
          LK (K,N)=-B
          DK1(K,N)=B+E
```

Print file "hslb4pc.for"

```
          DK2(K,N)=B-E
        ELSE
          A=2*CK(ITYPE(K+1,J+1))*DY(IYSZ(2))/DX(IXSZ(J+1))
          B=2*CK(ITYPE(K+1,J  ))*DY(IYSZ(2))/DX(IXSZ(J  ))
          C=(CK(ITYPE(K+1,J  ))*DX(IXSZ(J  ))+
     $       CK(ITYPE(K+1,J+1))*DX(IXSZ(J+1)))/DY(IYSZ(2  ))
          D=C
          E=2*DY(IYSZ(2  ))*
     $      (ROCP(ITYPE(K+1,J+1))*DX(IXSZ(J+1))+
     $       ROCP(ITYPE(K+1,J  ))*DX(IXSZ(J  )))/DT(L)
          UJ (1,J)=C+D
          LJ (1,J)=0
          DJ1(1,J)=-(C+D-E)
          DJ2(1,J)=-(C+D+E)
          UK (K,J)=-A
          LK (K,J)=-B
          DK1(K,J)=A+B+E
          DK2(K,J)=A+B-E
        ENDIF
      ELSE
C  TREAT VERTICAL INTERIOR CONDITIONS
        IF(J.EQ.N)THEN
C   TREAT VERTICAL INTERIOR WALL
          B=(CK(ITYPE(K+1,J  ))*DY(IYSZ(K+1))+
     $       CK(ITYPE(K  ,J  ))*DY(IYSZ(K  )))/DX(IXSZ(J  ))
          C=2*CK(ITYPE(K+1,N))*DX(IXSZ(N))/DY(IYSZ(K+1))
          D=2*CK(ITYPE(K  ,N))*DX(IXSZ(N))/DY(IYSZ(K  ))
          E=2*DX(IXSZ(N))*
     $      (ROCP(ITYPE(K+1,N))*DY(IYSZ(K+1))+
     $       ROCP(ITYPE(K  ,N))*DY(IYSZ(K  )))/DT(L)
          UJ (K,J)=C
          LJ (K,J)=D
          DJ1(K,J)=-(C+D-E)
          DJ2(K,J)=-(C+D+E)
          UK (K,N)=0
          LK (K,N)=-B
          DK1(K,N)=B+E
          DK2(K,N)=B-E
        ELSE
C  TREAT VERTICAL INTERIOR RADIAL INTERIOR AND CENTER
          A=(CK(ITYPE(K+1,J+1))*DY(IYSZ(K+1))+
     $       CK(ITYPE(K  ,J+1))*DY(IYSZ(K  )))/DX(IXSZ(J+1))
          B=(CK(ITYPE(K+1,J  ))*DY(IYSZ(K+1))+
     $       CK(ITYPE(K  ,J  ))*DY(IYSZ(K  )))/DX(IXSZ(J  ))
          C=(CK(ITYPE(K+1,J  ))*DX(IXSZ(J  ))+
     $       CK(ITYPE(K+1,J+1))*DX(IXSZ(J+1)))/DY(IYSZ(K+1))
          D=(CK(ITYPE(K  ,J  ))*DX(IXSZ(J  ))+
     $       CK(ITYPE(K  ,J+1))*DX(IXSZ(J+1)))/DY(IYSZ(K  ))
          E=((ROCP(ITYPE(K+1,J+1))*DY(IYSZ(K+1))+
     $        ROCP(ITYPE(K  ,J+1))*DY(IYSZ(K  )))*DX(IXSZ(J+1))+
     $       (ROCP(ITYPE(K+1,J  ))*DY(IYSZ(K+1))+
     $        ROCP(ITYPE(K  ,J  ))*DY(IYSZ(K  )))*DX(IXSZ(J  )))/DT(L)
          UJ (K,J)=C
          LJ (K,J)=D
          DJ1(K,J)=-(C+D-E)
          DJ2(K,J)=-(C+D+E)
          UK (K,J)=-A
          LK (K,J)=-B
          DK1(K,J)=A+B+E
          DK2(K,J)=A+B-E
        ENDIF
      ENDIF
   40 CONTINUE
C  BEGIN TIME STEPS
      DO 200 I=1,NSTEP(L)
```

Print file "hslb4pc.for"

```
      TME=TME+DT(L)
      CALL IADSLV(M,N,UK,DK1,LK,UJ,DJ2,LJ,T,TS)
      IF(AMOD(REAL(I),REAL(NPRT(L))).EQ.0)THEN
        WRITE(6,25)TME,(J,J=NSKP(L),N,NSKP(L))
        DO 140 K=M,MSKP(L),-MSKP(L)
  140   WRITE(6,26)(T(K,J),J=NSKP(L),N,NSKP(L))
C  CALCULATE HEAT FLUX LOCAL TO X=0 AND H, AVERAGE H (HAVE)
        DO 150 K=1,M
        IF(K.EQ.1)THEN
          Q2P(1)=(CENT-T(K,1))/DX(IXSZ(1))*CK(ITYPE(2,1))
          H(1)  =Q2P(1)/CENT
          HAVE  =H(1)*DY(IYSZ(2))/2
        ELSEIF(K.EQ.M)THEN
          Q2P(M)=(CENT-T(K,1))/DX(IXSZ(1))*CK(ITYPE(M,1))
          H(M)  =Q2P(M)/CENT
          HAVE  =HAVE+H(M)*DY(IYSZ(M))/2
        ELSE
          Q2P(K)=(CENT-T(K,1))*(CK(ITYPE(K+1,1))*DY(IYSZ(K+1))
     $                          +CK(ITYPE(K  ,1))*DY(IYSZ(K  )))/
     $                (DX(IXSZ(1))*(DY(IYSZ(K+1))+DY(IYSZ(K))))
          H(K)  =Q2P(K)/CENT
          HAVE  =HAVE+H(K)*(DY(IYSZ(K))+DY(IYSZ(K+1)))/2
        ENDIF
 150    CONTINUE
        HAVE=HAVE/YLEN
C  WRITE HEAT FLUX, H, HAVE AND WRITE TO FILE HNAME FOR PLOTTING
        WRITE(6,27)
        WRITE(6,28)(K,Q2P(K),H(K),K=M,MSKP(L),-MSKP(L))
        WRITE(6,29)TME,HAVE
        IF(HNAME.NE.' ')WRITE(7,30)TME,HAVE
      ENDIF
 200  CONTINUE
C  DUMP FINAL RESULTS TO RESTART FILE
      IF(DNAME.NE.' ')THEN
        OPEN(8,FILE=DNAME,FORM='UNFORMATTED')
        WRITE(8)CENT,A,M,N,NXSZ,NYSZ,NPROP,IXDX,IYDX,DX,DY,CK,ROCP,INDX,
     $          ITYPE,IXSZ,IYSZ,T,TS,TME
        CLOSE(8)
      ENDIF
      CLOSE(7)
      STOP
    1 FORMAT(A)
    2 FORMAT('1',A)
    5 FORMAT(' INPUT REVIEW'//' CENTER TEMPERATURE',T35,1PE12.6/' NUMBER
     $OF AXIAL NODES',T35,I3/' NUMBER OF RADIAL NODES',T35,I3/' NUMBER O
     $F AXIAL STEP CARDS READ',T35,I2/' NUMBER OF RADIAL STEP CARDS READ
     $',T35,I2/' NUMBER OF PROPERTY CARDS READ',T35,I2/' NUMBER OF TIME
     $STEP CARDS READ',T35,I2/' H PLOT FILE NAME',T35,A/' DUMP FILE NAME
     $',T35,A//' AXIAL STEP CARDS'/' ID',T13,'DX')
   32 FORMAT(//' HORIZ STEP CARDS'/' ID',T13,'DY')
   36 FORMAT(//' PROPERTY CARDS'/' ID',T13,'K',T25,'RHO*CP')
    7 FORMAT(' ',I2,2(3X,1PE12.6))
    8 FORMAT(//' TIME STEP CARDS'/' NUMBER',T15,'DT',T25,'NPRT',T32,'MSK
     $P',T38,'NSKP')
   37 FORMAT(//' AXIAL  NODE SIZE (RIGHT=TOPMOST)')
   38 FORMAT(//' RADIAL NODE SIZE')
   39 FORMAT(//' PROPERTY')
    9 FORMAT(' ',I6,2X,1PE12.5,3(2X,I4))
   18 FORMAT(/' RESTART DATA FROM FILE ',A)
   20 FORMAT(13OI1)
   21 FORMAT(' ',13OI1)
   23 FORMAT(//' TOTAL RADIAL LENGTH',T30,1PE12.6/' TOTAL VERTICAL LENGT
     $H',T30,E12.6,//' H SOLUTION FOR ',E12.6,' TO ',E12.6,' SECONDS'//)
   24 FORMAT(' PRINT TEMPERATURE MAP EVERY ',I4,1X,1PE12.5,' SECOND TIME
     $ STEPS FOR EVERY ',I3,' HORIZ NODES AND ',I3,' VERT NODES'/)
```

Print file "hslb4pc.for"

```
  25  FORMAT(' TEMPERATURE MAP AT ',1PE12.5,' SECONDS'/10(5X,I3,5X))
  26  FORMAT(' ',10E13.6)
  27  FORMAT(/6X,'HEAT FLUX',8X,'H')
  28  FORMAT(' ',I3,1P2E12.5)
  29  FORMAT(/' AVERAGE H @ ',1PE12.5,' SECONDS: ',E12.5//)
  30  FORMAT(' ',1P2E12.5)
      END

      FUNCTION RHS(ITIM,T,K,J)
C  RETURNS THE VALUE OF THE RIGHT HAND SIDE OF THE IAD EQUATIONS
C    ITIME - HALF (1) /FULL (2) TIME STEP (IN)
C    T     - TEMPERATURE ARRAY (IN)
C    K,J   - COLUMN, ROW INDICES (IN)
      COMMON UK(50,50),LK(50,50),DK2(50,50),UJ(50,50),
     $LJ(50,50),DJ1(50,50),F,M,N
      DIMENSION T(50,50)
      REAL LK,LJ
C BE CERTAIN UJ(M,J) AND UK(K,N) ARE 0 TO TREAT TOP CONDITIONS CORRECTLY
      IF(ITIM.EQ.1)THEN
C COMPUTE RHS AT HALF TIME STEP
        IF(J.EQ.1)THEN
          IF(K.EQ.1)THEN
            RHS=UJ(1,1)*T(2,1)+DJ1(1,1)*T(1,1)-LK(1,1)*F
          ELSE
            RHS=UJ(K,1)*T(K+1,1)+LJ(K,1)*T(K-1,1)+DJ1(K,1)*T(K,1)-
     $          LK(K,1)*F
          ENDIF
        ELSE
          RHS=UJ(K,J)*T(K+1,J)+LJ(K,J)*T(K-1,J)+DJ1(K,J)*T(K,J)
        ENDIF
      ELSEIF(ITIM.EQ.2)THEN
C COMPUTE RHS AT FULL TIME STEP
        IF(J.EQ.1)THEN
          RHS=UK(K,1)*T(K,2)+LK(K,1)*F+DK2(K,1)*T(K,1)
        ELSE
          RHS=UK(K,J)*T(K,J+1)+LK(K,J)*T(K,J-1)+DK2(K,J)*T(K,J)
        ENDIF
      ENDIF
      RETURN
      END

      SUBROUTINE IADSLV(M,N,UK,DK,LK,UJ,DJ,LJ,T,TS)
C  SOLVES THE IAD EQUATIONS USING GAUSSIAN ELIMINATION FOR A FULL TIME STEP
C    M                  - NUMBER OF COLUMNS (IN)
C    N                  - NUMBER OF ROWS    (IN)
C    UK,DK,LK,UJ,DJ,LJ  - COEFFICIENTS FOR IAD EQUATIONS (IN)
C    T                  - FULL TIME STEP TEMPERATURE ARRAY (OUT,IN)
C    TS                 - HALF TIME STEP TEMPERATURE ARRAY (OUT,IN)
      REAL LK(50,50),LJ(50,50)
      DIMENSION DK(50,50),DJ(50,50),UK(50,50),UJ(50,50),
     $T(50,50),B(50),TS(50,50)
      EXTERNAL RHS
C  COMPUTE TEMPERATURES AT END DF HALF TIME STEP IMPLICIT BY COLUMNS
      DO 70 K=1,M
      B(1)=DK(K,1)
      TS(K,1)=RHS(1,T,K,1)/B(1)
C  FORWARD GUASSIAN ELIMINATION
      DO 65 J=2,N
      B(J)=DK(K,J)-LK(K,J)*UK(K,J-1)/B(J-1)
   65 TS(K,J)=(RHS(1,T,K,J)-LK(K,J)*TS(K,J-1))/B(J)
C BACK SOLUTION
      DO 70 J=N-1,1,-1
   70 TS(K,J)=TS(K,J)-UK(K,J)*TS(K,J+1)/B(J)
C COMPUTE TEMPERATURES AT END OF FULL TIME STEP IMPLICIT BY ROWS
      DO 130 J=1,N
```

Print file "hslb4pc.for"

```
      B(1)=DJ(1,J)
      T(1,J)=RHS(2,TS,1,J)/B(1)
C  FORWARD GUASSIAN ELIMINATION
      DO 110 K=2,M
      B(K)=DJ(K,J)-LJ(K,J)*UJ(K-1,J)/B(K-1)
  110 T(K,J)=(RHS(2,TS,K,J)-LJ(K,J)*T(K-1,J))/B(K)
C BACK SOLUTION
      DO 130 K=M-1,1,-1
  130 T(K,J)=T(K,J)-UJ(K,J)*T(K+1,J)/B(K)
      RETURN
      END

      SUBROUTINE WRTHD(N)
C  WRITE MAP POSITION HEADING
      CHARACTER HEAD*130
      HEAD=' '
      L=1
      DO 6 I=1,N/10
      HEAD=HEAD(1:L)//'^.........'
    6 L=I*10+1
      WRITE(6,12)HEAD
   12 FORMAT(' LOCATION MAP (BY ID)'//A)
      RETURN
      END
```

HCYL9PC.FOR

```
      PROGRAM BLAUSIS
C  CALCULATES TEMPERATURES AND HEAT TRANSFER COEFFICIENTS FOR TWO DIMENSIONAL CYLINDER
C  VARIABLE NODE SIZE AND PROPERTIES ALLOWED
C  PC VERSION
      REAL LJ,LK
      DIMENSION T(50,50),ITYPE(50,50),DK1(50,50),DJ2(50,50),
     $         TS(50,50),Q2P(50),H(50),IRSZ(50),IXSZ(50),
     $IRDX(10),DX(10),DR(10),NSTEP(10),CK(10),ROCP(10),DT(10),NPRT(10),
     $NSKP(10),MSKP(10),INDX(10),IXDX(10)
      COMMON UK(50,50),LK(50,50),DK2(50,50),UJ(50,50),
     $LJ(50,50),DJ1(50,50),F,M,N
      CHARACTER TITLE*80,HNAME*40,DNAME*40,RNAME*40
C INPUT PREPARATION
C  RECORD 1:
C    TITLE - 80 CHARACTER PROBLEM DESCRIPTION
C  RECORD 2:
C    NTM   - NUMBER OF TIME STEP CARDS TO BE READ
C    RNAME - RESTART FILE NAME.  IF PRESENT READ ONLY TIME STEP CARDS AFTER THIS CARD
C    HNAME - H PLOT FILE NAME.  IF PRESENT WRITE T,HAVE(T) TO HNAME.
C    DNAME - DUMP FILE NAME.  IF PRESENT WRITE DUMP FILE TO DNAME.
C  RECORD 3:
C    CENT  - TEMPERATURE @ R=0
C    A     - INNER RADIUS OF CYLINDER
C    M     - TOTAL NUMBER OF AXIAL NODE ENDPOINTS (=TOTAL NODES - 1)
C    N     - TOTAL NUMBER OF RADIAL NODES
C    NXSZ  - NUMBER OF AXIAL  NODE SIZE CARDS TO BE READ
C    NRSZ  - NUMBER OF RADIAL NODE SIZE CARDS TO BE READ
C    NPROP - NUMBER OF PROPERTY CARDS TO BE READ
C  READ NXSZ AXIAL NODE SIZE CARDS:
C    IXDX  - INDEX OF NODE SIZE (0-9)
C    DY    - NODE SIZE
C  READ NRSZ RADIAL NODE SIZE CARDS:
C    IRDX  - INDEX OF NODE SIZE (0-9)
C    DX    - NODE SIZE
C  READ NPROP PROPERTY CARDS:
C    INDX  - INDEX OF PROPERTY (0-9)
C    CK    - THERMAL CONDUCTIVITY
C    ROCP  - DENSITY*SPECIFIC HEAT
C  READ NTM TIME STEP CARDS:
C    NSTEP - TOTAL NUMBER OF TIME STEPS ACTIVE FOR THIS CARD
C    DT    - TIME STEP SIZE
C    NPRT  - NUMBER OF TIME STEPS A TEMPERATURE/H COEFF SUMMARY IS PRINTED
C    MSKP  - PRINT FOR EACH MSKP AXIAL  NODES
C    NSKP  - PRINT FOR EACH NSKP RADIAL NODES
C  READ AXIAL  NODE SIZE MAP FOR M-1 NODES FROM TOP MOST POSITION (1 CARD)
C  READ RADIAL NODE SIZE MAP FOR N NODES FROM RIGHT MOST POSITION (1 CARD)
C  READ PROPERTY LOCATION MAP (M-1 ROWS WITH N COLUMNS)
C END OF INPUT
C  READ DATA
      READ(5,1) TITLE
      WRITE(6,2)TITLE
      READ(5,*) NTM,RNAME,HNAME,DNAME
      IF(RNAME.EQ.' ')THEN
        READ(5,*) CENT,A,M,N,NXSZ,NRSZ,NPROP
        WRITE(6,5)CENT,A,M,N,NXSZ,NRSZ,NPROP,NTM,HNAME,DNAME
C  READ AXIAL STEP SIZE CARDS
        DO 31 I=1,NXSZ
        READ(5,*) IXDX(I),DX(IXDX(I)+1)
  31    WRITE(6,7)IXDX(I),DX(IXDX(I)+1)
        WRITE(6,32)
C  READ RADIAL STEP SIZE CARDS
        DO 34 I=1,NRSZ
        READ(5,*) IRDX(I),DR(IRDX(I)+1)
  34    WRITE(6,7)IRDX(I),DR(IRDX(I)+1)
        WRITE(6,36)
```

```
Print file "hcyl9pc.for"

C  READ PROPERTY CARDS
        DO 3 I=1,NPROP
        READ(5,*) INDX(I),CK(INDX(I)+1),ROCP(INDX(I)+1)
   3    WRITE(6,7)INDX(I),CK(INDX(I)+1),ROCP(INDX(I)+1)
C  READ TIME STEP CARDS
        WRITE(6,8)
        DO 4 I=1,NTM
        READ(5,*) NSTEP(I),DT(I),NPRT(I),MSKP(I),NSKP(I)
   4    WRITE(6,9)NSTEP(I),DT(I),NPRT(I),MSKP(I),NSKP(I)
C  READ AXIAL  STEP SIZE LOCATION MAP
        WRITE(6,37)
        CALL WRTHD(M)
        READ(5,20) (IXSZ(K),K=M,2,-1)
        WRITE(6,21)(IXSZ(K),K=M,2,-1)
C  READ RADIAL STEP SIZE LOCATION MAP
        WRITE(6,38)
        CALL WRTHD(N)
        READ(5,20) (IRSZ(J),J=1,N)
        WRITE(6,21)(IRSZ(J),J=1,N)
C  READ PROPERTY LOCATION MAP
        WRITE(6,39)
        CALL WRTHD(N)
        DO 10 K=M,2,-1
        READ(5,20) (ITYPE(K,J),J=1,N)
  10    WRITE(6,21)(ITYPE(K,J),J=1,N)
C  ADJUST SIZE AND TYPE ID TO AVOID ZERO ARRAY INDEX
        DO 11 K=2,M
        IXSZ(K)=IXSZ(K)+1
        DO 11 J=1,N
  11    ITYPE(K,J)=ITYPE(K,J)+1
        DO 41 J=1,N
  41    IRSZ(J)=IRSZ(J)+1
        TME=0.
      ELSE
C PERFORM RESTART FROM FILE RNAME
        OPEN(8,FILE=RNAME,FORM='UNFORMATTED')
        READ(8)CENT,A,M,N,NXSZ,NRSZ,NPROP,IXDX,IRDX,DX,DR,CK,ROCP,INDX,
     $          ITYPE,IXSZ,IRSZ,T,TS,TME
        CLOSE(8)
        WRITE(6,18) RNAME
        WRITE(6,5)CENT,A,M,N,NXSZ,NRSZ,NPROP,NTM,HNAME,DNAME
        DO 42 I=1,NXSZ
  42    WRITE(6,7)IXDX(I),DX(IXDX(I)+1)
        DO 43 I=1,NRSZ
  43    WRITE(6,7)IRDX(I),DR(IRDX(I)+1)
        WRITE(6,36)
        DO 13 I=1,NPROP
  13    WRITE(6,7)INDX(I),CK(INDX(I)+1),ROCP(INDX(I)+1)
        WRITE(6,8)
        DO 14 I=1,NTM
        READ(5,*) NSTEP(I),DT(I),NPRT(I),MSKP(I),NSKP(I)
  14    WRITE(6,9)NSTEP(I),DT(I),NPRT(I),MSKP(I),NSKP(I)
        WRITE(6,37)
        CALL WRTHD(M)
        WRITE(6,21)(IXSZ(K)-1,K=M,2,-1)
        WRITE(6,38)
        CALL WRTHD(N)
        WRITE(6,21)(IRSZ(J)-1,J=1,N)
        WRITE(6,39)
        CALL WRTHD(N)
        DO 16 K=M,2,-1
  16    WRITE(6,21)(ITYPE(K,J)-1,J=1,N)
      ENDIF
      F=CENT
C  SUM INTERVALS TO FIND TOTAL LENGTH
```

Print file "hcyl9pc.for"

```
      XLEN=0
      DO 17 K=2,M
   17 XLEN=XLEN+DX(IXSZ(K))
      RLEN=0
      DO 19 J=1,N
   19 RLEN=RLEN+DR(IRSZ(J))
      IF(HNAME.NE.' ') OPEN(7,FILE=HNAME)
      DO 200 L=1,NTM
      WRITE(6,23)RLEN,XLEN,TME,DT(L)*NSTEP(L)+TME
      WRITE(6,24)NPRT(L),DT(L),NSKP(L),MSKP(L)
C  PREPARE TRIDIAGONAL COEFFICIENT MATRIXES
C  TREAT WALL AS INSULATED BOUNDARY
C  CENTER CONDITIONS FOR CONSTANT TEMPERATURE
      R=A
      DO 40 J=1,N
      R=R+DR(IRSZ(J))
      DO 40 K=1,M
      IF(K.EQ.M)THEN
C  TREAT TOP CONDITIONS
        IF(J.EQ.N)THEN
C    TREAT TOP WALL
          B=2*CK(ITYPE(M,N))*DX(IXSZ(M))*(R-DR(IRSZ(N))/2)/DR(IRSZ(N))
          C=2*CK(ITYPE(M,N))*DR(IRSZ(N))* R/DX(IXSZ(M))
          D=C
          E=4*R*DR(IRSZ(N))*DX(IXSZ(M))*ROCP(ITYPE(M,N))/DT(L)
          UJ (M,N)=0
          LJ (M,N)=C+D
          DJ1(M,N)=-(C+D-E)
          DJ2(M,N)=-(C+D+E)
          UK (M,N)=0
          LK (M,N)=-B
          DK1(M,N)=B+E
          DK2(M,N)=B-E
        ELSE
C    TREAT TOP INTERIOR AND CENTER
          A=2*CK(ITYPE(M,J+1))*DX(IXSZ(M))*(R+DR(IRSZ(J+1))/2)/
     $        DR(IRSZ(J+1))
          B=2*CK(ITYPE(M,J  ))*DX(IXSZ(M))*(R-DR(IRSZ(J  ))/2)/
     $        DR(IRSZ(J  ))
          C=(CK(ITYPE(M  ,J  ))*DR(IRSZ(J  ))*(R-DR(IRSZ(J  ))/4)+
     $       CK(ITYPE(M  ,J+1))*DR(IRSZ(J+1))*(R+DR(IRSZ(J+1))/4))/
     $       DX(IXSZ(M  ))
          D=C
          E=2*DX(IXSZ(M))*
     $      (ROCP(ITYPE(M  ,J+1))*DR(IRSZ(J+1))*(R+DR(IRSZ(J+1))/4)+
     $       ROCP(ITYPE(M  ,J  ))*DR(IRSZ(J  ))*(R-DR(IRSZ(J  ))/4))
     $      /DT(L)
          UJ (M,J)=0
          LJ (M,J)=C+D
          DJ1(M,J)=-(C+D-E)
          DJ2(M,J)=-(C+D+E)
          UK (K,J)=-A
          LK (K,J)=-B
          DK1(K,J)=A+B+E
          DK2(K,J)=A+B-E
        ENDIF
      ELSEIF(K.EQ.1)THEN
C   TREAT BOTTOM CONDITIONS
        IF(J.EQ.N)THEN
C     TREAT BOTTOM WALL
          B=2*CK(ITYPE(2,N))*DX(IXSZ(2))*(R-DR(IRSZ(N))/2)/DR(IRSZ(N))
          C=2*CK(ITYPE(2,N))*DR(IRSZ(N))* R/DX(IXSZ(2))
          D=C
          E=4*R*DR(IRSZ(N))*DX(IXSZ(2))*ROCP(ITYPE(2,N))/DT(L)
          UJ (1,J)=C+D
```

Print file "hcyl9pc.for"

```
          LJ (1,J)=0
          DJ1(1,J)=-(C+D-E)
          DJ2(1,J)=-(C+D+E)
          UK (K,N)=0
          LK (K,N)=-B
          DK1(K,N)=B+E
          DK2(K,N)=B-E
        ELSE
          A=2*CK(ITYPE(K+1,J+1))*DX(IXSZ(2))*(R+DR(IRSZ(J+1))/2)/
     $        DR(IRSZ(J+1))
          B=2*CK(ITYPE(K+1,J  ))*DX(IXSZ(2))*(R-DR(IRSZ(J  ))/2)/
     $        DR(IRSZ(J  ))
          C=(CK(ITYPE(K+1,J  ))*DR(IRSZ(J  ))*(R-DR(IRSZ(J  ))/4)+
     $       CK(ITYPE(K+1,J+1))*DR(IRSZ(J+1))*(R+DR(IRSZ(J+1))/4))/
     $       DX(IXSZ(2  ))
          D=C
          E=2*DX(IXSZ(2  ))*
     $      (ROCP(ITYPE(K+1,J+1))*DR(IRSZ(J+1))*(R+DR(IRSZ(J+1))/4)+
     $       ROCP(ITYPE(K+1,J  ))*DR(IRSZ(J  ))*(R-DR(IRSZ(J  ))/4))
     $      /DT(L)
          UJ (1,J)=C+D
          LJ (1,J)=0
          DJ1(1,J)=-(C+D-E)
          DJ2(1,J)=-(C+D+E)
          UK (K,J)=-A
          LK (K,J)=-B
          DK1(K,J)=A+B+E
          DK2(K,J)=A+B-E
        ENDIF
      ELSE
C  TREAT AXIAL INTERIOR CONDITIONS
        IF(J.EQ.N)THEN
C   TREAT AXIAL INTERIOR WALL
          B=(CK(ITYPE(K+1,J  ))*DX(IXSZ(K+1))+
     $       CK(ITYPE(K  ,J  ))*DX(IXSZ(K  )))*(R-DR(IRSZ(J  ))/2)/
     $       DR(IRSZ(J  ))
          C=2*CK(ITYPE(K+1,N))*DR(IRSZ(N))*R/DX(IXSZ(K+1))
          D=2*CK(ITYPE(K  ,N))*DR(IRSZ(N))*R/DX(IXSZ(K  ))
          E=2*R*DR(IRSZ(N))*(ROCP(ITYPE(K+1,N))*DX(IXSZ(K+1))+
     $                       ROCP(ITYPE(K  ,N))*DX(IXSZ(K  )))/DT(L)
          UJ (K,J)=C
          LJ (K,J)=D
          DJ1(K,J)=-(C+D-E)
          DJ2(K,J)=-(C+D+E)
          UK (K,N)=0
          LK (K,N)=-B
          DK1(K,N)=B+E
          DK2(K,N)=B-E
        ELSE
C  TREAT AXIAL INTERIOR RADIAL INTERIOR AND CENTER
          A=(CK(ITYPE(K+1,J+1))*DX(IXSZ(K+1))+
     $       CK(ITYPE(K  ,J+1))*DX(IXSZ(K  )))*(R+DR(IRSZ(J+1))/2)/
     $       DR(IRSZ(J+1))
          B=(CK(ITYPE(K+1,J  ))*DX(IXSZ(K+1))+
     $       CK(ITYPE(K  ,J  ))*DX(IXSZ(K  )))*(R-DR(IRSZ(J  ))/2)/
     $       DR(IRSZ(J  ))
          C=(CK(ITYPE(K+1,J  ))*DR(IRSZ(J  ))*(R-DR(IRSZ(J  ))/4)+
     $       CK(ITYPE(K+1,J+1))*DR(IRSZ(J+1))*(R+DR(IRSZ(J+1))/4))/
     $       DX(IXSZ(K+1))
          D=(CK(ITYPE(K  ,J  ))*DR(IRSZ(J  ))*(R-DR(IRSZ(J  ))/4)+
     $       CK(ITYPE(K  ,J+1))*DR(IRSZ(J+1))*(R+DR(IRSZ(J+1))/4))/
     $       DX(IXSZ(K  ))
          E=((ROCP(ITYPE(K+1,J+1))*DX(IXSZ(K+1))+
     $        ROCP(ITYPE(K  ,J+1))*DX(IXSZ(K  )))*
     $        DR(IRSZ(J+1))*(R+DR(IRSZ(J+1))/4)+
```

Print file "hcyl9pc.for"

```
     $       (ROCP(ITYPE(K+1,J  ))*DX(IXSZ(K+1))
     $       +ROCP(ITYPE(K  ,J  ))*DX(IXSZ(K  )))*
     $        DR(IRSZ(J  ))*(R-DR(IRSZ(J  ))/4))/DT(L)
          UJ (K,J)=C
          LJ (K,J)=D
          DJ1(K,J)=-(C+D-E)
          DJ2(K,J)=-(C+D+E)
          UK (K,J)=-A
          LK (K,J)=-B
          DK1(K,J)=A+B+E
          DK2(K,J)=A+B-E
        ENDIF
      ENDIF
   40 CONTINUE
C  BEGIN TIME STEPS
      DO 200 I=1,NSTEP(L)
      TME=TME+DT(L)
      CALL IADSLV(M,N,UK,DK1,LK,UJ,DJ2,LJ,T,TS)
      IF(AMOD(REAL(I),REAL(NPRT(L))).EQ.0)THEN
        WRITE(6,25)TME,(J,J=NSKP(L),N,NSKP(L))
        DO 140 K=M,MSKP(L),-MSKP(L)
  140   WRITE(6,26)(T(K,J),J=NSKP(L),N,NSKP(L))
C  CALCULATE HEAT FLUX LOCAL TO R=0 AND H, AVERAGE H (HAVE)
        DO 150 K=1,M
        IF(K.EQ.1)THEN
          Q2P(1)=(CENT-T(K,1))/DR(IRSZ(1))*CK(ITYPE(2,1))
          H(1)  =Q2P(1)/CENT
          HAVE  =H(1)*DX(IXSZ(2))/2
        ELSEIF(K.EQ.M)THEN
          Q2P(M)=(CENT-T(K,1))/DR(IRSZ(1))*CK(ITYPE(M,1))
          H(M)  =Q2P(M)/CENT
          HAVE  =HAVE+H(M)*DX(IXSZ(M))/2
        ELSE
          Q2P(K)=(CENT-T(K,1))*(CK(ITYPE(K+1,1))*DX(IXSZ(K+1))
     $                         +CK(ITYPE(K  ,1))*DX(IXSZ(K  )))/
     $                 (DR(IRSZ(1))*(DX(IXSZ(K+1))+DX(IXSZ(K))))
          H(K)  =Q2P(K)/CENT
          HAVE  =HAVE+H(K)*(DX(IXSZ(K))+DX(IXSZ(K+1)))/2
        ENDIF
  150   CONTINUE
        HAVE=HAVE/XLEN
C  WRITE HEAT FLUX, H, HAVE AND WRITE TO FILE HNAME FOR PLOTTING
        WRITE(6,27)
        WRITE(6,28)(K,Q2P(K),H(K),K=M,MSKP(L),-MSKP(L))
        WRITE(6,29)TME,HAVE
        IF(HNAME.NE.' ')WRITE(7,30)TME,HAVE
      ENDIF
  200 CONTINUE
C  DUMP FINAL RESULTS TO RESTART FILE
      IF(DNAME.NE.' ')THEN
        OPEN(8,FILE=DNAME,FORM='UNFORMATTED')
        WRITE(8)CENT,A,M,N,NXSZ,NRSZ,NPROP,IXDX,IRDX,DX,DR,CK,ROCP,INDX,
     $        ITYPE,IXSZ,IRSZ,T,TS,TME

        CLOSE(8)
      ENDIF
      CLOSE(7)
      STOP
    1 FORMAT(A)
    2 FORMAT('1',A)
    5 FORMAT(' INPUT REVIEW'//' CENTER TEMPERATURE',T35,1PE12.6/' INNER
     $RADIUS',T35,E12.6/' NUMBER OF AXIAL NODES',T35,I3/' NUMBER OF RADI
     $AL NODES',T35,I3/' NUMBER OF AXIAL STEP CARDS READ',T35,I2/' NUMBE
     $R OF RADIAL STEP CARDS READ',T35,I2/' NUMBER OF PROPERTY CARDS REA
     $D',T35,I2/' NUMBER OF TIME STEP CARDS READ',T35,I2/' H PLOT FILE N
```

Print file "hcyl9pc.for"

```
     $AME',T35,A/' DUMP FILE NAME',T35,A//' AXIAL STEP CARDS'/' ID',T13,
     $'DX')
  32  FORMAT(//' RADIAL STEP CARDS'/' ID',T13,'DR')
  36  FORMAT(//' PROPERTY CARDS'/' ID',T13,'K',T25,'RHO*CP')
   7  FORMAT(' ',I2,2(3X,1PE12.6))
   8  FORMAT(//' TIME STEP CARDS'/' NUMBER',T15,'DT',T25,'NPRT',T32,'MSK
     $P',T38,'NSKP')
  37  FORMAT(//' AXIAL  NODE SIZE (RIGHT=TOPMOST)')
  38  FORMAT(//' RADIAL NODE SIZE')
  39  FORMAT(//' PROPERTY')
   9  FORMAT(' ',I6,2X,1PE12.5,3(2X,I4))
  18  FORMAT(/' RESTART DATA FROM FILE ',A)
  20  FORMAT(130I1)
  21  FORMAT(' ',130I1)
  23  FORMAT(//' TOTAL RADIAL LENGTH',T30,1PE12.6/' TOTAL AXIAL LENGTH',
     $ T30,E12.6,//' H SOLUTION FOR ',E12.6,' TO ',E12.6,' SECONDS'//)
  24  FORMAT(' PRINT TEMPERATURE MAP EVERY ',I4,1X,1PE12.5,' SECOND TIME
     $ STEPS FOR EVERY ',I3,' RADIAL NODES AND ',I3,' AXIAL NODES'/)
  25  FORMAT(' TEMPERATURE MAP AT ',1PE12.5,' SECONDS'/10(5X,I3,5X))
  26  FORMAT(' ',10E13.6)
  27  FORMAT(/6X,'HEAT FLUX',8X,'H')
  28  FORMAT(' ',I3,1P2E12.5)
  29  FORMAT(/' AVERAGE H @ ',1PE12.5,' SECONDS: ',E12.5//)
  30  FORMAT(' ',1P2E12.5)
      END

      FUNCTION RHS(ITIM,T,K,J)
C  RETURNS THE VALUE OF THE RIGHT HAND SIDE OF THE IAD EQUATIONS
C    ITIME - HALF (1) /FULL (2) TIME STEP (IN)
C    T     - TEMPERATURE ARRAY (IN)
C    K,J   - COLUMN, ROW INDICES (IN)
      COMMON UK(50,50),LK(50,50),DK2(50,50),UJ(50,50),
     $LJ(50,50),DJ1(50,50),F,M,N
      DIMENSION T(50,50)
      REAL LK,LJ
C BE CERTAIN UJ(M,J) AND UK(K,N) ARE 0 TO TREAT TOP CONDITIONS CORRECTLY
      IF(ITIM.EQ.1)THEN
C COMPUTE RHS AT HALF TIME STEP
        IF(J.EQ.1)THEN
          IF(K.EQ.1)THEN
            RHS=UJ(1,1)*T(2,1)+DJ1(1,1)*T(1,1)-LK(1,1)*F
          ELSE
            RHS=UJ(K,1)*T(K+1,1)+LJ(K,1)*T(K-1,1)+DJ1(K,1)*T(K,1)-
     $          LK(K,1)*F
          ENDIF
        ELSE
          RHS=UJ(K,J)*T(K+1,J)+LJ(K,J)*T(K-1,J)+DJ1(K,J)*T(K,J)
        ENDIF
      ELSEIF(ITIM.EQ.2)THEN
C COMPUTE RHS AT FULL TIME STEP
        IF(J.EQ.1)THEN
          RHS=UK(K,1)*T(K,2)+LK(K,1)*F+DK2(K,1)*T(K,1)
        ELSE
          RHS=UK(K,J)*T(K,J+1)+LK(K,J)*T(K,J-1)+DK2(K,J)*T(K,J)
        ENDIF
      ENDIF
      RETURN
      END

      SUBROUTINE IADSLV(M,N,UK,DK,LK,UJ,DJ,LJ,T,TS)
C  SOLVES THE IAD EQUATIONS USING GAUSSIAN ELIMINATION FOR A FULL TIME STEP
C    M                 - NUMBER OF COLUMNS (IN)
C    N                 - NUMBER OF ROWS    (IN)
C    UK,DK,LK,UJ,DJ,LJ - COEFFICIENTS FOR IAD EQUATIONS (IN)
C    T                 - FULL TIME STEP TEMPERATURE ARRAY (OUT,IN)
```

Print file "hcyl9pc.for"

```
C     TS                  - HALF TIME STEP TEMPERATURE ARRAY (OUT,IN)
      REAL LK(50,50),LJ(50,50)
      DIMENSION DK(50,50),DJ(50,50),UK(50,50),UJ(50,50),
     $T(50,50),B(50),TS(50,50)
      EXTERNAL RHS
C  COMPUTE TEMPERATURES AT END OF HALF TIME STEP IMPLICIT BY COLUMNS
      DO 70 K=1,M
      B(1)=DK(K,1)
      TS(K,1)=RHS(1,T,K,1)/B(1)
C  FORWARD GUASSIAN ELIMINATION
      DO 65 J=2,N
      B(J)=DK(K,J)-LK(K,J)*UK(K,J-1)/B(J-1)
   65 TS(K,J)=(RHS(1,T,K,J)-LK(K,J)*TS(K,J-1))/B(J)
C BACK SOLUTION
      DO 70 J=N-1,1,-1
   70 TS(K,J)=TS(K,J)-UK(K,J)*TS(K,J+1)/B(J)
C COMPUTE TEMPERATURES AT END OF FULL TIME STEP IMPLICIT BY ROWS
      DO 130 J=1,N
      B(1)=DJ(1,J)
      T(1,J)=RHS(2,TS,1,J)/B(1)
C  FORWARD GUASSIAN ELIMINATION
      DO 110 K=2,M
      B(K)=DJ(K,J)-LJ(K,J)*UJ(K-1,J)/B(K-1)
  110 T(K,J)=(RHS(2,TS,K,J)-LJ(K,J)*T(K-1,J))/B(K)
C BACK SOLUTION
      DO 130 K=M-1,1,-1
  130 T(K,J)=T(K,J)-UJ(K,J)*T(K+1,J)/B(K)
      RETURN
      END

      SUBROUTINE WRTHD(N)
C  WRITE MAP POSITION HEADING
      CHARACTER HEAD*130
      HEAD=' '
      L=1
      DO 6 I=1,N/10
      HEAD=HEAD(1:L)//'`.........'
    6 L=I*10+1
      WRITE(6,12)HEAD
   12 FORMAT(' LOCATION MAP (BY ID)'//A)
      RETURN
      END
```

Appendix E
Experimental Data

Table E.1. Table of Experimental Conditions and Heat Transfer Coefficients for Glass Beads.

k_s = 1.04 W/m-K
C_{ps} = 1080 J/kg-K
ρ_s = 2500 kg/m^3

ρ_b = 1500 kg/m^3 d_p = 0.00018 m

Power (W)	Linear Solids Velocity (m/s)	Mass Flow Rate (kg/s)	T_w (C)	T_s (C)	Contact Time (s)	Heat Transfer Coefficient (W/m^2-K)	% Error
147.	.03860	.0599	127.5	28.2	3.948	243.4	4.4
203.	.03860	.0599	156.7	25.0	3.948	253.5	3.2
97.	.03860	.0599	97.6	30.2	3.948	236.7	6.6
98.	.07730	.1199	80.3	31.2	1.972	328.4	7.1
150.	.07730	.1199	107.6	31.9	1.972	325.9	4.7
200.	.07730	.1199	132.6	33.7	1.972	332.3	3.5
200.	.10840	.1682	121.3	35.1	1.406	381.4	3.7
148.	.10840	.1682	98.9	35.7	1.406	385.0	5.0
99.	.10840	.1682	76.5	35.7	1.406	399.5	7.5
104.	.00700	.0109	167.4	30.8	21.771	125.2	5.5
106.	.01200	.0186	148.2	33.3	12.700	151.7	5.6
107.	.02300	.0357	124.9	34.0	6.626	193.5	5.8

107.	.03200	.0496	113.6	34.2	4.762	221.5	5.9
107.	.05200	.0807	99.3	34.4	2.931	271.3	6.2
106.	.07500	.1163	90.2	34.6	2.032	313.3	6.5
107.	.09300	.1443	85.0	33.5	1.639	341.5	6.6
106.	.11950	.1854	80.0	34.9	1.275	386.2	6.9
106.	.16650	.2583	74.5	34.5	.915	435.8	7.2
106.	.26000	.4033	67.2	33.6	.586	519.5	7.7
105.	.24700	.3832	67.8	33.9	.617	506.4	7.7
105.	.29000	.4499	65.9	33.9	.526	539.9	7.9

ρ_b = 1500 kg/m^3 d_p = 0.0008 m

Power (W)	Linear Solids Velocity (m/s)	Mass Flow Rate (kg/s)	T_w (C)	T_s (C)	Contact Time (s)	Heat Transfer Coefficient (W/m^2-K)	% Error
100.	.02570	.0399	119.8	28.0	5.930	179.2	6.1
148.	.02130	.0330	170.6	29.3	7.155	172.2	4.1
146.	.00487	.0076	248.1	29.9	31.294	110.0	3.9
100.	.00590	.0092	182.8	30.3	25.831	107.9	5.7
100.	.04530	.0703	111.7	32.0	3.364	206.4	6.3
148.	.04380	.0679	145.3	33.1	3.479	216.9	4.3
147.	.07730	.1199	129.4	33.9	1.972	253.1	4.5
98.	.07700	.1194	102.3	33.9	1.979	235.7	6.6
98.	.14200	.2203	93.9	33.6	1.073	267.4	6.8
149.	.14320	.2221	119.4	33.6	1.064	285.6	4.5
149.	.25300	.3925	116.9	34.2	.602	296.3	4.6
101.	.23800	.3692	92.3	34.3	.640	286.6	6.7
98.	.23500	.3645	90.8	34.4	.649	284.4	6.9

ρ_b = 1435 kg/m^3 d_p = 0.000044 m

Power (W)	Linear Solids Velocity (m/s)	Mass Flow Rate (kg/s)	T_w (C)	T_s (C)	Contact Time (s)	Heat Transfer Coefficient (W/m^2-K)	% Error
93.	.00794	.0118	153.2	29.1	19.194	122.6	6.2
148.	.00750	.0111	220.2	29.3	20.320	127.6	3.9
149.	.00980	.0145	204.3	30.8	15.551	141.2	3.9
100.	.00945	.0140	161.3	32.2	16.127	127.4	5.8
100.	.01705	.0253	126.8	34.3	8.938	177.8	6.1
100.	.02250	.0334	116.3	34.4	6.773	200.9	6.2
100.	.07830	.1162	91.9	33.5	1.946	282.0	6.7
100.	.04450	.0660	96.3	34.3	3.425	265.4	6.6
118.	.00448	.0066	216.1	27.1	34.018	102.7	4.8
74.	.00560	.0083	148.2	27.2	27.214	100.6	7.6
76.	.01410	.0209	110.7	31.7	10.809	157.2	7.9
101.	.01460	.0217	132.9	31.9	10.438	164.5	5.9
101.	.01660	.0246	128.8	33.5	9.181	174.4	6.0
101.	.02330	.0346	116.0	34.0	6.541	202.7	6.2
101.	.03500	.0519	102.3	34.1	4.354	243.6	6.4
102.	.04520	.0671	96.0	34.2	3.372	271.5	6.5
102.	.07100	.1054	83.9	33.5	2.146	332.8	6.9

Table E.2. Table of Experimental Conditions and Heat Transfer Coefficients for Sand.

k_s = 0.80 W/m-K
C_{ps} = 780 J/kg-K
ρ_s = 2700 kg/m^3

ρ_b = 1280 kg/m^3 d_p = 0.00011 m

Power (W)	Linear Solids Velocity (m/s)	Mass Flow Rate (kg/s)	T_w (C)	T_s (C)	Contact Time (s)	Heat Transfer Coefficient (W/m^2-K)	% Error
100.	.01860	.0246	123.0	25.7	8.194	169.1	6.0
126.	.01740	.0230	149.9	27.3	8.759	169.0	4.8
126.	.04140	.0548	123.2	28.6	3.681	219.0	5.0
101.	.04140	.0548	103.1	29.3	3.681	225.3	6.3
101.	.08180	.1083	90.6	30.1	1.863	274.7	6.6
125.	.08180	.1083	103.8	30.1	1.863	279.0	5.4
126.	.15200	.2012	93.8	30.7	1.003	327.2	5.6
100.	.15200	.2012	81.1	30.6	1.003	325.5	7.0
99.	.22700	.3005	76.0	30.7	.671	359.2	7.3
128.	.22300	.2952	88.7	30.9	.683	362.9	5.7
128.	.22700	.3005	91.0	31.6	.671	353.1	5.6
147.	.03370	.0446	144.8	26.3	4.522	204.1	4.2
147.	.06150	.0814	122.5	30.2	2.478	261.9	4.5
147.	.08570	.1134	116.4	30.7	1.778	282.0	4.6
146.	.02115	.0280	162.0	27.3	7.206	178.2	4.2

100.	.02115	.0280	117.8	29.3	7.206	185.9	6.1
98.	.05430	.0719	95.8	30.8	2.807	248.0	6.6
150.	.05380	.0712	127.0	30.9	2.833	256.7	4.4
101.	.05380	.0712	101.2	31.9	2.833	239.8	6.4
50.	.05380	.0712	67.5	32.6	2.833	235.9	12.9
50.	.08200	.1085	63.6	33.3	1.859	271.1	13.3
100.	.08200	.1085	92.8	33.5	1.859	277.6	6.7
148.	.08200	.1085	122.8	34.3	1.859	274.1	4.5

ρ_b = 1400 kg/m^3 d_p = 0.0008 m

Power (W)	Linear Solids Velocity (m/s)	Mass Flow Rate (kg/s)	T_w (C)	T_s (C)	Contact Time (s)	Heat Transfer Coefficient (W/m^2-K)	% Error
100.	.01930	.0281	121.1	27.1	7.896	174.8	6.1
125.	.01920	.0280	145.4	29.0	7.937	176.6	4.9
100.	.02430	.0354	121.3	31.1	6.272	182.3	6.1
125.	.02920	.0426	137.1	30.5	5.219	192.8	4.9
100.	.06040	.0881	103.0	31.3	2.523	229.5	6.4
151.	.06080	.0887	133.6	31.4	2.507	243.0	4.3
151.	.09900	.1444	126.4	32.0	1.539	263.2	4.4
101.	.09840	.1435	99.5	32.1	1.549	246.2	6.4
100.	.18300	.2668	92.8	31.6	.833	268.9	6.6
148.	.18400	.2683	120.3	31.9	.828	274.5	4.5
148.	.16100	.2348	122.5	32.0	.947	268.9	4.5
99.	.16500	.2406	95.6	32.3	.924	257.3	6.6
148.	.01500	.0219	189.7	32.0	10.160	154.4	4.0
147.	.01270	.0185	184.2	27.7	12.000	154.5	4.0

147.	.02400	.0350	160.3	33.6	6.350	190.8	4.2
145.	.05700	.0831	138.1	30.0	2.674	220.5	4.4
148.	.06600	.0962	139.9	31.6	2.309	224.7	4.3
50.	.02170	.0316	83.4	32.8	7.023	162.4	12.0
100.	.02170	.0316	129.0	32.9	7.023	171.2	6.0
151.	.02170	.0316	170.3	33.1	7.023	181.0	4.0
146.	.05150	.0751	139.8	30.3	2.959	219.4	4.3
100.	.05150	.0751	109.5	32.0	2.959	212.1	6.3
50.	.05150	.0751	71.6	32.7	2.959	211.2	12.6

ρ_b = 1440 kg/m^3 d_p = 0.0012 m

Power (W)	Linear Solids Velocity (m/s)	Mass Flow Rate (kg/s)	T_w (C)	T_s (C)	Contact Time (s)	Heat Transfer Coefficient (W/m^2-K)	% Error
100.	.06500	.0968	105.3	32.8	2.345	226.9	6.4
100.	.06500	.0968	152.3	30.3	2.345	134.8	5.8
150.	.01740	.0259	120.3	28.5	8.759	268.7	4.4
149.	.02500	.0372	114.8	27.9	6.096	282.0	4.5
96.	.04130	.0615	138.4	27.9	3.690	142.9	6.1
150.	.05740	.0855	132.0	29.8	2.655	241.4	4.3
100.	.05740	.0855	97.8	28.9	2.655	238.9	6.5
100.	.06200	.0923	101.2	29.6	2.458	229.8	6.4

Table E.3. Table of Experimental Conditions and Heat Transfer Coefficients for Copper.

k_s = 384 W/m-K
C_{ps} = 386 J/kg-K
ρ_s = 8950 kg/m^3
ρ_b = 5200 kg/m^3
d_p = 0.00021 m

Power (W)	Linear Solids Velocity (m/s)	Mass Flow Rate (kg/s)	T_w (C)	T_s (C)	Contact Time (s)	Heat Transfer Coefficient (W/m^2-K)	% Error
153.	.10700	.5931	84.2	28.7	1.424	453.5	5.1
100.	.10700	.5931	65.6	29.4	1.424	455.1	7.8
200.	.10700	.5931	104.4	29.8	1.424	440.7	3.8
198.	.03770	.2090	136.7	30.1	4.042	305.3	3.5
150.	.03770	.2090	111.4	31.9	4.042	310.3	4.6
100.	.01840	.1020	113.7	32.5	8.283	202.4	6.2
150.	.01840	.1020	158.1	32.3	8.283	196.1	4.1
200.	.01840	.1020	185.0	32.3	8.283	215.3	3.2

The % Error term of Tables E.1 to E.3 was derived using the following relations:

$$h = \frac{P}{A\ \Delta T}$$

$$\frac{dh}{h} = \frac{dP}{P} + \frac{dA}{A} + \frac{d\Delta T}{\Delta T}$$

where $\Delta T = T_W - T_S$. After application of measurement precision,

$$\frac{dh}{h} = \frac{5}{P} + \frac{.5}{A} + \frac{1}{\Delta T}$$

$$\%\ \text{Error} = 100 * \frac{dh}{h}.$$

Table E.4. Table of Experimental Conditions and Heat Transfer Coefficients for Falling Solids.

Particle Diameter (m)	Linear Solids Velocity (m/s)	Heat Transfer Coefficient (W/m^2-K)	Material
0.11	0.52	98.72	Sand
0.11	0.52	112.75	Sand
0.11	0.52	98.0	Sand
0.11	0.52	103.93	Sand
0.8	1.84	68.	Sand
0.8	1.84	64.3	Sand
0.8	1.84	54.	Sand
1.2	1.89	57.	Sand
1.2	1.89	50.	Sand
0.214	1.65	89.	Copper
0.214	1.65	107.	Copper

Appendix F
Statistical analysis

Table F.1. Regression Analysis of Model.

Linear model: $\frac{t_{cr}}{d_p \rho_s} = a + bL$

Parameter	Estimate	Standard Error	T Value
Intercept (a)	0.362193	0.017465	20.7375
Slope (b)	9.69099	0.254237	38.118

Analysis of Variance

Source	Sum of Squares	Df	Mean Square	F-ratio
Model	3.0933	1	3.0933	1452.98
Error	0.017031	8	0.0021289	
Total (Corr.)	3.110348	9		

Correlation Coefficient = 0.997258
Stnd. Error of Est. = 0.046140
R-squared = 99.45%

Table F.2. List of All Data used to Fit the Model.

Heated Length (m)	Particle Diameter (m)	$\frac{t_{cr}}{\rho_s d_p}$ (m^2 s/kg)	Material	Author
0.005	0.0002	0.432	sand	Ernst
0.005	0.0004	0.421	sand	Ernst
0.005	0.0006	0.439	sand	Ernst
0.0116	0.00016	0.519	sand	Desai
0.0116	0.0008	0.472	sand	Desai
0.0116	0.00015	0.461	copper	Desai
0.0116	0.00017	0.407	copper	Desai
0.0116	0.00063	0.449	copper	Desai
0.1524	0.00018	1.776	glass	This study
0.1524	0.0008	1.905	glass	This study

Appendx G
Particle Size Distribution

Table G.1. Size Distributions of Particles

Silica Sand

$\overline{d_p} \approx 0.11$mm

Tyler Mesh	%Weight
-42 + 60	2.18
-60 + 80	5.5
-80 + 100	9.57
-100 + 115	17.83
-115 + 150	19.2
-150 + 170	16.37
-170 + 200	13.4
-200 + 250	6.77
-250 + 270	5.25
-270 + 325	2.5
-325	1.43

$\overline{d_p} \approx 0.8$mm

Tyler Mesh	%Weight
-20 + 24	35
-24 + 28	21.37
-28 + 35	21.16
-35 + 48	15.21
-48	7.26

$\overline{d_p} \approx 1.2$mm

Tyler Mesh	%Weight
-10 + 14	67.84
-14 + 20	31.25
-20 + 24	0.693
-24	0.218

Copper

$\overline{d_p} \approx 0.214$mm

Tyler Mesh	%Weight
-20 + 24	0.3
-24 + 28	0.78
-28 + 32	5.24
-32 + 48	43.3
-48 + 60	1.75
-60 + 80	17.52
-80 + 100	11.70
-100 + 115	3.35
-115 + 150	3.78
-150 + 170	4.98
-170	7.26

Glass

$\overline{d_p} \approx 0.8$mm Tyler Mesh	%Weight
-14 + 20	23.94
-20 + 24	72.2
-24 + 28	3.05
-28 + 32	0.39
-32 + 35	0.2
-35 + 40	0.17
-40	0.05

$\overline{d_p} \approx 0.18$mm Tyler Mesh	%Weight
-45 + 60	0.5
-60 + 70	38.8
-70 + 80	49.7
-80 + 100	6.0
-100 + 120	2.0
-120 + 140	3.0